AD-A136 181 THE GRAND BANKS EXPERIMENT: A SATELLITE/AIRCRAFT/SHIP EXPERIMENT TO EXPLO..(U) NAVAL OCEAN RESEARCH AND DEVELOPMENT ACTIVITY NSTL STATION MS.. P E LA VIOLETTE 1/2

UNCLASSIFIED JUL 83 NORDA-49 F/G 17/9 NL

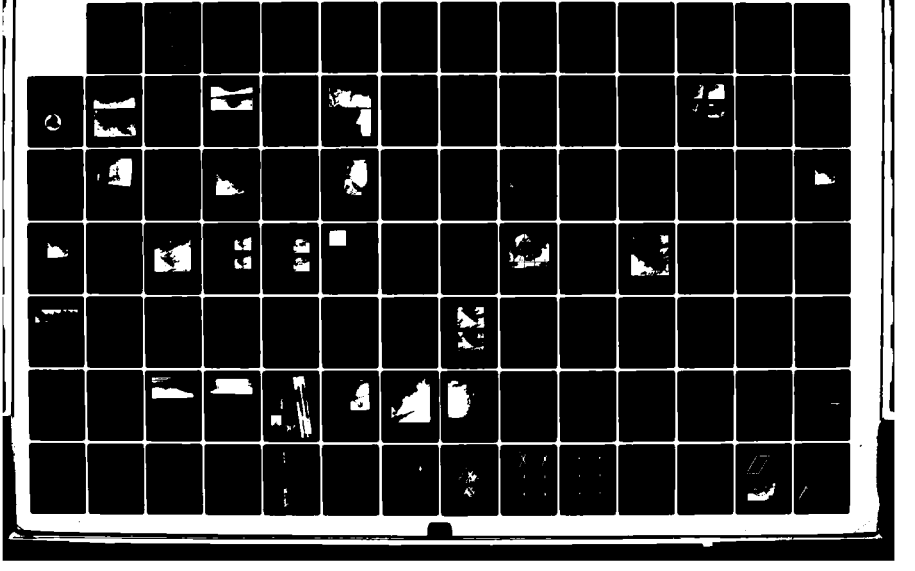

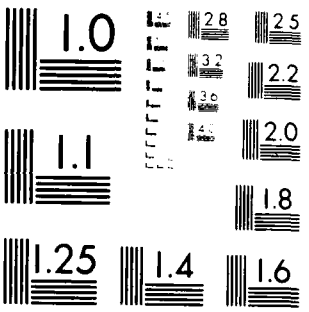

NORDA Report 49

The Grand Banks Experiment:

A Satellite/Aircraft/Ship Experiment to Explore the Ability of Specialized Radars to Define Ocean Fronts

Paul E. La Violette

Oceanography Division
Ocean Science and Technology Laboratory

July 1983

Naval Ocean Research and Development Activity
NSTL Station, Mississippi 39529

Foreword

The Grand Banks Experiment was designed to examine the ability of satellite- and aircraft-specialized radars to monitor ocean fronts. Data from these types of radars provide information on aspects of the ocean we have only recently learned to be important and at a scale with which we are just becoming familiar. The results of the experiment documented in this report should help develop these radars into powerful oceanographic research tools.

G.T. Phelps, Captain, USN
Commanding Officer, NORDA

Executive Summary

At various times during 1978-1979, a joint U.S.-Canadian experiment involving ships, buoys, aircraft, and satellites was conducted in the waters southeast of the Grand Banks. The purpose was to determine the ability of satellite- and aircraft-specialized radars (SAR and SLAR) to monitor ocean fronts. The experiment results, detailed in this report, show that these radars are capable of defining thermal fronts under most weather conditions. The degree, as well as type, of definition depended on the angle the wind made with the thermal front and associated currents. Winds blowing parallel to the fronts produced shear lines in the SAR and SLAR imagery. Winds blowing orthogonal to the front produced broad patterns whose changes mark the location of the thermal fronts. This latter definition produced the best delineation of the thermal fronts; however, delineation was more gradual than the sharp thermal gradients marking the fronts seen in satellite infrared imagery. The possible causes of these effects are detailed in this report.

Preface

The Grand Banks Experiment is a U.S.-Canadian effort to explore the utility of microwave sensors to define ocean fronts. Chief among the sensors to be studied are the synthetic and real aperture radars (SAR and SLAR). These specialized radars are the subject of this report.

A U.S.-Canadian investigative group called the Grand Banks Experiment Team was assembled to conduct the experiment and to analyze the resulting data. While the author of this report is the U.S. principal investigator, the report has been assessed by the team members (listed opposite) who worked on the SAR and SLAR data. In this regard, the results should be considered a collective report on that portion of the team's work.

The text of the report has a definite purpose: to document the ability of SAR and SLAR to define ocean thermal fronts and currents. Thus, extensive analyses by the various team members toward results only partially related to this objective have been re-edited for inclusion in this report. The original papers have been referenced for any reader who seeks further information.

Preface

Robert W. Fett
Naval Environmental
Prediction Research Facility
Monterey, California, USA

James Gallagher
U.S. Navy Underwater
Systems Center
New London, Connecticut, USA

James F. R. Gower
Institute of Ocean Sciences
Patricia Bay, BC, Canada

Nordan E. Huang
NASA-Wallops Flight Center
Wallops Island, Virginia, USA

Jeffrey Kerling
U.S. Naval Oceanographic Office
NSTL Station, Mississippi, USA

Paul E. La Violette
Naval Ocean Research
and Development Activity
NSTL Station, Mississippi, USA

Charles McClain
NASA-Goddard Space Flight Center
Greenbelt, Maryland, USA

Steve Peteherych
Environment Canada
Downsview, Ontario, Canada

Contents

Contents

Illustrations and Tables

Illustrations

Tables

The Grand Banks Experiment:

A Satellite/Aircraft/Ship Experiment to Explore the Ability of Specialized Radars to Define Ocean Fronts

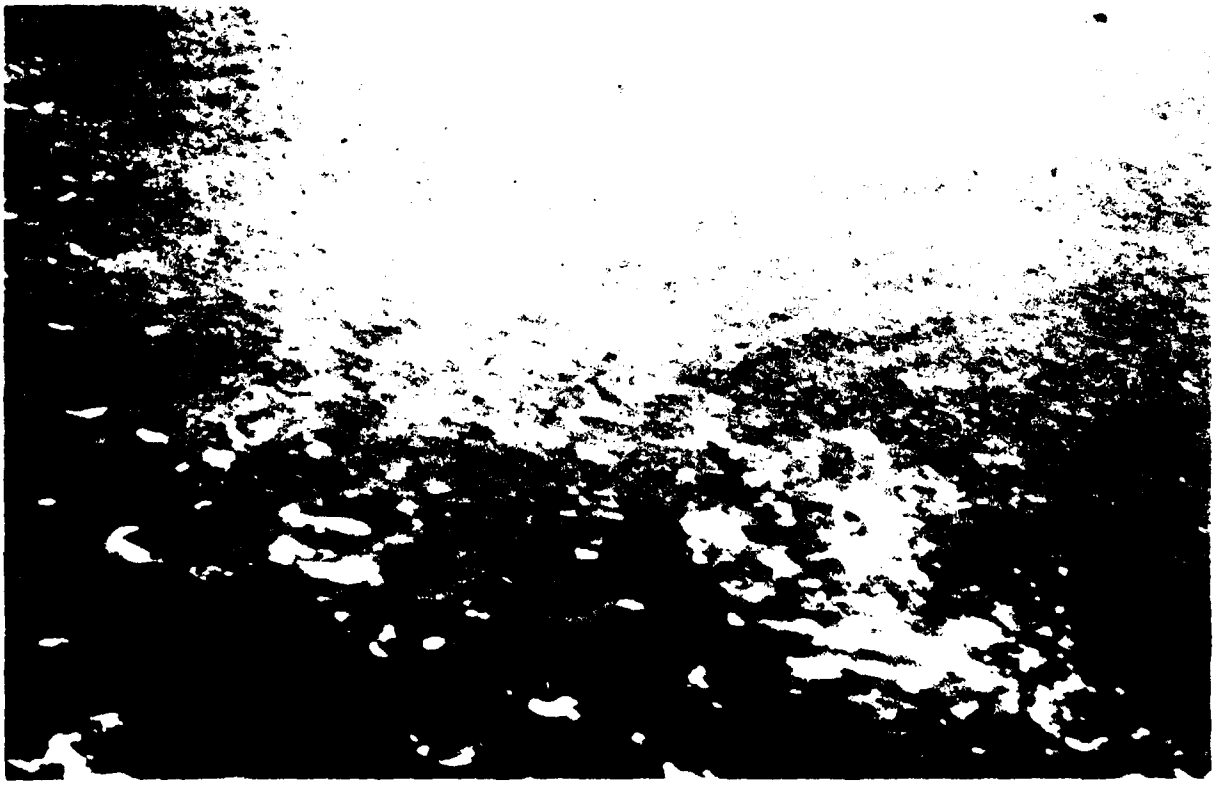

Part I. General

The sun was shining on the sea,
Shining with all his might
He did his very best to make
The billows smooth and bright ...

"Through the Looking Glass"
by Lewis Carroll

1. Introduction

The recent development and installation of synthetic and real aperture radars (SAR and SLAR) aboard satellites and aircraft offers a unique opportunity to utilize radar backscatter (σ_o) data to synoptically examine the roughness patterns of the ocean surface. One of the most important oceanographic applications of this information is the capability to monitor the location of ocean frontal boundaries during all weather conditions.

Several mechanisms have been shown to cause the surface roughness to change across an ocean front. One of the important ones is the interaction of the wind and the ocean surface. Studies such as Jones (1953), Kondo (1975), and Sweet et al. (1981) have shown that wind stress on the ocean surface is markedly dependent on the thermal stability of the air immediately above the surface. For surface winds, the water temperature (T_s) affects the vertical wind profile so that the surface stress is greater when the water is warmer than the air temperature (T_a) and less when the water is cooler than the air. Increasing wind speeds, however, have been shown to diminish this effect (Deacon, 1961). A large decrease or negative sign to the air-sea surface temperature difference (T_a-T_s) can result in increased boundary-layer turbulence and, consequently, increased wave growth. Such a situation occurs abruptly in the region of an ocean front where (T_a-T_s) is positive on one side of the front and is negative on the opposite side. This effect is regularly observed from research aircraft, especially along the northern and western edge of the Gulf Stream as shown in Figure 1.

Another important mechanism that causes changes to surface roughness across an ocean front is wave-current interaction. Changes in either the amplitude or the orientation of surface waves across current boundaries is a phenomenon often observed at sea. Early studies attributed the abrupt changes in ocean roughness to sharp fluctuations in the current field, such as observed in an inlet during the ebb and flood of the tides (Bowden, 1948; Barber, 1949). A good example of such changes is shown in Figure 2.

The kinematic and dynamic relationships that govern wave refraction and

Figure 1. Variations in the roughness patterns across the north wall of the Gulf Stream looking south from a research aircraft at 300 m altitude. The smooth areas in both photographs are regions of slope water. (Photograph by J. Kerling, NAVOCEANO).

Figure 2. Tidal-current produced surface features in the sunglint in Discovery Passage, British Columbia, Canada (Hughes, 1978).

energy exchange between a shearing current and a gravity wave component in terms of radiation stress were developed by Longuet-Higgins and Stewart (1960), and Longuet-Higgins (1961 and 1964). Their results indicate that wave components are modified by the current in a manner dependent upon the phase speed of the wave and the initial angle of the wave-current encounter. Kenyon (1971) noted that wave components can be reflected, trapped, or transmitted by such currents as the Gulf Stream. Corresponding changes have been observed by Sugimori (1973) in the Kuroshio and by Hayes (1980) in the Gulf Stream. As an illustration of the importance of wave-current interactions, Huang et al. (1971) applied the theoretical results of each component of wind-propagated waves to Pierson-Moskowitz spectra for the two simple conditions of the wind directly following the current and the wind opposed to the current. In their study, Huang et al. indicated that significant changes in the spectra should be expected to occur under actual ocean conditions.

In addition to current- and thermal-associated roughness changes, other mechanisms exist which, to various degrees, are responsible for the variations in surface roughness found near or across ocean fronts. Chief among these are the dampening effects of organic

films, internal wave motions, and variations in bottom topography. Few indepth studies have been made that directly relate these effects to changes in ocean frontal roughness.

A number of investigators have shown that abrupt roughness changes in the ocean surface are visible from satellites and that these changes are indicative of oceanographic events taking place. (e.g. Soules, 1970; Strong and De Rycke, 1973; Fett and Rabe, 1977; Fett et al., 1978; and La Violette et al., 1980). These roughness changes are seen in the satellite visible data as changes in the reflective response of the ocean surface to the sun's rays. Figure 3 is a good example of this phenomenon.

In a similar fashion, the σ_o derived from SAR and SLAR instruments should be capable of delineating surface roughness features associated with thermal and current boundary effects. Since these instruments respond to surface roughness, their σ_o should be the response to the same surface roughness effects as those that create sunglint patterns and, in many instances, the radar imagery should show features similar to those seen in the sunglint imagery.

Some differences should be expected, of course, when comparing sunglint patterns and radar imagery. For example, the geometry for the radar is simpler since the instrument transmits its own illuminating radiation. More important than this, is the fact that the reflection mechanism of the radar involves resonant or Bragg scattering. The importance of the resonant scattering to this study is discussed in Parts IV and V using SLAR and SAR imagery. In essence, however, the origin of radar and sunglint images are similar, and this similiarity is used to help show the type of changes in ocean roughness that create the variations in σ_o seen in the radar imagery.

The main purpose of the Grand Banks Experiment is to show that:

- thermal fronts, and their related currents and local weather conditions modify, or create conditions which modify, the amplitude and orientation of local waves,

- these modifications form distinctive roughness patterns in the ocean surface, and the radar backscatter of aircraft and satellite SAR and SLAR off these roughened surfaces can be used to define the region of these patterns.

Since these radars are not affected by fog, mist, or time of day, the conclusions show these radars to be useful all-weather tools for ocean research.

2. The Grand Banks Experiment

The Grand Banks Experiment took place in the waters off the coast of Newfoundland southeast of the Grand Banks. Satellite data were collected for the broad area located between 40° and 51° West and 35° and 50° North. Ship and aircraft data were collected for a relatively smaller area--44° to 51° West and 39° to 45° North (Fig. 4).

The experiment was conducted in two survey phases. The first phase, called "Baseline," occurred during two weeks in late June 1978. The second phase, called "New Look," occurred in early May and again in July/August 1979. To provide continuity between the two phases, satellite data were collected during the intervening months.

Baseline had two purposes. The first was to establish that there is a relationship between the regional surface roughness patterns and the thermal fronts and surface flow. The second was to derive a synoptic understanding of the physical oceanography of the study region. The launch of SEASAT-A was delayed until after the June survey and no SAR data

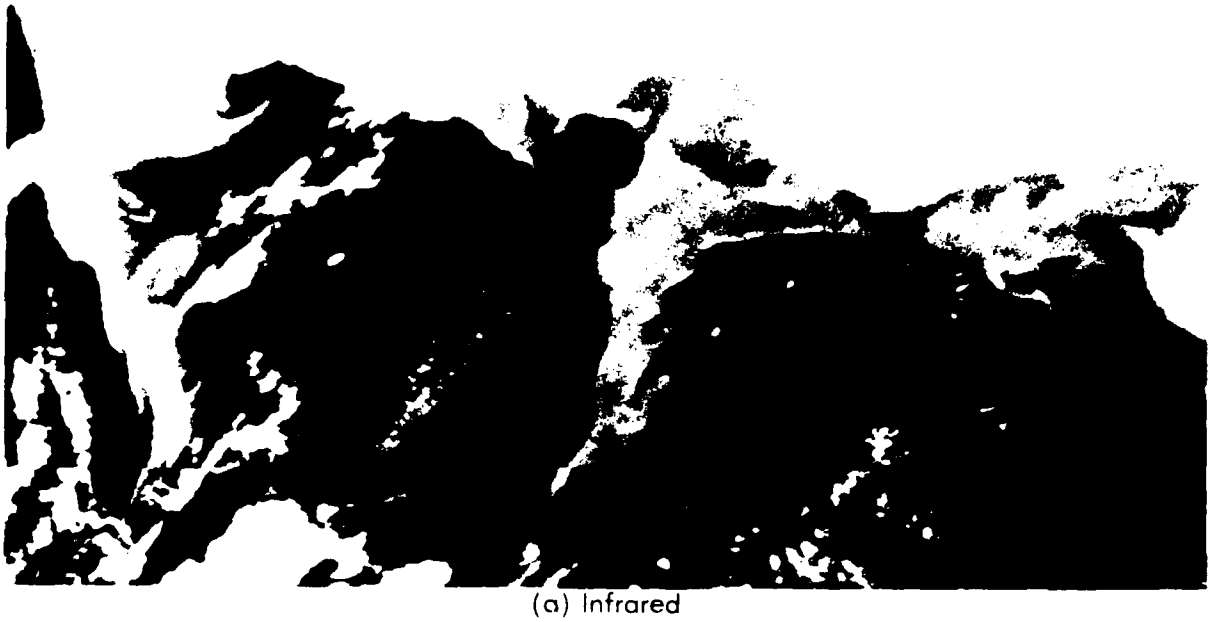

(a) Infrared

(b) Visible

Figure 3 (left). Imagery of sunglint and thermal patterns in the Gulf Stream derived from visible and infrared TIROS N data for 15 May 1979. These images represent spectral radiation from the same earth scene that was received by the satellite sensor and then split to show the scene's electromagnetic radiation for the visible and thermal ranges. Note that the visible image shows a continuous north south swath of sun glint rather than a point source. This is a product of the rotation of the sensor and mirror coupled with the forward movement of the satellite. A fuller explanation for this phenomenon may be found in La Violette et al., 1980. The infrared image is a gray tone depiction of the thermal radiation of the oceans and clouds. Lighter tones represent cold features, darker tones represent warm features.

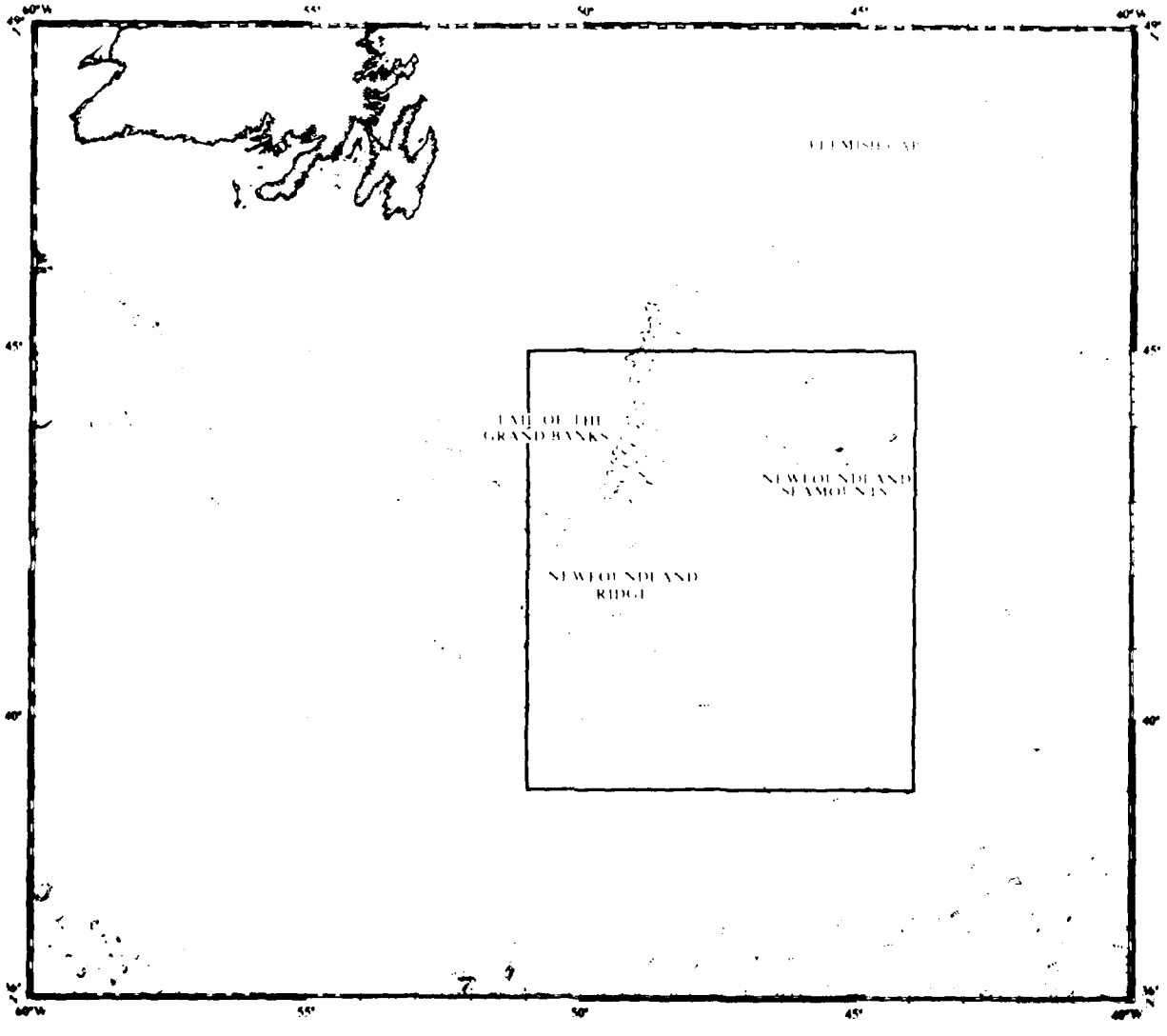

Figure 4. Grand Banks Experiment study area. The square represents the major ship and aircraft survey area.

Table A. Platforms and sensors used during BASELINE and NEW LOOK

BASELINE (June 1978)

Platforms		Main Instrumentation Sensors
Ships:	USNS LYNCH (T-AGOR-7)	CTD[1], XBT[2], surface temperatures[3], surface salinities[4], satellite drifter buoy, and meteorological sensors
	USCGC EVERGREEN	XBT, surface temperatures, and satellite drifter buoy
Aircraft:	U.S. NAVOCEANO BIRDSEYE (P-3)	PRT[5], AXBT[5], IR scanner, and meteorological sensors
Satellites:	NOAA-4 and 5	IR and visible

NEW LOOK (May 1979)

Aircraft:	U.S. NAVOCEANO SEASCAN (P-3)	PRT, AXBT, and meteorological sensors
Satellite:	TIROS-N	IR and visible

NEW LOOK (July/August 1979)

Ship:	USNS LYNCH (T-AGOR-7)	CTD, XBT
Aircraft:	U.S. NAVOCEANO SEASCAN (P-3)	PRT, AXBT, and meteorological sensors
Satellite:	TIROS-N	IR and visible

NOTES:

Data Collection and calibration methods:

[1]Presurvey calibration and field rosette sample checks
[2]Standard Sippican XBTs, no field calibration
[3]Bucket temperature with calibrated thermometers
[4]Autosal model 8400 salinometer
[5]Barnes PRT-5 inflight bath calibration with upward-looking PRT's for sky correction
[6]Pre-survey bath calibration

are available for the period of Baseline. However, SLAR data were collected by a U. S. Coast Guard C-130 aircraft. Details on the instrumentation and survey platforms used during Baseline can be found in Table A.

New Look was planned so that SAR and SLAR data could be obtained during an in situ survey of the regional fronts. Unfortunately, several critical setbacks occurred prior to and during New Look which required altering the experiment approach. The most important setback was the abrupt failure of SEASAT-A prior to New Look and the resultant loss of a SAR for the New Look phase of the experiment. An aircraft SAR was planned as a replacement, but at the start of New Look this aircraft developed mechanical problems, and was forced to withdraw from the survey without collecting any SAR data.

Another major setback was a severe storm that prevented the USNS LYNCH from entering the study area in time to participate in New Look. Thus, the in situ wave measurements that the ship scientists would have made for comparison with the remotely sensed data are not available. A second ship, the CCS GADUS ATLANTICUS, developed engine trouble and was also forced to withdraw.

Despite these difficulties, the New Look survey team was able to collect extensive and, at times, unique data sets. As will be shown, these data are of sufficient quality to be used to resolve the objectives of the SAR/SLAR portion of the Grand Banks Experiment.

3. Analytical Approach

The analysis of the experimental data in this study utilizes the following approach:

- Prove that the satellite infrared imagery reliably depicts ocean boundaries of major significance and may be used in a hindcast study with SEASAT SAR data (Part II).
- Show that these boundaries have roughness variations discernible by SAR and SLAR using (1) ship reports; (2) aircraft laser, sonobuoy and camera data; and (3) NOAA (TIROS-N) infrared and visible data (Part III).
- Compare SLAR data with ship, aircraft and satellite data taken during Baseline and New Look (Part IV).
- Conduct a hindcast study to compare SEASAT-A SAR data taken in September-October 1978 with NOAA-5 infrared imagery, local weather data, and ship reports collected during the same period (Part V).
- Coalesce these results to show that the radar backscatter σ_0 of SAR and SLAR can be used to define ocean fronts (Part VI).

The next to last step is extremely critical. Since no ship or aircraft data were collected in the area for the period when SEASAT-A SAR was functioning, registered NOAA-5 infrared imagery, regional weather analyses, and local ship reports will be the only sources of surface truth. The first three steps will be used to prove that the use of satellite infrared imagery as surface truth in the fourth step is a valid concept.

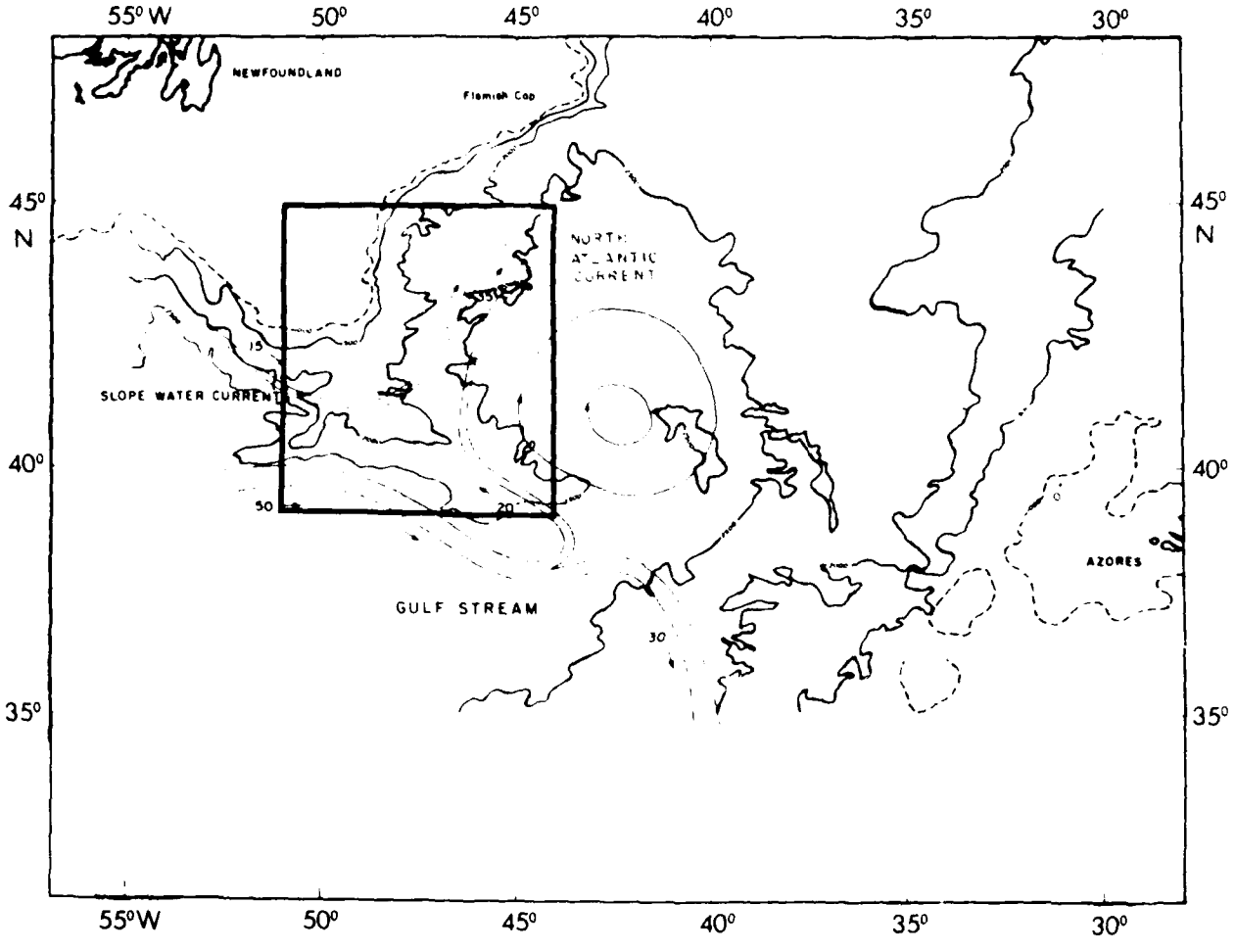

Figure 5. Schematic positions of currents southeast of Grand Banks according to Mann (1967). Contours represent nominal transports in 10^6 m^3/sec. The square represents the major survey area of the Grand Banks Experiment.

Part II. Baseline and New Look

1. Introduction

Recently developed computer techniques using a blend of ship, aircraft, and satellite data (Holyer et al., 1980) now enable oceanographers to study the synoptic details of an ocean area as complex as that lying southeast of the Grand Banks. La Violette (1974, 1981a) and La Violette et al. (1975) show that data from satellites can be used in the field to operationally control the survey of a complex area, and can be used in combination with conventionally collected data for the post-survey analysis. In such a survey, remotely sensed data from satellites would be used to provide broad, synoptic area coverage, and in situ data from aircraft and ships would be used to intensely examine small critical regions within the larger study area. Baseline and New Look were conducted in this fashion.

The main purpose of this portion of the study is to describe the oceanography of the region as derived from ship/aircraft/satellite surveys, and to show that satellite infrared imagery can be used to accurately locate the position of the region's thermal fronts.

A more complete report on the oceanographic conditions found during the Grand Banks surveys can be found in La Violette (1981b).

2. Previous Studies

Historical aircraft and ship data indicate that the ocean region southeast of the Grand Banks is the confluence of the Gulf Stream, North Atlantic, and Slope waters. On the Grand Banks, the cold, generally southward-moving waters of the Labrador Current form a dynamic buttress to these warmer, northward- and eastward-moving waters. The interface of these water masses composes the Labrador Front, a complex pattern of meanders, extrusions, and eddies which, in the historical data, seems to generate confusing patterns that change position and strength from season to season and from year to year (Worthington, 1962, 1976; Mann, 1967, 1971; and Clarke et al., 1980).

A controversy exists over what happens to the Gulf Stream once it enters the region of confluence. This conflict centers around the claim by Worthington (1962, 1976) that a permanent low-pressure trough exists over the bathymetric rise, known as the Newfoundland Ridge, blocking further eastward flow of the stream. According to Worthington, the total flow of the Gulf Stream is therefore deflected southward toward the Sargasso Sea and little, if any, mixing occurs between the waters of the Gulf Stream and the North Atlantic current moving northward on the other side of the bathymetric ridge.

Mann (1967), on the other hand, elaborates on a theory first advanced by Islin (1936) that the stream splits into two branches south of the Grand Banks (Fig. 5). Using April/May 1963 and June/July 1964 data collected by CSS BAFFIN, Mann states that although much of the Gulf Stream flows south, a branch of the Gulf Stream loops back at 38°30'N, 44°W to join the North Atlantic Current. Mann also notes that in the shallower regions of the Newfoundland Ridge closer to the Grand Banks, slope water overrides the ridge and also joins the North Atlantic Current.

Clarke et al. (1980), reporting on the results of a 1972 three-ship survey, show what they consider conclusive proof that the Gulf Stream does indeed split into two branches, with the greatest

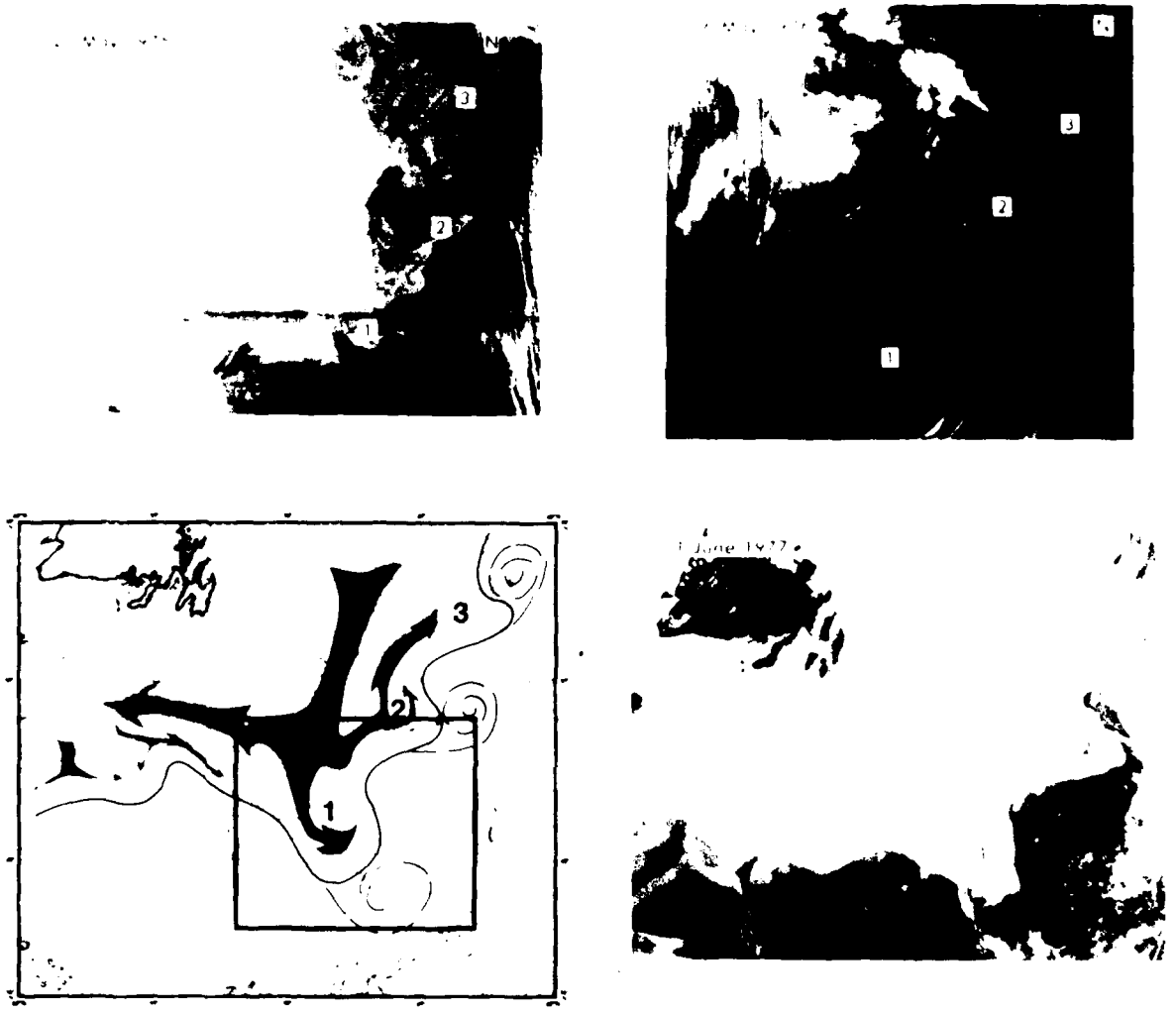

Figure 6. Samples of satellite infrared imagery for the Grand Banks Experiment area for the period January 1975 through October 1979. These imagery show that three frontal extrusions were always present in the cloud free data. However, imagery showing all three structures at one time are rare. The ones presented here are meant only as examples of these features. Newfoundland is the dark land mass in the upper left corner of each image. The line drawing on the bathymetry chart is a composite of all the imagery for 1978, and is drawn by hand on a common grid. The solid line represents the edge of the cold water of the Labrador Front. The dashed line represents the direction and type of extrusion away from the front. The shaded area northwest of the front represents the dominant position of the Labrador Current as seen in the imagery. The smaller shaded areas in the west are smaller slope water current features that also appeared in the 1978 imagery. Composites drawn from other years' imagery show similar results.

amount of Gulf Stream water turning southward and the smaller portion joining the northern Atlantic waters.

Much of the oceanographic data collected in the area have been taken by vessels of the International Ice Patrol, which began systematically collecting ocean station data in 1922. Based on these data, mean dynamic topographies (using 1000 m as a reference level) for the months of the iceberg season (April, May and June) were calculated by Soule (1964).

Mountain and Shuhy (1980), after examining STD data taken by the USCGC EVERGREEN and USCGC SHERMAN in June 1976 and USCGC HAMILTON in August 1977, conclude that mesoscale eddies were present along the Newfoundland Ridge and that these had a temporal and spatial variability on a scale that had not been resolved in previous surveys. Their data indicated the circulation pattern varied from one in which the Gulf Stream branched around the Ridge to one in which a portion of the Gulf Stream crossed the Ridge.

The author feels that the problems encountered by the researchers studying the dynamics of this complex region have not been caused by insufficient data, but rather by a lack of synoptic data. Certainly, the International Ice Patrol data set is not a small amount. However, the International Ice Patrol data represent repeated looks at standard locations, with no account being taken that these positions in any one year may not best describe the regional dynamic structure. Compilations of these data into mean dynamic topographies, such as composed by Soule, can easily hide transient variations that may not be trivial. As will be shown in the analyses of the Baseline and New Look data, translations of the main features of only a few kilometers would introduce drastic variations in point measurements such as those made by STD's taken at standard locations.

3. Pre-Survey Satellite Data

In preparation for the Baseline and New Look surveys, NOAA-4 and NOAA-5 satellite imagery for the three-year period, January 1975 through May 1978 were examined. During Baseline and New Look, as well as during the intervening months in between, additional satellite data (NOAA-5 and TIROS-N) were collected to aid in the survey operations and post-survey analyses. Altogether, over five years of satellite data were examined for use in this study (Fig. 6).

The data collected by ship and aircraft during Baseline and New Look were handled in the conventional manner for these types of survey platforms. Remarks describing the collection, limitations, and application of satellite data have been included as an appendix for readers unfamiliar with these types of data.

A problem in the use of NOAA-4 and 5 data (that does not occur with TIROS-N data) is that quantitative image-to-image comparison of the NOAA data is difficult because of variations in geographic distortion (see the appendix). Therefore, the pre-survey analysis of satellite imagery was done qualitatively by hand-transferring the main gradient features onto a common grid. Although this method is crude, the analysis of the thermal front between the cold, southwest-moving Labrador Current water and the warmer, northward-moving Atlantic waters show certain persistent features. These features appear as extrusions of cold water that are continuously being extended away from the Labrador Front into the warmer Atlantic waters. Moreover, these extrusions extend from nodal points overlaying three bathymetric features: The Newfoundland Ridge, the Newfoundland Seamounts and the Flemish Cap. The first two features lie within the study area and are addressed in detail in this report.

A composite drawing resulting from the examination of the satellite infrared imagery for one year (1978) is shown in Figure 6 to compare with samples of

cloud-free imagery from the several years of imagery.

Clouds are always a problem in utilizing infrared satellite data for oceanographic analysis since they block the satellites' view of the ocean. Thus, monitoring a region as cloudy as the study area for any extended period using satellite infrared data is difficult. Nonetheless, the pre-survey study showed that large amounts of cold water were always in some phase of extrusion away from the common nodal points. There appears to be no periodicity to the growth and decline of the extrusions. In addition, the speed of their movement varies considerably--at times a feature will show little movement and then begin to move rapidly. Because of the regional cloud cover and the NOAA 4 and 5 data registration problems mentioned with NOAA-4 and 5 data, it is difficult to make quantitative measurements of the movements. Since the initial three years of satellite data were examined only as a pre-survey study, a more extensive examination was not instigated.

It is interesting to note that few completely separate eddies were found in the several years of satellite imagery (the average was three each year). Thin filaments of cold-water tying the developing eddies or gyres to the Labrador Front are found to be normally present. The significance of these unexpected filaments is covered in the discussion section.

4. Baseline Data—June 1978

Baseline took place during the period of 14-27 June 1978. The survey platforms and the sensor instrumentation relevant to this study are listed in Table A. During the survey, the Navy P-3 aircraft made seven survey flights, beginning 14 June and finishing 25 June.

The USNS LYNCH entered the area 14 June and departed 24 June. A satellite drifter was released from the ship 22 June. The USCGC EVERGREEN entered the area 19 June and departed 21 June. This ship had also been equipped with a satellite drifter buoy that was released 13 April north of the study area. As will be shown, the movement of these buoys through the study area defined two of the main thermal features.

Analyses of the data collected by aircraft, ships, and buoys show that the cold features delineated in the simultaneously collected satellite infrared imagery were the surface manifestations of large ocean frontal structures that extended more than 1500 m below the surface (Figs. 7-13 give correlative evidence of this). In addition, analyses show that these frontal structures moved during the survey period. Most of the interesting movement occurred in the water over the Newfoundland Ridge, and it was there that the ship and aircraft data collection was concentrated.

By the end of the two-week survey, a major structure with a large eddy-like feature at its terminus had extruded more than 140 km from the southwest corner of the Labrador Front. The initial position of this movement can be seen in the 12 June satellite infrared imagery and the aircraft precision radiation thermometer (PRT) data for 17/18 June in Figure 7. The movement culminates in the frontal position shown by the 25 June satellite image and the 27 June aircraft PRT analysis in Figure 9. The step-by-step extrusion away from the initial position is shown in the overlay of major thermal gradients derived from PRT data in Figure 10. As this figure suggests (and the satellite data show more positively), the main movement began abruptly 18 June and continued to the position shown for 27 June, which was the end of the Baseline survey. Unfortunately, clouds and the onset of seasonal high humidity obscured satellite views of the sea surface temperature gradients for the next two months. Because of this, no further tracking of the extruded cold feature could be made.

Plane views of the 300 m temperatures show that the thermal gradients at this depth closely follow the surface patterns of thermal extrusion (Fig. 11). Cross sections constructed from ship 750 m expendable bathythermographs (XBTs) show that the cold feature extended at least to the bottom of the XBT traces (Fig. 12). Finally, STD casts taken by the ship show that the salinity and temperature within the cold feature differed from the salinity and temperature outside the feature as deep as 1200 m (Fig. 13).

Two other extrusive features were examined during Baseline. The first of these features--a southward extrusion of cold water along 49°30'W--is shown by the satellite imagery to have slowly developed into an eddy 100 km in diameter. In situ examination by the aircraft and ships was limited to the filament connecting the main portion of the feature with the Labrador Front (Figs. 7 and 12). However, positive evidence for genetic circulation was furnished by the track of a satellite drifter buoy (Fig. 14) released into the Labrador Current at 48°31'N, 48°59'W by the USCGC EVERGREEN on 13 April (P. Richardson, WHOI, unpublished data).

It is interesting to compare the southward movement of the buoy with the position of the thin, cold core of the Labrador Current visible in the 12 June satellite image (Fig. 7). At 51°30'W, the buoy turned eastward, and on 30 May it became caught in the flow of the southward extension at 49°30'W. The data show that the buoy then became entrained within the newly formed eddy and remained there rotating in a counter-clockwise direction until the end of tracking 22 June. The eddy is visible in the NOAA-5 infrared image of 23 June in Figures 8 and 14.

The examination of the several years of collected satellite imagery indicates that, although a cold feature near the region of 49°30'W is often found, it does not appear to be a persistent feature in the imagery. On those occasions when it is found, it seems to form one element of a bifurcated ridge feature, with the position of the second Newfoundland Ridge feature being moved more to the northeast than when only one feature is present.

Wave data were collected by a member of the Canadian Wave Climate Study group using a wave buoy deployed from USNS LYNCH. The data from four of these deployments are discussed in detail in Part IV.

The third feature of interest--the cold frontal feature over the Newfoundland Seamounts--also showed strong extension during Baseline. Although neither the aircraft nor the ships entered this region (except to show the beginning of northeast arcing of the thermal gradients north of 43°N in the 17/18 June aircraft data analysis), the satellite imagery did show feature development from 12 to 25 June that was similar to the cold extrusion over the Newfoundland Ridge (Figs. 7 and 9). A satellite-drifter buoy, dropped by the USNS LYNCH on the eastern side of the Newfoundland Ridge feature, followed the thermal gradients northeastward at an average speed of slightly over 100 cm/sec (Fig. 14). North of 43°N, the drifter began to follow a course which outlines the cold water feature over the Seamounts shown in the northern portion of the 25 June satellite image (Fig. 9).

5. New Look Data—May 1979

The second phase of the Grand Banks Experiment--New Look--was made in 1979. This phase was accomplished in two steps--the first during the period 9-19 May; the second from 28 July to 14 August. The instruments used and their platforms are listed in Table A.

During the May survey, only aircraft and satellites were used as data collection platforms. As mentioned in Part I, two ships that were to have participated in the May survey were forced to withdraw. Despite this loss, the May aircraft and satellite data furnished information

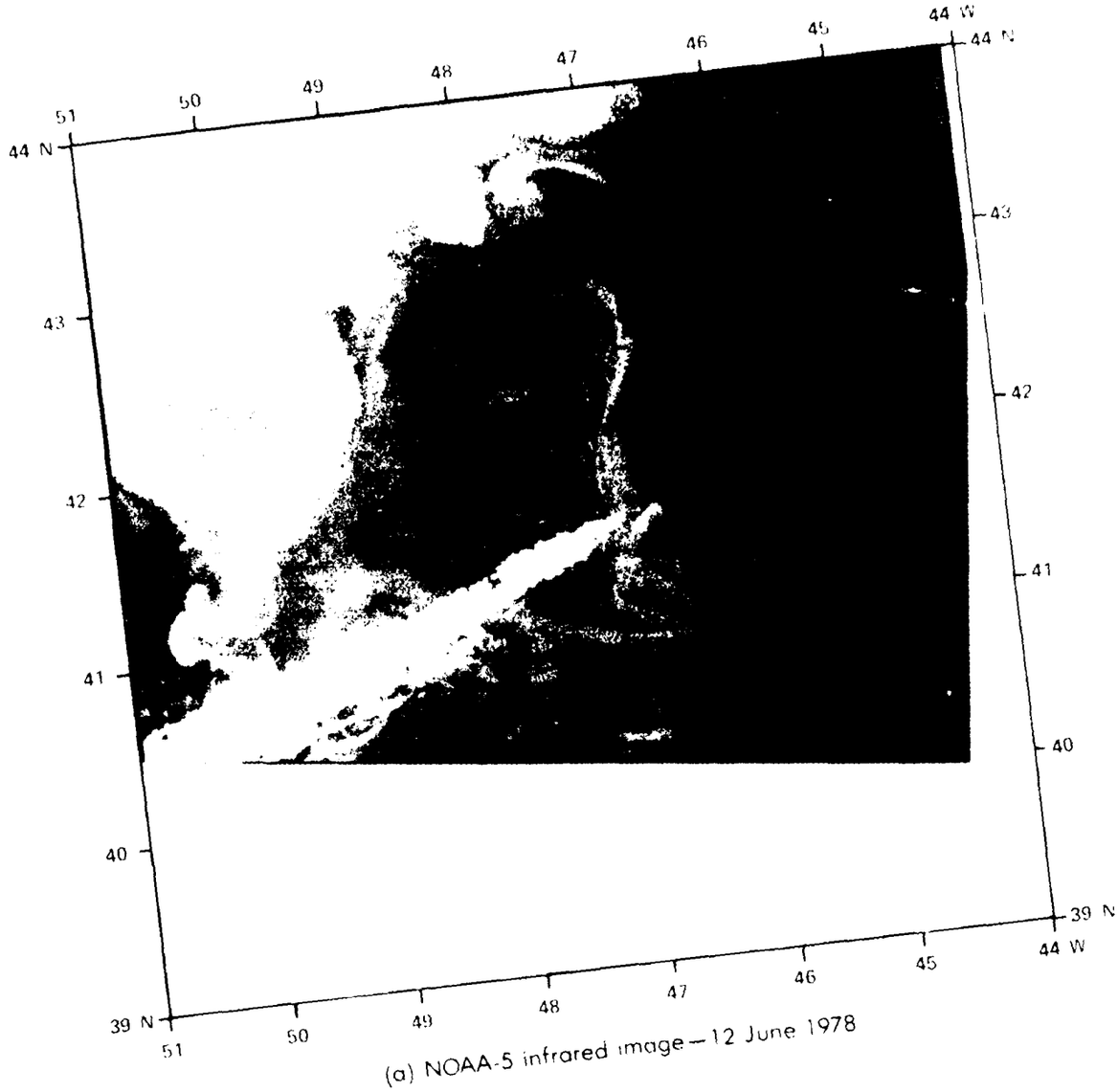

(a) NOAA-5 infrared image—12 June 1978

Figure 7. NOAA 5 infrared image of study area for 12 June 1978 and analyses of aircraft PRT data in °C for 14/15 and 17/18 June 1978. The infrared image is in the original NOAA projection. In the PRT data for 14/15 June, the western side was flown on 17 June. The diagonals in the PRT analyses refer to the drop locations of the ship XBTs, and these data are analyzed in the cross section in Figure 12. (Image enhancement by Canadian Atmospheric Environment Service.)

(b) Aircraft PRT analysis for 14/15 June 1978

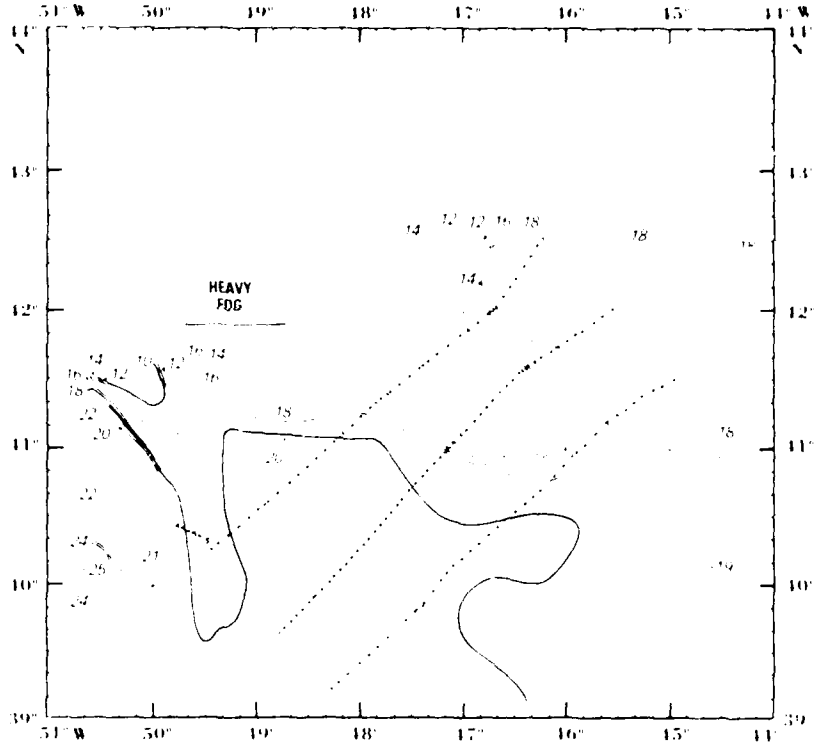

(c) Aircraft PRT analysis for 17/18 June 1978

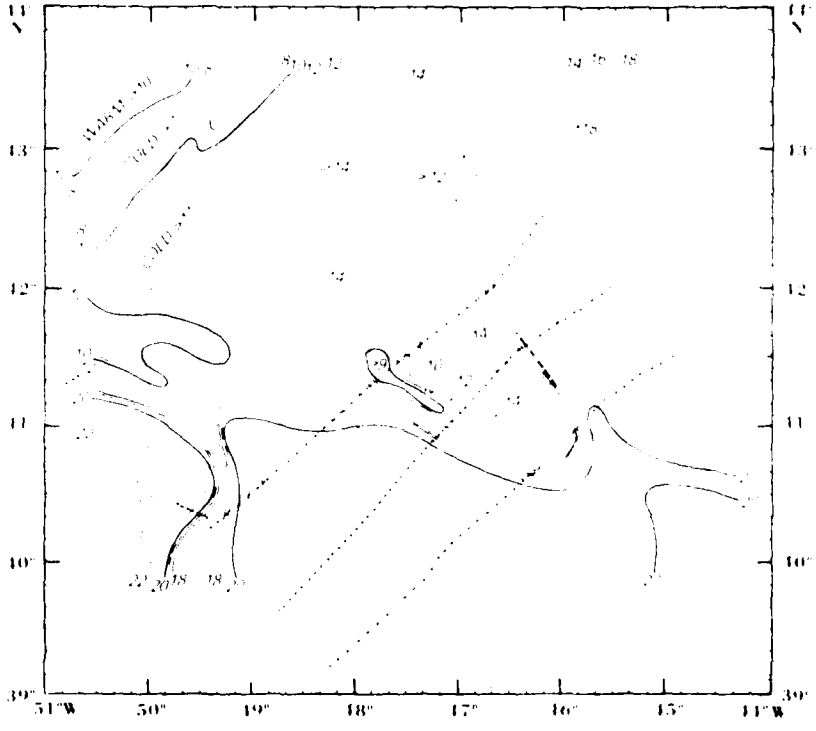

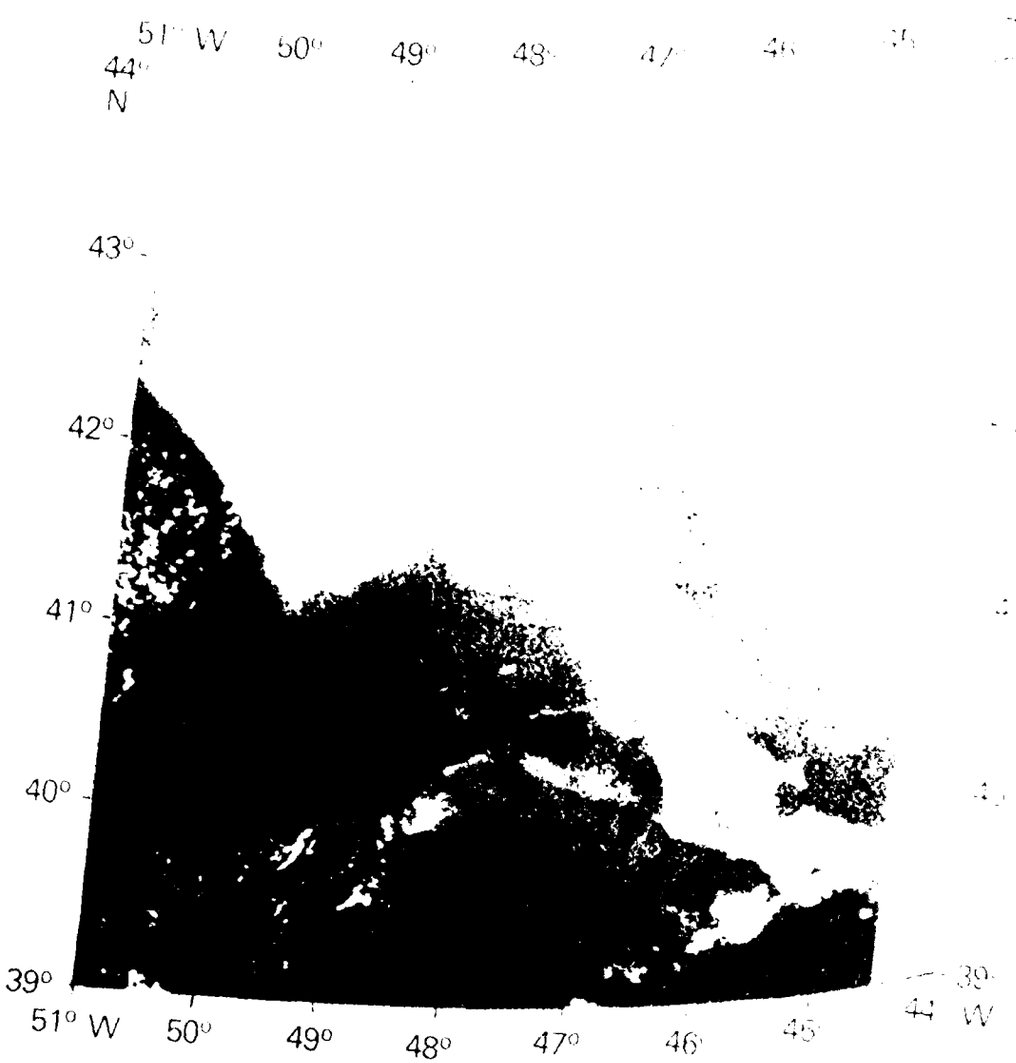

(a) NOAA 5 infrared image—23 June 1978

Figure 8. NOAA 5 infrared image of study area for 23 June 1978 and analyses of aircraft PRT data in °C for 23 June 1978. The infrared image is in the original NOAA projection. The diagonals in the PRT analyses refer to the drop locations of the stars XBTs, and these data are analyzed in the cross section in Figure 1. (Image enhancement by Canadian Atmospheric Environment Service.)

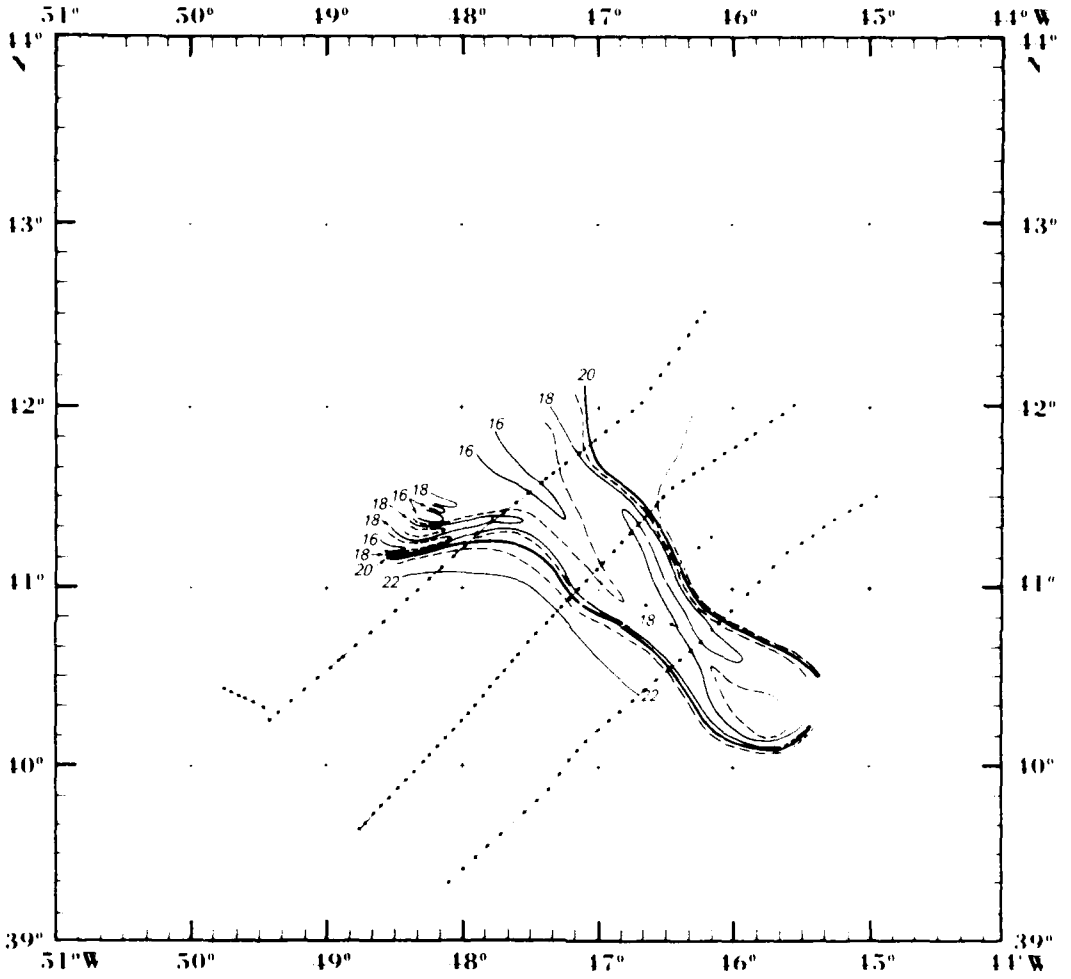

(b) Analysis of PRT data for 23 June 1978

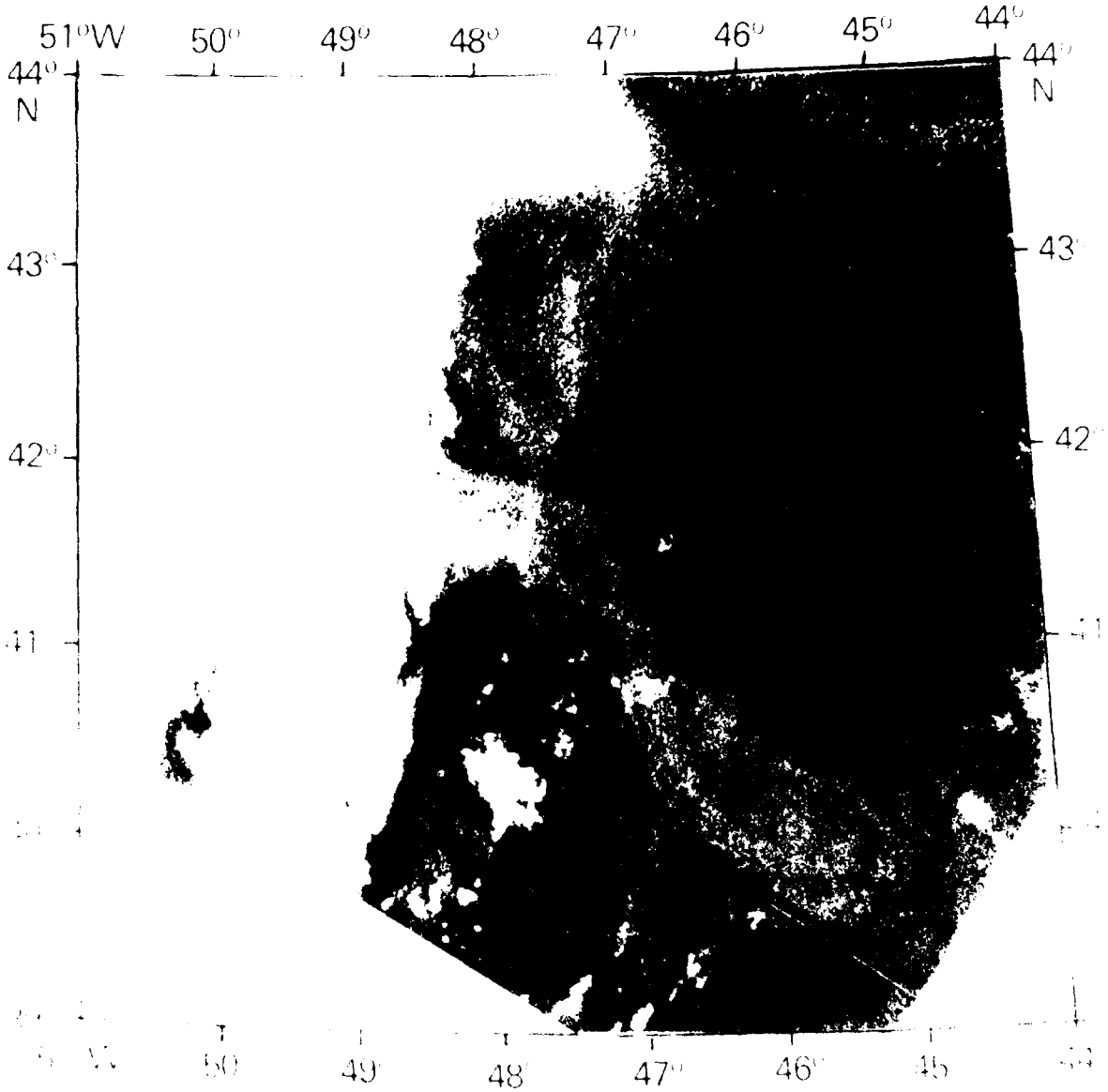

NOAA [illegible] Experiment study area for 25 June [illegible] analysis [illegible] PRT data in °C for 2nd June 1978. The infrared image is [illegible] NOAA [illegible] satellite. The dropsonde in the PRT analysis refer to the [illegible] the ship XBTs, and the dots are analyzed in the cross section in Figure [illegible] enhancement by Canadian Atmospheric Environment Service.)

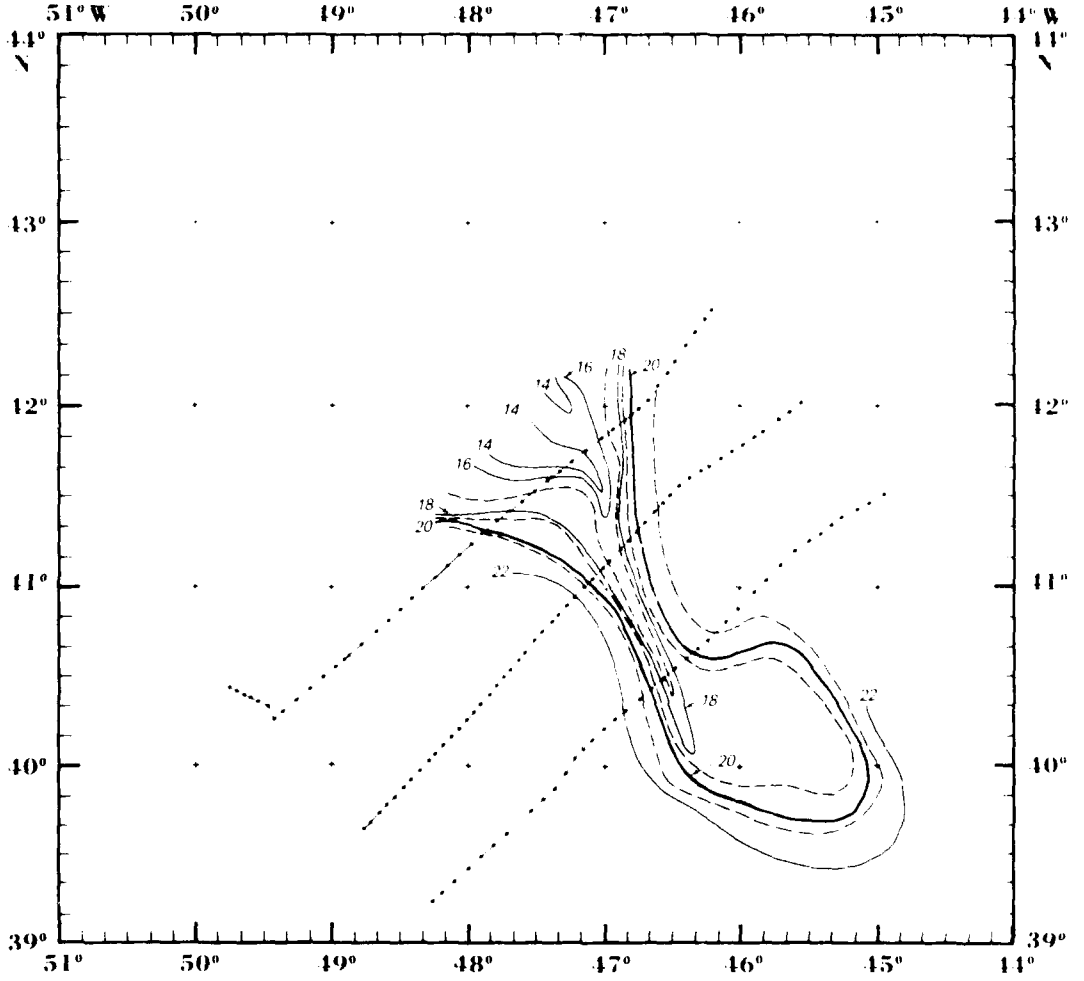

(b) Analysis of PRT data for 27 June 1978

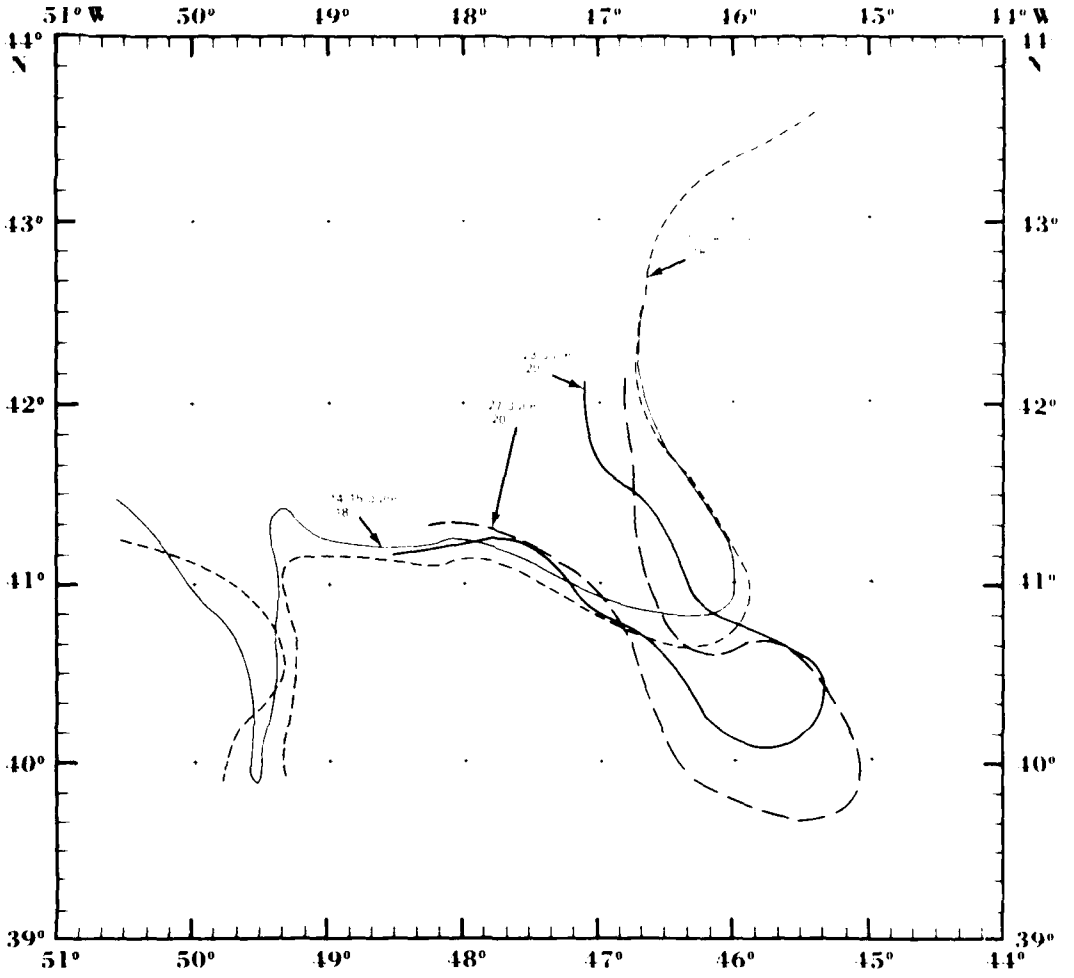

Figure 10. Progression of the extruding cold frontal feature of the Newfoundland Ridge between 14 and 27 June, 1978. Each isoline represents the position of the main thermal gradient for the representative day's flight.

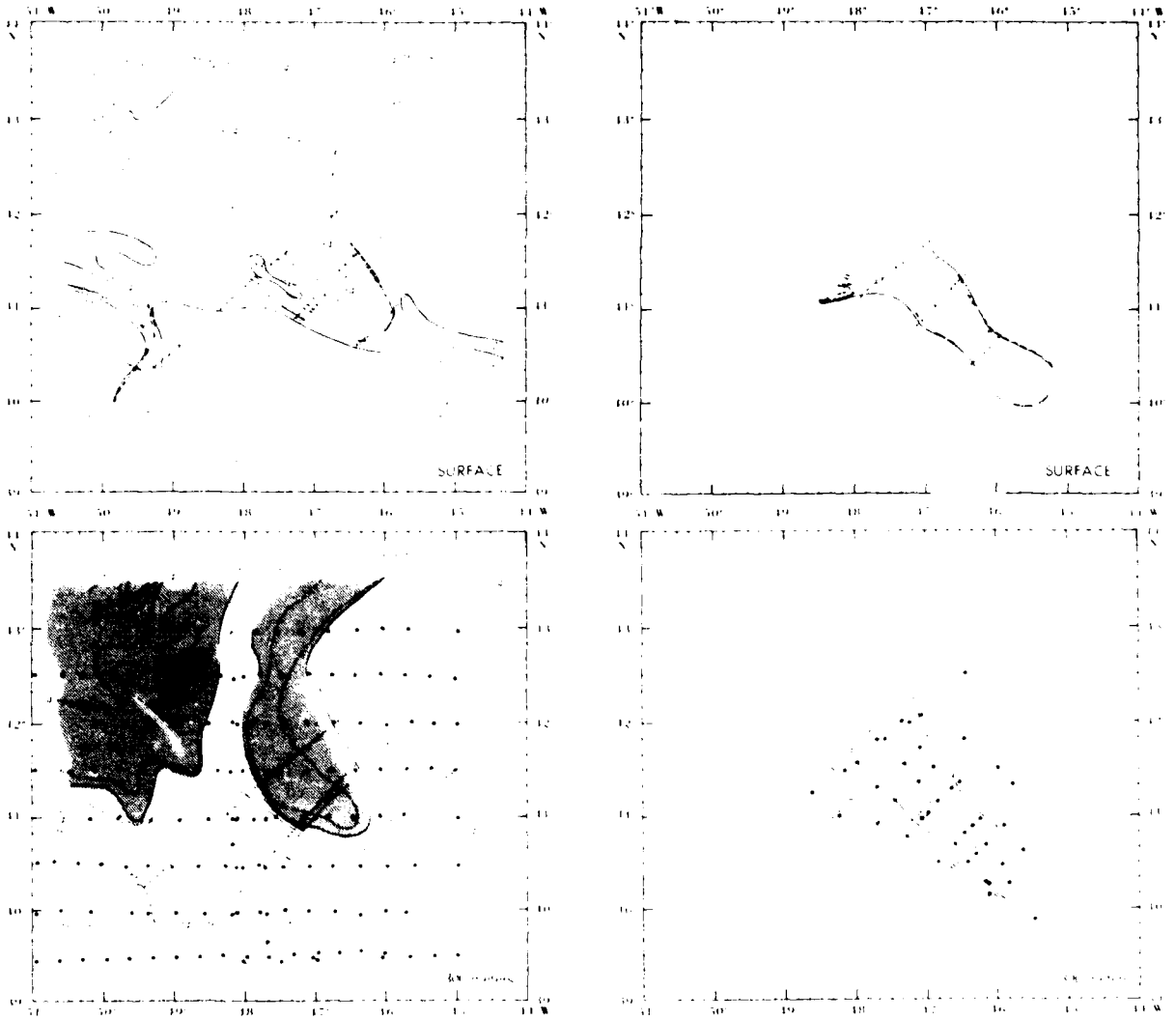

(a) 17/18 June 1978

(b) 23 June 1978

Figure 11. Sea surface and 300 m horizontal temperature analysis in °C derived from PRT and aircraft XBT data for 17/18 and 23 June 1978. The analyses are presented to show the continuity with depth of the cold structure as the structure extruded away from the Labrador Front. The diagonal lines refer to the drop locations of the ship XBTs, and these data are analyzed in the cross sections in Figure 12.

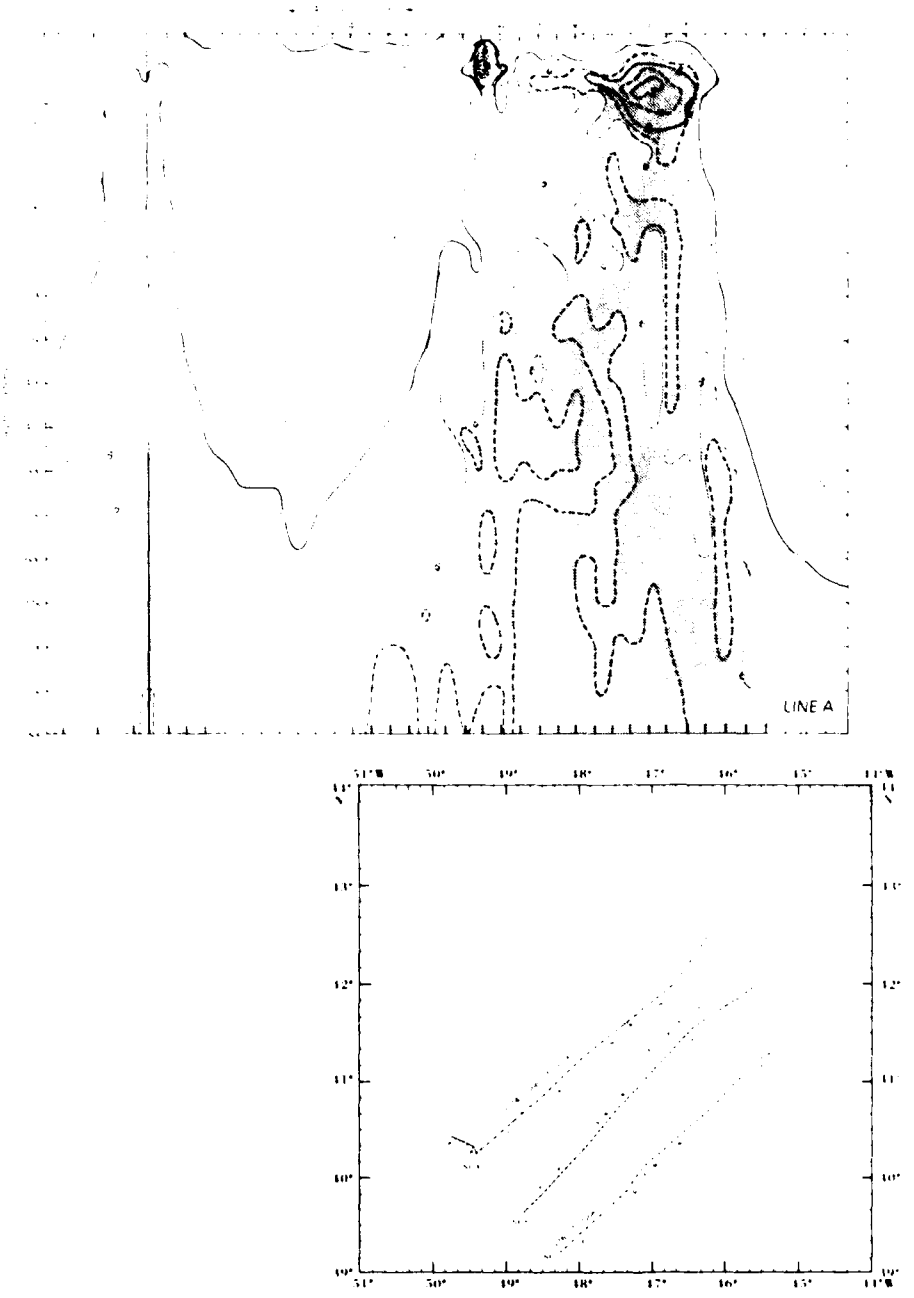

Figure 12. Vertical analyses in °C of ship 750 m XBT data during Baseline. The XBTs were dropped every 1/2 hour. Values at the top analyses refer to the time of the XBT drop in Greenwich Mean Time (GMT) as well as the drop location. The vertical line at 1830 GMT, 14 June, of Line A refers to the change in direction shown in the location chart. The XBT data from 1030 to 1130 GMT, 17 June, of Line C are considered unreliable, and no analysis is presented for that period.

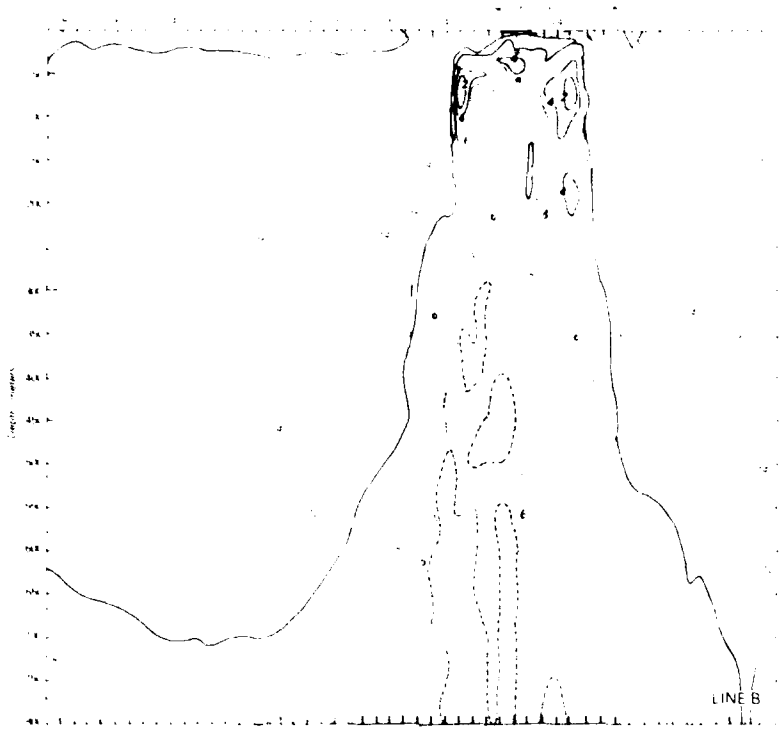
LINE B

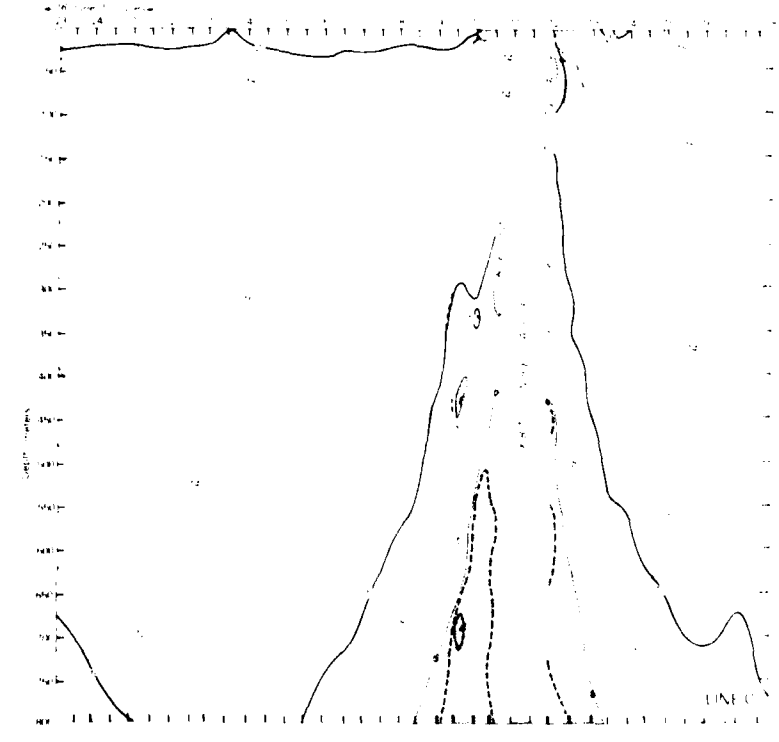

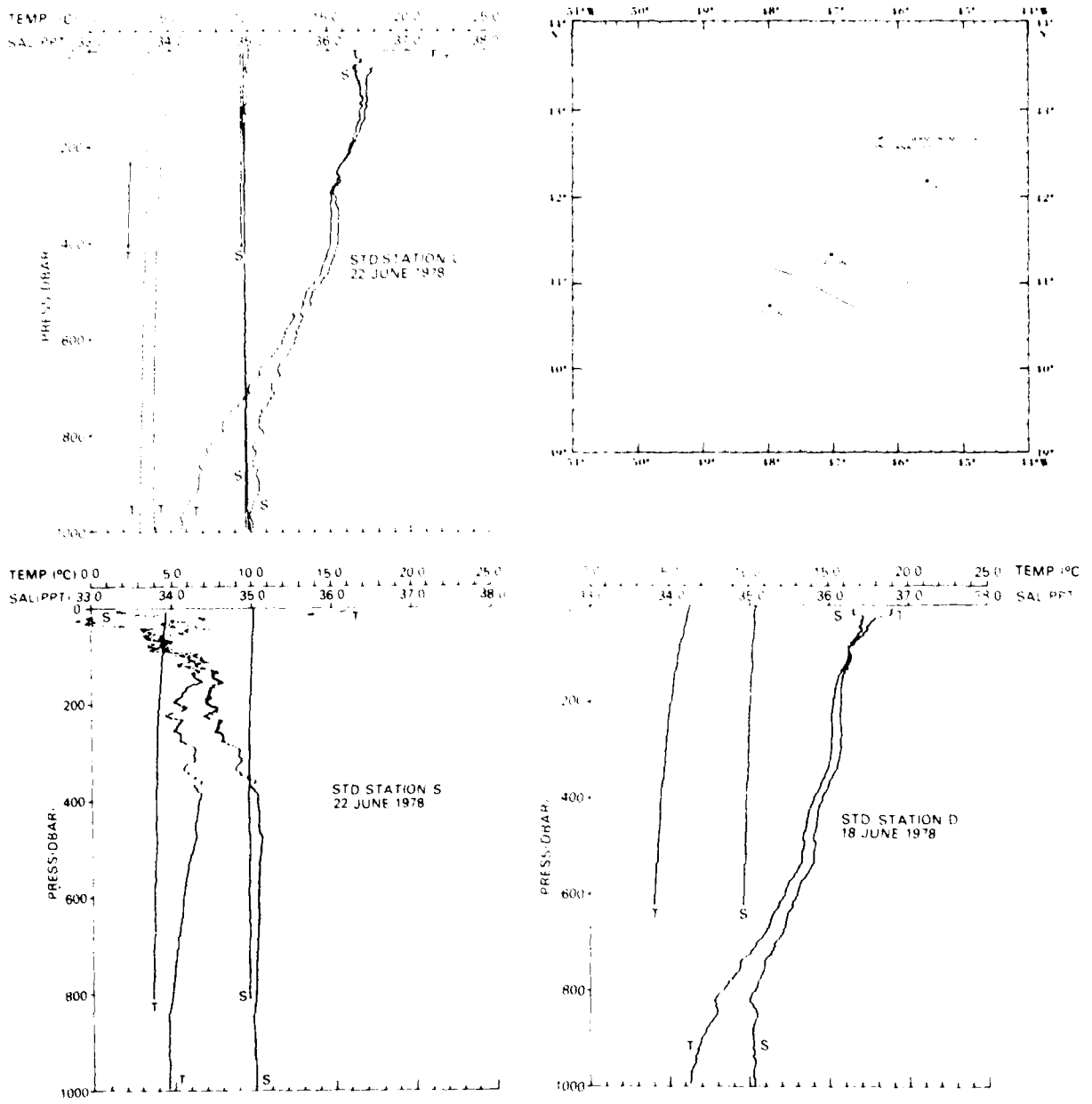

Figure 13. Representative STD station data taken across the Newfoundland Ridge feature during BASELINE. Note that in order to conserve space, the data are folded for values below 1000 decibars.

complementary to that provided by the Baseline data. The satellite data covered the entire area, while the aircraft measurements concentrated on details of the frontal features over the Newfoundland Ridge and the Newfoundland Seamounts. The satellite image for Figure 15 is a good example of the frontal features present in the waters off the study area during May 1979.

The storm that plagued the ships created cloud conditions that covered the area extensively during New Look. However, those satellite imagery clear enough to display ocean thermal gradients show that the Ridge feature did not move appreciably during the survey. A comparison of the 9/10 May aircraft PRT analysis with the 15 May satellite image in Figure 16 verifies that very little southeast extension of the cold feature occurred despite the five-day difference in the data sets.

The aircraft data analyses for the 9/10 May flights proved interesting. Although heavy fog and low clouds prevented collection of surface radiation data by the aircraft along and north of the 42°N track lines, analysis of the subsurface AXBT data shows that the main cold water feature in the area was actually being extended from 49°30'W and that a second feature, very much smaller in comparison, was present at 48°W, 42°45'N.

The TIROS-N data collected during New Look are capable of more accurate registration than the data from NOAA- collected during Baseline (see the Appendix). Thus, the data from this satellite can be rigorously compared with the aircraft survey data analysis.

The horizontal distribution of the smaller ridge feature indicated by the point AXBT measurements of 9/10 May is shown more clearly in the 15 May satellite image. Thus, during New Look, as during Baseline, a bifurcated Newfoundland Ridge feature was present with the eastern member of the bifurcation being comparatively underdeveloped.

Upon examining the satellite and aircraft data in the field, the western member of the ridge feature was deemed the more important structure, and intensive measurements of its surface roughness were planned. On 16 and 17 May intensive frontal surveys were made that cut a 150 km cross section across the cold extrusion. Synoptic measurements involving the temperature, currents, and wave spectra of the ocean and temperature, humidity, and pressure variations in the atmosphere were made along the section. These measurements were designed to show an instantaneous view of the physical conditions in the atmosphere and ocean across the feature. A detailed account of the intensive surveys conducted during these two days is presented in Part III of this study.

On 19 May, an aerial survey was made of the cold water gyre lying over the Newfoundland Seamounts. The feature had been visible in the satellite infrared imagery for several days, but became hidden under clouds two days prior to the flight. The gyre, seen in best detail in the satellite image for 15 May (Fig. 17), extended over an area 200 km on its east-west axis and 100 km on its north-south axis. Analysis of the aircraft XBT data collected during the 19 May flight (Fig. 17) shows surface structure similar to the gyre appearing in the previous day's imagery. The analysis shows that the complexities seen at the surface extended at least to the bottom of the aircraft XBT traces, with strong movement extending through all levels.

6. New Look Data—July and August, 1979

The final portion of the New Look survey took place during July and August 1979. This portion of New Look was designed to show that the cold water feature over the Newfoundland Ridge was present during a period when seasonal high humidity often obscures the region from the view of infrared satellite sensors.

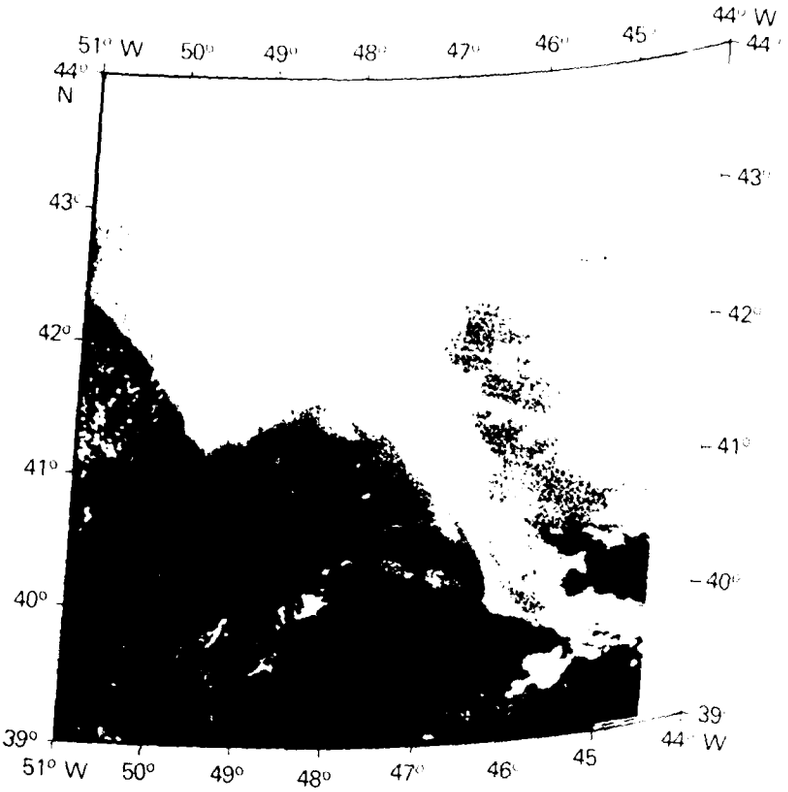
51° W
50°
49°
48°
47°
46°
45°
44° W
44° N
43°
42°
41°
40°
39°

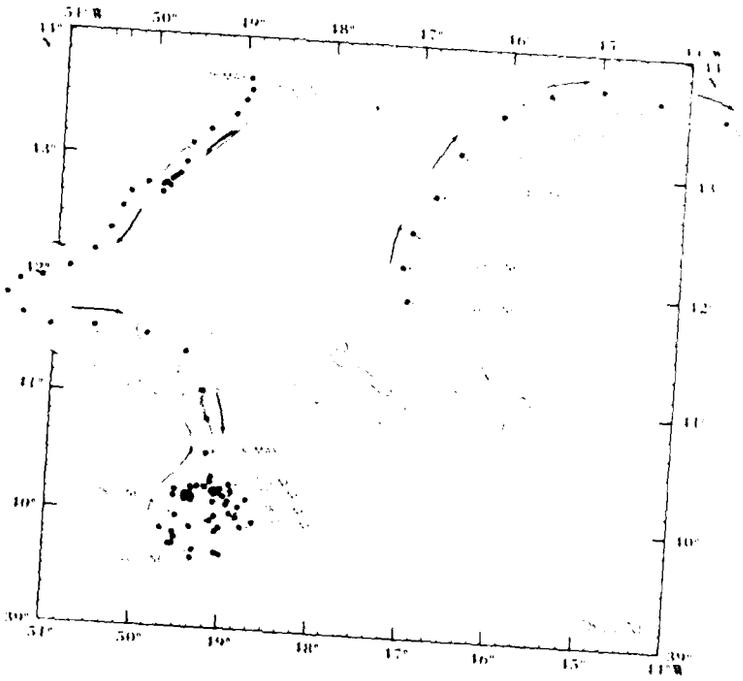

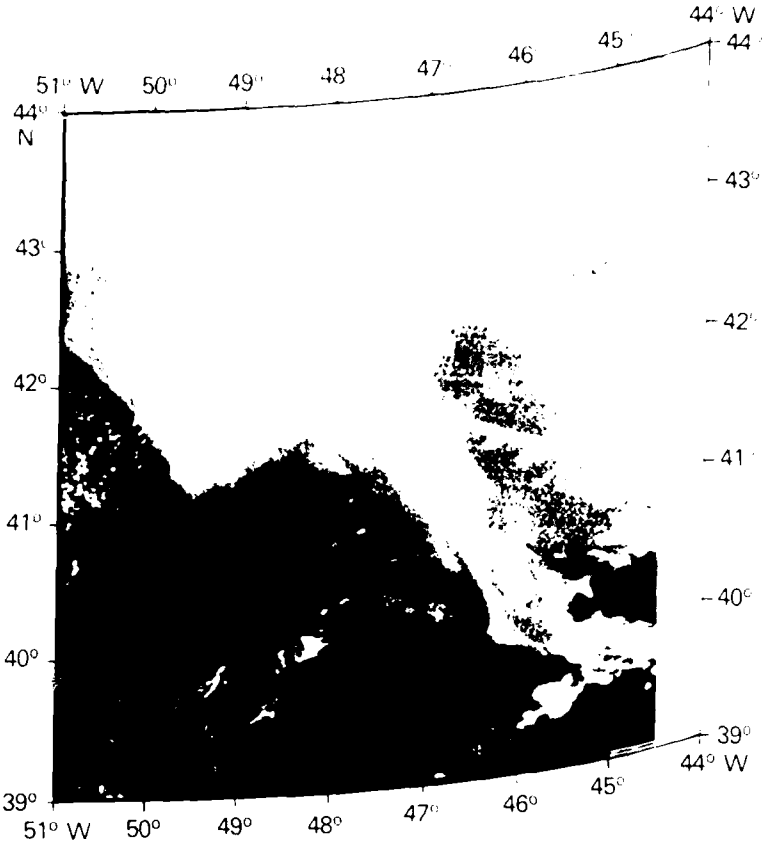
44° W
51° W
50°
49°
48°
47°
46°
45°
44° N
43°
42°
41°
40°
39°

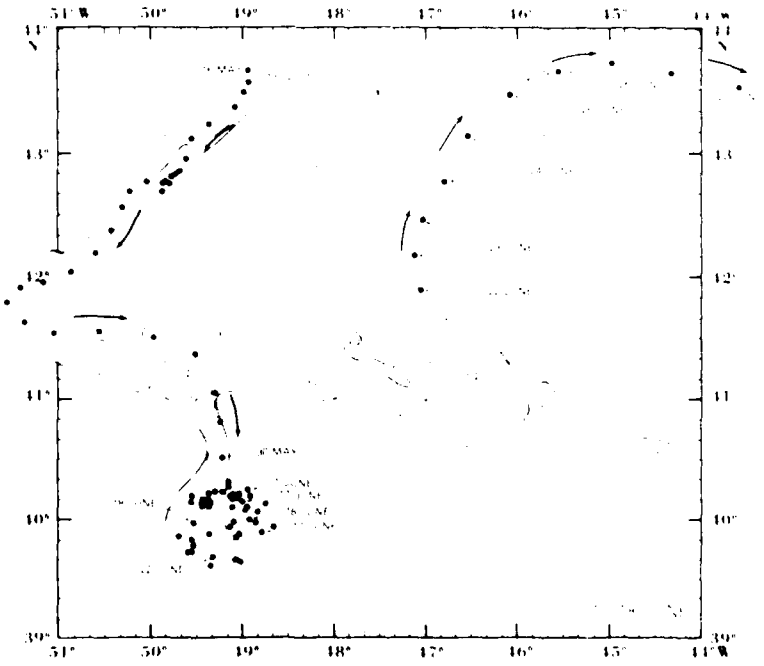

The survey consisted of the USNS LYNCH making 750 m XBT drops while running a diagonal cut across the Newfoundland Ridge and partially over the Newfoundland Seamounts. Two runs were made two weeks apart. Analysis of XBT data obtained from the first run, made 28-31 July (Fig. 18) differs very little from the second run made two weeks later, 11-14 August. Analyses of aircraft PRT and XBT data collected along the same tracklines at the same times produced essentially the same results as the ship data.

Only one satellite image received during the July-August New Look survey was sufficiently low in atmospheric moisture to allow the ocean thermal gradients to be seen in the study region. This image, plus the aircraft and ship data, shows that the Newfoundland Ridge and the Newfoundland Seamounts features were definitely present during the summer months. An examination of the data indicates that the Newfoundland Seamount feature was fully extended, whereas the Newfoundland Ridge feature seems to be withdrawn almost as far to the northwest as the eastern ridge feature in May.

The infrared image also shows a cold feature, partially hidden by clouds, southwest of the ridge feature. From this general location, it may be inferred that this cold feature is similar to the feature found at 49°30'W during May and in the previous year during Baseline. An indication of the subsurface structure of this secondary feature may be seen in the southern portion of the 28-31 July cross section. Unfortunately, time constraints prevented any aircraft investigation of this feature.

7. Discussion

The cold water extrusion over the Newfoundland Ridge lies in the region where Worthington places his "permanent low-pressure trough" and, indeed, a low-pressure trough is seen in the vertical cross sections of a number of past surveys (Worthington, 1962; Mann, 1967; Reininger and Clarke, 1975; and Clarke et al., 1980). During Baseline, the XBTs along Line C in Figure 12 were deliberately dropped along a track near where a line of XBTs were dropped from R/V HUDSON 18 May 1972 (Reininger and Clarke, 1975). The cross sectional analysis of the data from these HUDSON XBTs shown in Figure 19 exhibits essentially the same structure as the analysis of LYNCH XBT data in Line C.

These analyses, as well as other analyses of XBT data showing similar thermal structures over the Newfoundland Ridge, give an initial impression that a low-pressure trough may indeed be a permanent feature. However, one wonders how

Figure 14. Movement of satellite drifter buoys within the Grand Banks Experiment area during Baseline (Richardson, unpublished data, 1980). The western drifter buoy was released by the USCGC EVERGREEN on 13 April; the eastern buoy was released by the USNS LYNCH on 22 June. The dots represent positions at time intervals of approximately twice a day (1200 and 2400 GMT). The 17/18 June PRT analysis is superposed on the draft chart to give perspective to the position of the thermal gradients during a portion of the buoy's movement. NOAA-5 infrared image for 23 June is presented to show the current features in which the drifter buoys were entrained. The newly formed eddy is visible in the image. Note that the image is not the same projection as the drift chart.

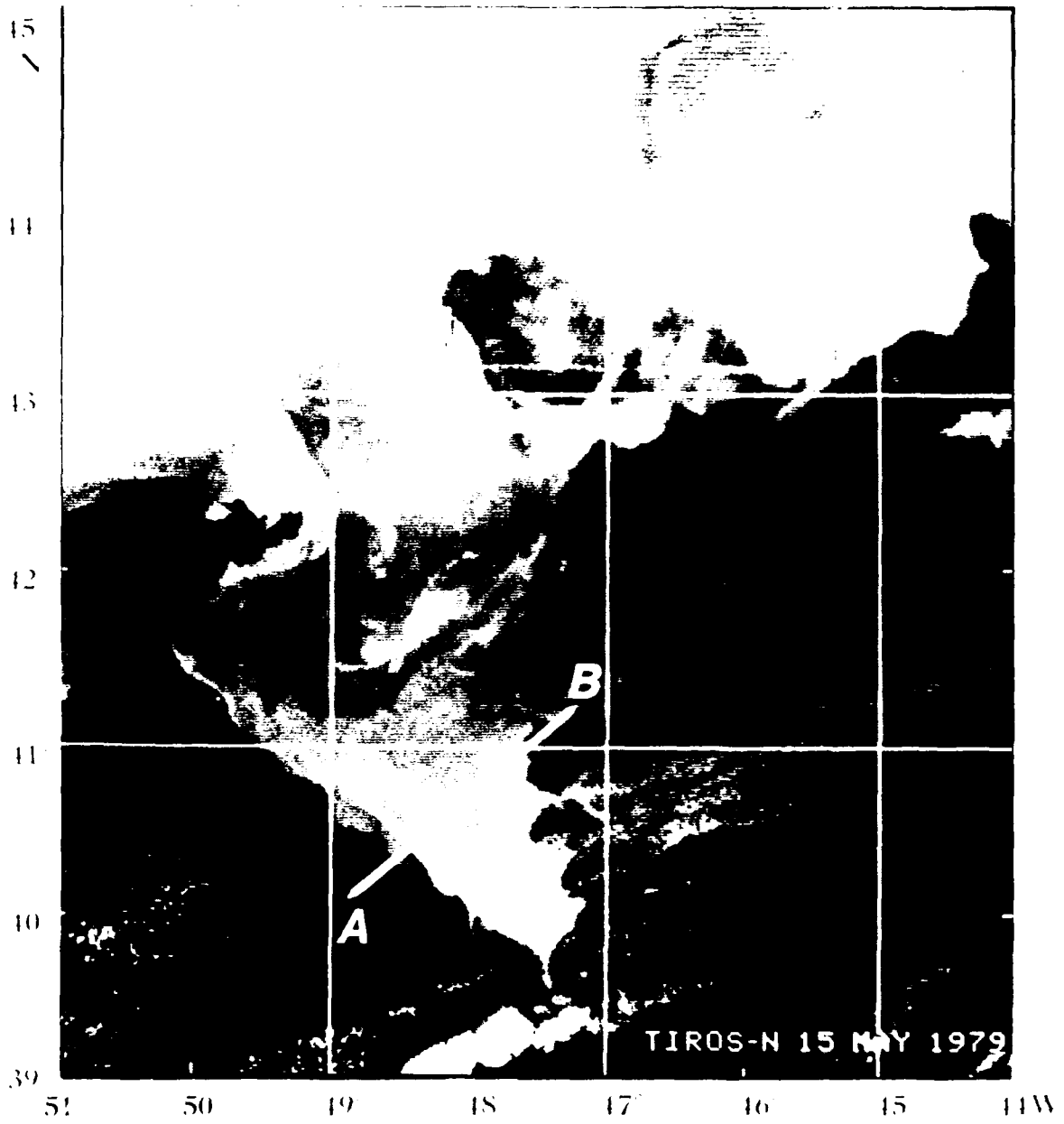

Figure 15. TIROS N infrared image for 15 May 1979 showing thermal extrusions over the Newfoundland Ridge and the Newfoundland Seamounts. TIROS N data, unlike NOAA 4 and 5 data, can be accurately registered and made into projections that correspond to various analytical needs (in this study mercator projections are used). This image has been registered to a mercator grid and digitally enhanced to show various oceanographic features. The dark filament in the enhancement to the right shows a branch of the Gulf Stream going around the Newfoundland Ridge feature. The line A B refers to the region of the profile flights of 16 17 May 1979.

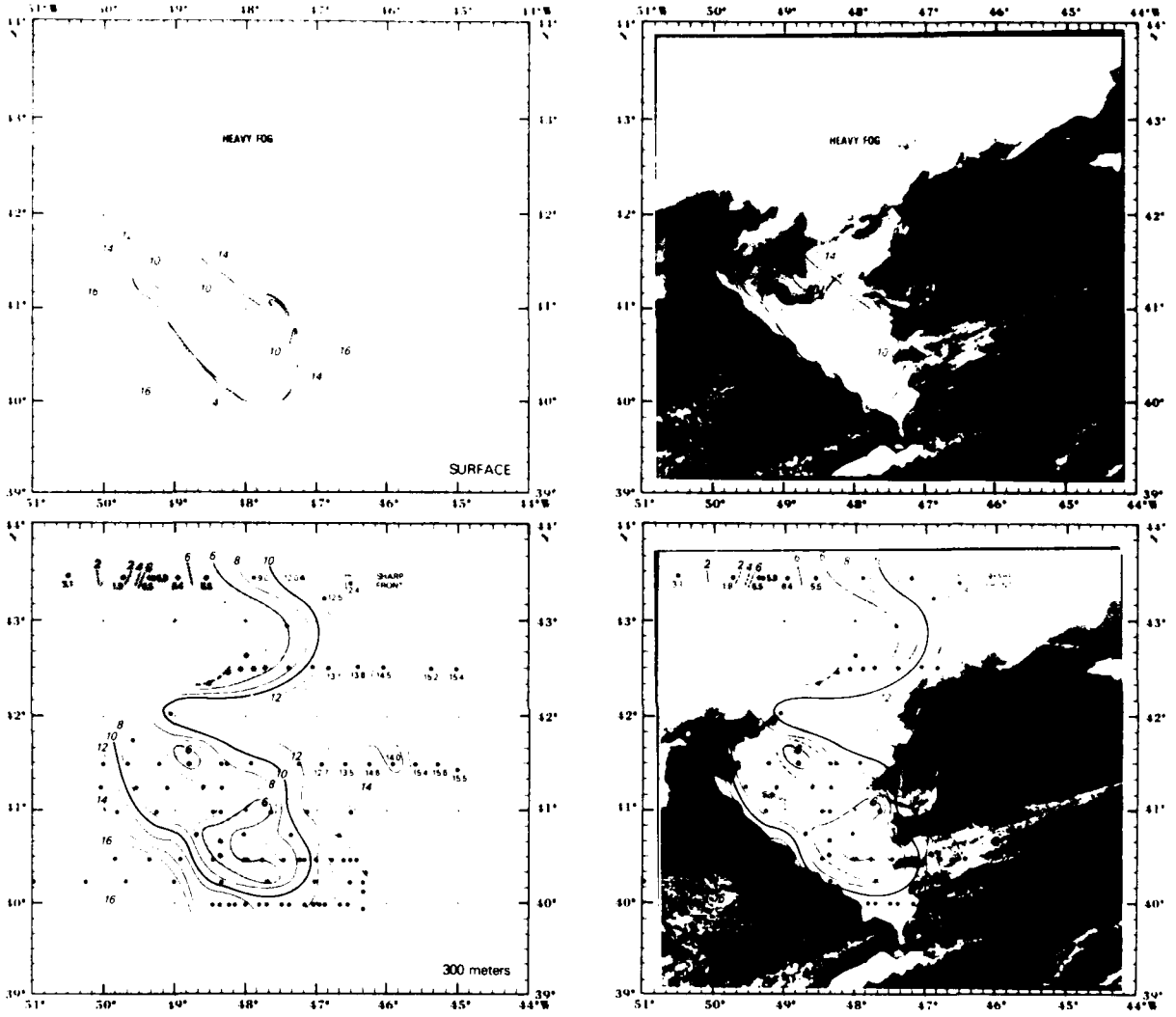

Figure 16. Sea surface and 300 m horizontal temperature analyses in °C of aircraft PRT and XBT data for 9/10 May 1979 compared with 15 May 1979 infrared image. The superposed analyses on the TIROS-N 15 May image show the small amount of movement that had taken place in the five days as well as the continuity of the cold structure with depth.

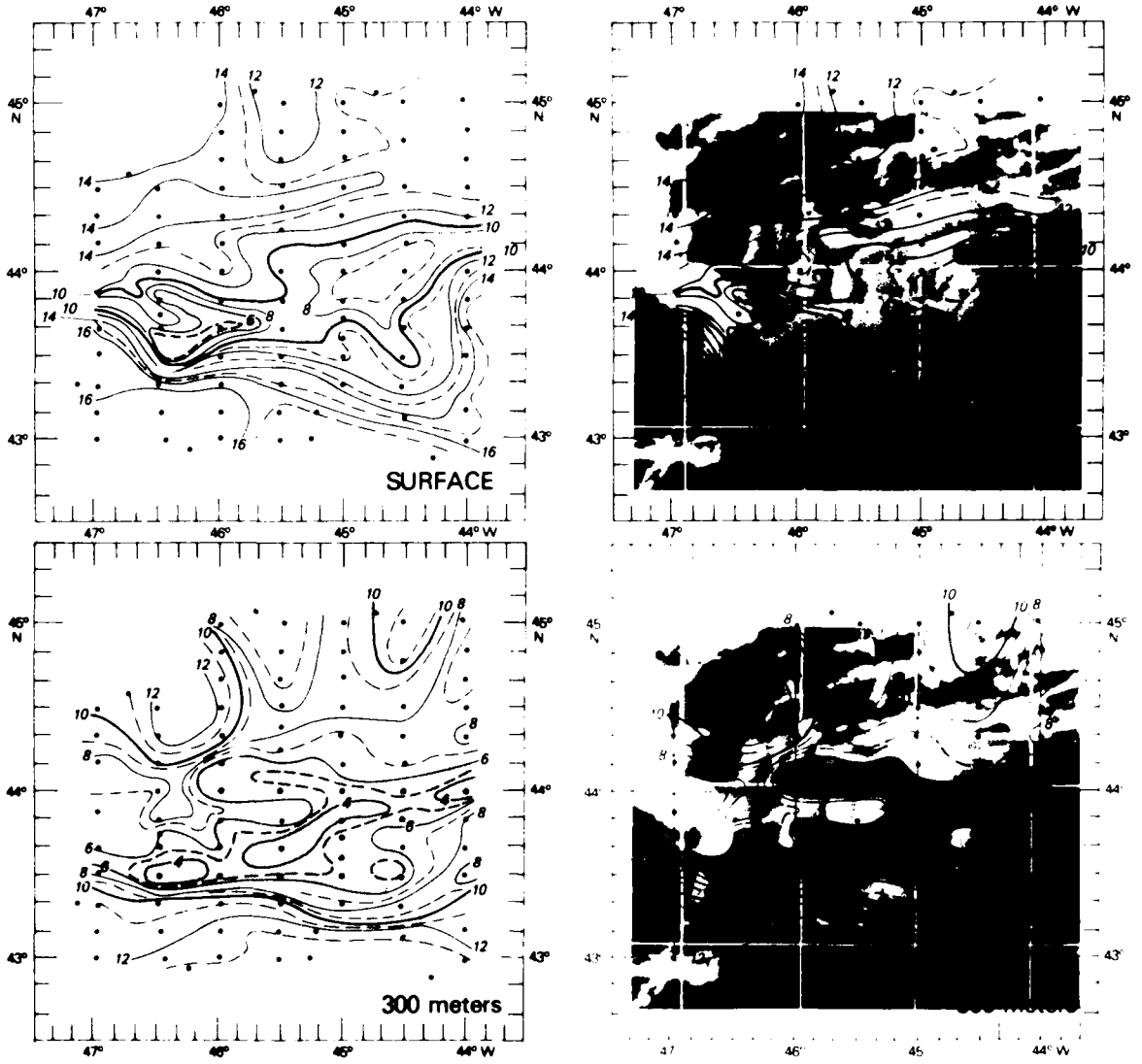

Figure 17. Sea surface and 300 m horizontal temperature analyses in °C (aircraft XBTs only) of the Newfoundland Seamount area for 19 May 1979 compared with a computer composite of satellite infrared data for 13, 14, 15, and 16 June. The superposed analyses on the image are presented to show the continuity of the cold feature with time and depth.

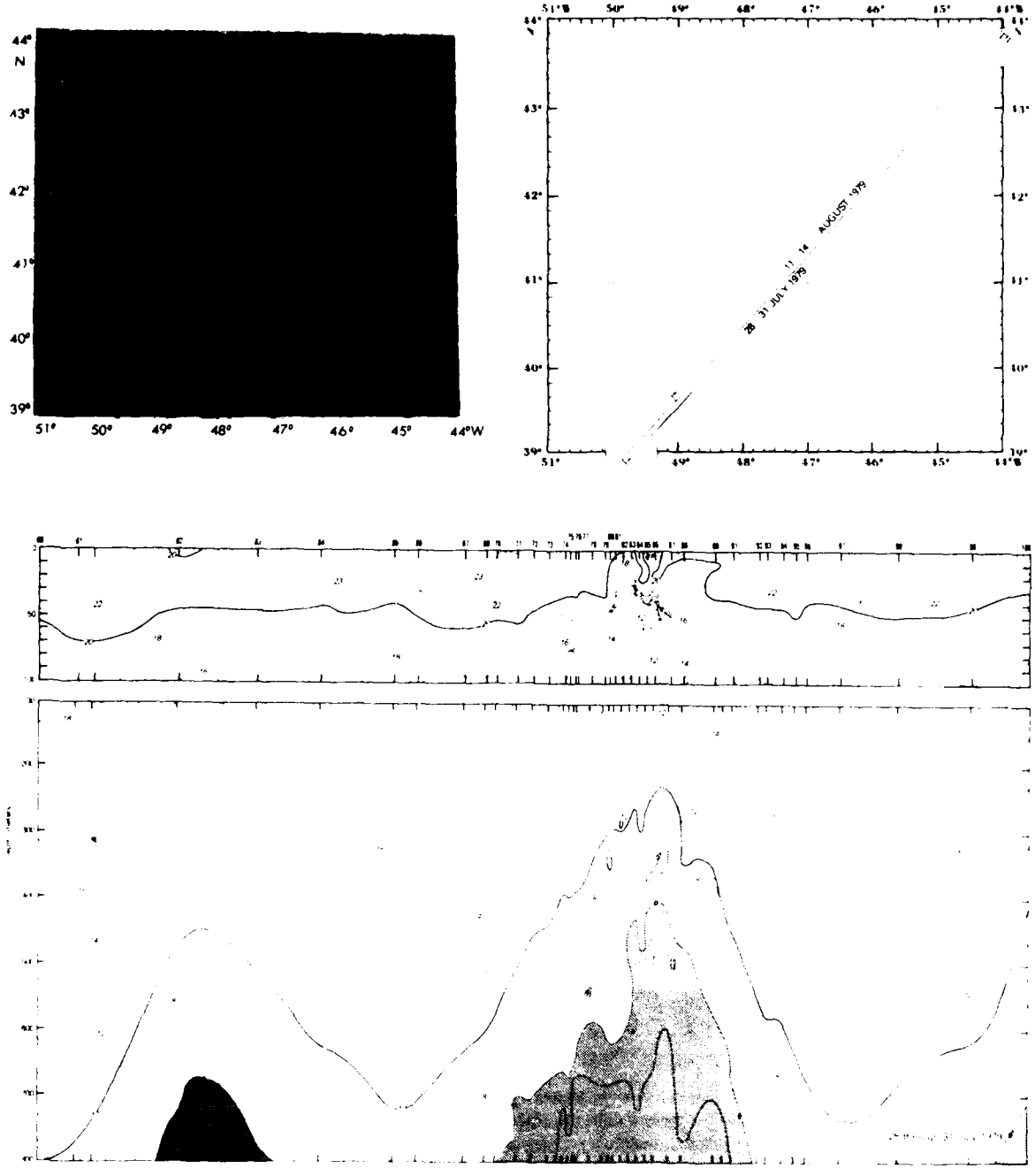

Figure 18. TIROS-N infrared image for 28 July 1979 and vertical analyses in °C of data from ship 750 m XBTs dropped in July 1979. The track of the USNS LYNCH is superposed on the figure to show the relationship of the cross section to the infrared image. In the XBT analysis, the depth scale for the first 100 m is expanded to show the details of this depth interval.

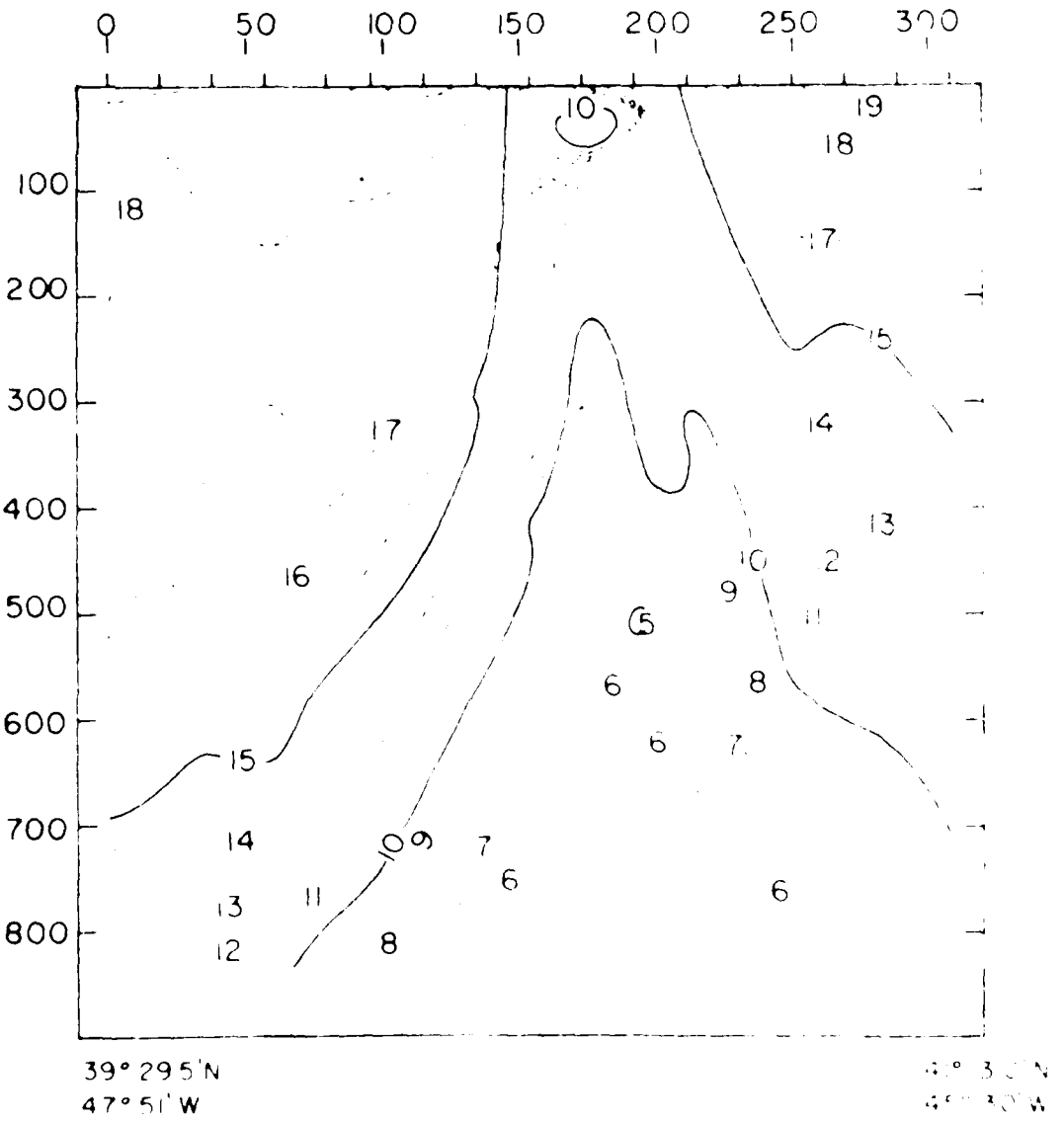

Figure 19. Vertical analysis in °C of R/V HUDSON XBT data for 18 May 1972 (after Reininger and Clarke, 1975). This section is essentially geographically coincident to line C of Figure 12. A comparison of the two cross sections will show them to be grossly the same with the exception of the thermal rise toward the developing eddy in the southern portion of the Baseline section.

the vertical structure would have looked had the LYNCH XBTs been dropped along Line C on 12 June 1978 when the feature was slightly more northwest. Would any evidence of a low-pressure trough have been present? In fact, XBTs dropped along the Line C track during the New Look surveys of May and July/August 1979 would not have revealed a low pressure trough. To even further emphasize the point, if XBTs had been dropped along the same track as Line B of Figure 12 during the July/August survey, analysis would not have shown a cold feature.

If, instead of a "permanent low-pressure trough," an intermittent one is considered, one that is constantly expanding in the form of extrusions and eddies, then the seeming inconsistency of the features being present on one occasion and not on another would be resolved. The analyses of the five years of satellite data and those of the Grand Banks Experiment surveys definitely show that an extensive cold-water feature, intermittently extending from the Labrador Front, is normally formed over the Newfoundland Ridge.

It is interesting to note that only rarely were eddies found in the historical satellite imagery that were not connected to the Labrador Front by thin filaments of cold water. During the survey phases, filaments were found connecting the front with the cold feature at 49°30'W (during Baseline) and the feature over the Newfoundland Seamount (during New Look). Both of these filaments extended below 300 m, with the filament at 49°30'W extending deeper than 800 m. Thus, the eddies found by Mountain and Shuhy (1980) were probably still connected to the Labrador Front by thin cold water filaments, although the filaments may not have been observed because of station spacing. If this is true, then such a filament would block the movement of Gulf Stream water directly across the Ridge between the eddies and the Labrador Front.

Although a cold water feature associated with the Newfoundland Ridge normally exists in some stage of extrusion, its actual position over the ridge varies and, as examination of these data shows, the feature can often be bifurcated rather than singular. Clarke et al. (1980) noticed a similar location disparity when comparing their data analysis on the low-pressure trough to that of Mann (1967). Examination of the five years of satellite imagery shows that the main feature wandered in location between the extreme eastern position shown in Baseline and a point only slightly west of the May 1979 location. This extreme variation appears to occur when the feature exhibits bifurcation.

The cold extrusions over the Newfoundland Seamounts, on the other hand, are found to be always singular in occurrence and to lie directly over their bathymetric counterpart (Fig. 20). The fact that gross fits of this nature are a consistent feature of the water over the Seamounts indicates that the slope of the bottom has a strong control on the surface thermal pattern.

8. Conclusions

The analyses of Grand Banks Experiment aircraft and ship data show that three dynamic frontal structures projected from the Labrador Front during 1978 and 1979: two extensions of cold water generally over the Newfoundland Ridge and a third directly over the Newfoundland Seamounts.

A study of satellite imagery for a five-year period, which includes these surveys, shows that the cold frontal features are always present in some phase of extrusion. Their persistence throughout the year, their extension as deep as 1500 m, and their close alignment with bathymetric features deeper than 4000 m, indicate that they are not minor features caused by the local wind stress on the surface layer, but are major oceanographic features related to the circulation of the entire water column.

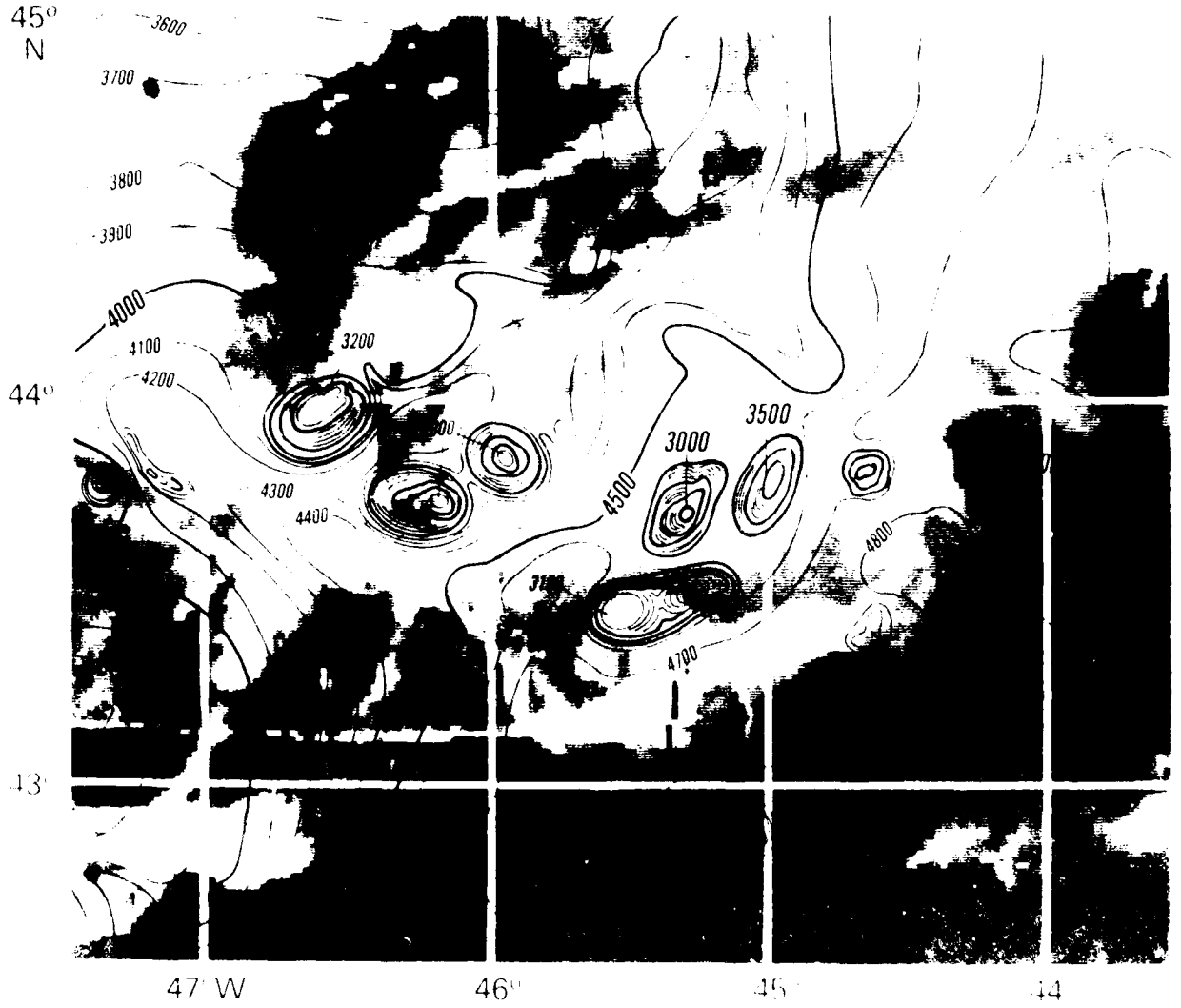

Figure 20. Bathymetric chart of seamounts superposed [illegible] of TIROS N infrared data for 13, 14, [illegible] May 1979. [illegible] dual days also exhibit a good fit with the bathymetry, [illegible] flux and do not individually show the strong control of the bathymetry on the feature movement as well as the composite.

Finally, a comparison of the Baseline and New Look ship and aircraft data analyses with simultaneously collected satellite data shows that the distribution of thermal gradients in the two data sets agree. It may be concluded, therefore, that in this area satellite imagery could be confidently used to monitor the movement of these major frontal features during those times when ship and aircraft data are not available. This conclusion is basic to the hindcast study of SEASAT-A SAR imagery in Part V.

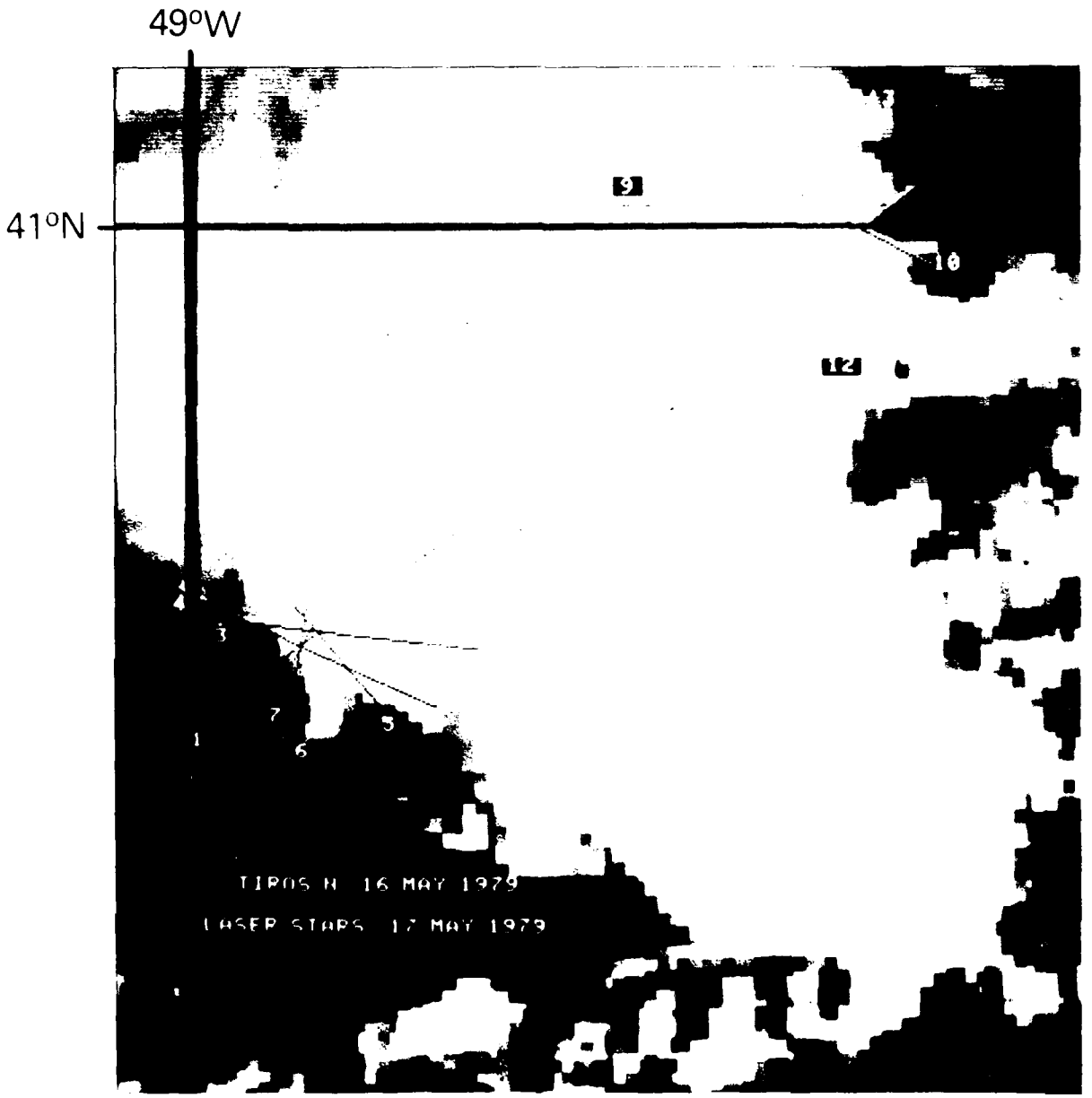

Figure 21. Infrared satellite image for 16 May 1979 superposed with the laser flight patterns for 17 May 1979.

Part III. The New Look Frontal Surveys of 16 and 17 May 1979

1. Introduction

The analyses discussed in Part II established that major cold frontal features are constantly being extruded from the Labrador Front and that under cloud-free conditions, satellite infrared imagery can reliably define these features. This portion of the report will use New Look data from the 16-17 May 1979 aircraft surveys to take a closer look at the cold features lying over the Newfoundland Ridge. Its main purpose is to show that surface roughness within the cold features is different from surface roughness of the surrounding warmer waters. An effort will also be made to identify the processes that created these roughness variations.

The flight patterns needed to make the 16-17 May surveys were quite complex. A description of the 16 May flight as detailed in La Violette (1981a) may be used as an example of how the flights were conducted.

2. The Frontal Surveys

Once the physical boundaries of the Newfoundland Ridge extrusions were established by the broad area surveys of 9-10 May (Fig. 16), two intensive aircraft surveys were planned for a 150 km cut across the tongue of cold water. These surveys were designed to show a synoptic view of the atmosphere and the ocean along the cut at the time of the flights.

Because of the nature of the data being collected, the two surveys required a cloud-free sky and, preferably, different wind conditions. Clear-sky conditions did not occur until 15 May. During the delay, TIROS-N and GOES imagery were continuously monitored to provide weather information and to see if any major oceanographic changes occurred. On 15 May, the satellite imagery showed the weather over the Ridge feature was clear and indicated conditions would remain clear for several days. The imagery also showed that surface thermal patterns over the Ridge feature had not drastically changed during the one-week delay. Based on this information, the cross sectional surveys were conducted 16-17 May.

Only one TIROS-N pass is available for computer registration for the two-day surveys. This is the 0630Z pass 16 May shown in Figure 21. The main line of the two-day survey was made along the line cutting across the cold feature in the figure.

On both days, the Navy P-3 aircraft dropped sonobuoys with approximately 9 km spacing at 15 positions across the front (Fig. 22). The sonobuoys at each drop point had their hydrophones set for a depth of 18 m. The purpose of the drops was to give a close approximation of the speed and direction of the currents across the Ridge feature by measuring the drifts of the various buoys. On 16 May, 2 hrs 20 min after the initial drops, the line was reflown and the drift position of the buoys established by the aircraft's inertial navigation system (INS). The current information derived from this tracking is shown in Figure 22.

On 17 May, the eastern front was found to be displaced 30 km southwest of the 16 May position. Since the western front did not move, the net result was a narrower feature (the reason for this narrowing will be covered in the discussion). The spacing of the drops was shortened accordingly and the sonobuoys released. After a time interval the line was reflown in a manner similar to the

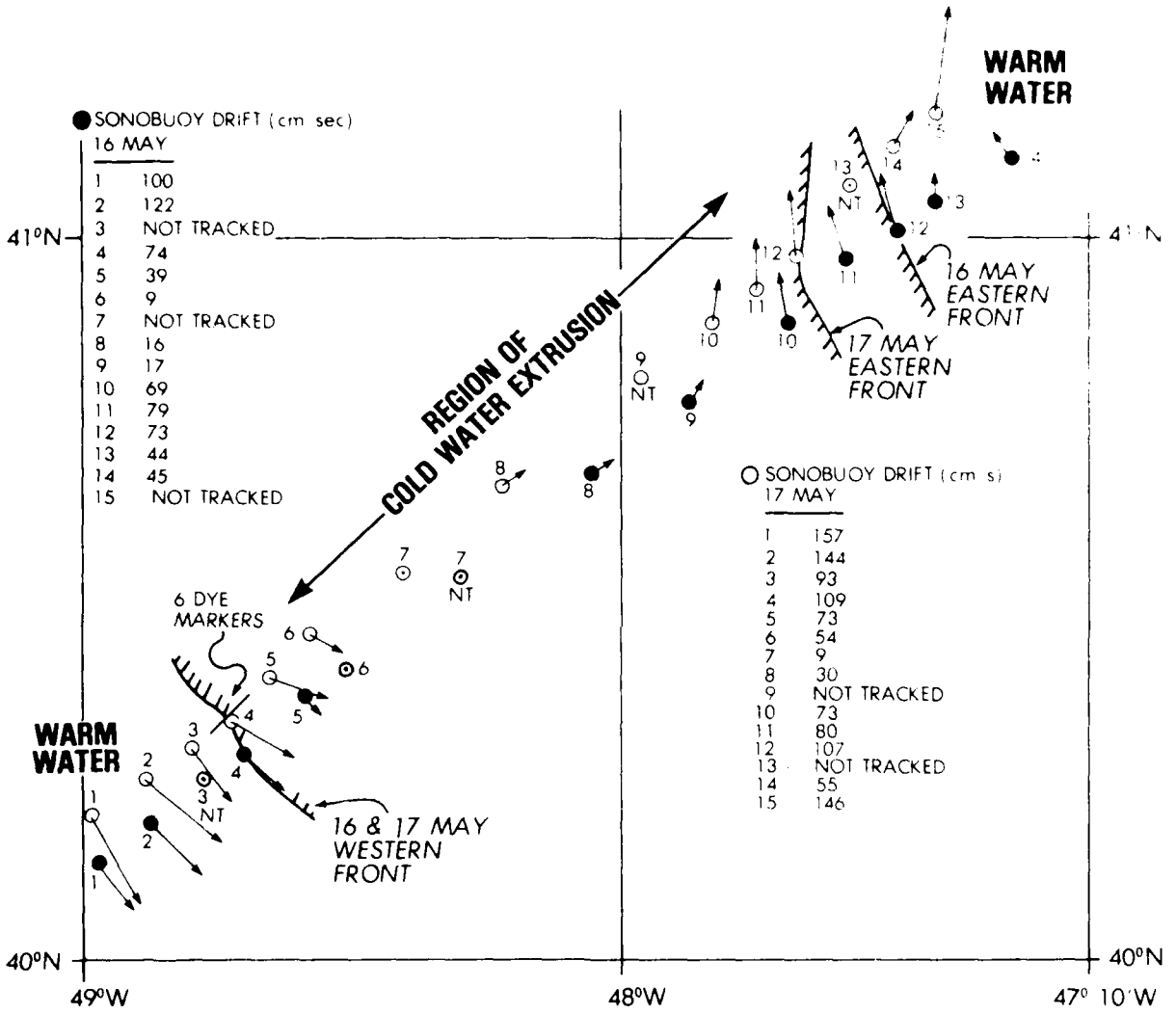

Figure 22. Current speeds and directions derived from 16 and 17 May 1979 sonobuoy data. The tracks for the drop positions correspond to the tracks taken for the data shown in Figures 23 and 24. The drop positions of the dye markers shown between positions 2 and 5 of 16 May are presented in greater detail in Figure 23.

16 May flight. Unfortunately, the initial post-survey analysis showed that the drift rates derived from this data were obviously erroneous. Recalculations of the navigation data indicated that the initial sonobuoy drop positions were in error. Fortunately, a third tracking run had been made. The drift positions of the sonobuoys along this third run appear to be accurate, and it is the drift data from this third track compared to the sonobuoy positions along the second track that were used to calculate the current data presented in Figure 22.

A problem with using the third track positions to calculate drift times rather than initial drop positions is that the times are minimal for the desired results. Also, because the aircraft flew a reverse course on the third tracking run, the drift time for each sonobuoy varies (on 16 May, the drift rate of each buoy was essentially the same). The variation is linear and ranges from 1 hr 2 min at sonobuoy 15 to 2 hrs 7 min at sonobuoy 1. Despite these problems, the current speed and directions derived from the 17 May sonobuoy tracking appear to be similar to those made from 16 May data, and reinforces the belief that the 17 May tracking data are representative of the current conditions.

As part of the 16 May sonobuoy drops, six dye markers were dropped between sonobuoys 3 and 5, with the third dye marker and sonobuoy 4 being dropped together exactly on the thermal border of the western front. The photomosaic of Figure 23 shows their drift positions after 1 hr 10 min.

Although not discernible in the nadir-oriented photographs, the front, lying almost exactly on dye marker 3 and at right angles to the plane's flight, was plainly visible from the aircraft as a definite linear feature in the water. The demarcation may have been caused by organic material contained by convergence along the front. However, from the aircraft the actual reason for the feature could not be determined. The coincidence of the linear feature with the thermal front was noted by the scientific crew of the aircraft by a characteristic sharp change in the aircraft PRT trace.

Although a linear feature defining the western front was visible 16 May, an overall sea state change across the front was not as obvious. However, the aircraft meteorological radar display showed marked changes in the sea clutter that coincided with the location of the thermal front. In the display, a region of greater clutter was shown on the warmer side of the front than on the colder side. It is important to note that during the Baseline and New Look flights, the ocean thermal fronts were almost always visible as sharp changes in the sea clutter on the aircraft meteorological radar. Indeed, on a number of occasions, instrument drops were made on these fronts based on sea clutter variations on the radar display.

Environmental data measured along the cross-sectional tracks are stacked using the same horizontal scale in Figure 24 (16 May) and Figure 25 (17 May). There are two caveats to remember in using these figures. The first is that the 17 May XBTs were not dropped along the same track as other environmental data, but were actually dropped along a parallel line 50 km to the southeast (this is noted in Fig. 25). The cross section is presented in the figure only as an indication of vertical thermal conditions. The second point to remember is that navigation inaccuracies of ±5 km may exist between the position of each pass along the standard track line. This error, created by precessional movement within the aircraft INS, was unavoidable due to the numerous severe turns the aircraft made to collect the necessary data.

INS-derived wind data for 17 May at all altitudes (75 through 3000 m) over the cross-section tracks and for 250 m for the rest of the area are shown in Figure 26.

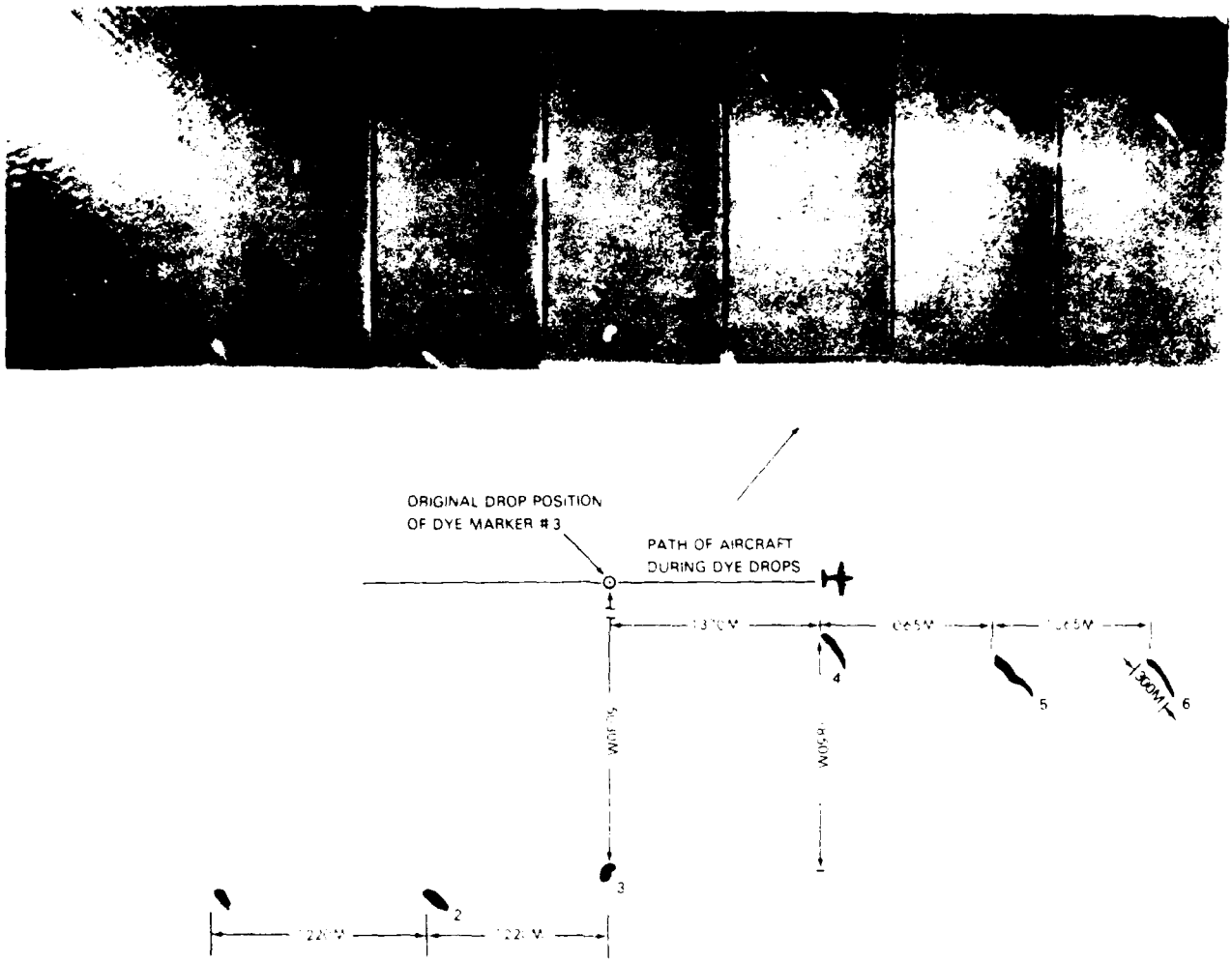

Figure 23. Photographic mosiac of the drift positions of the dye markers dropped on 16 May. The time between the dropping of the dyes and the photographs was one hour and ten minutes. At the time of the drop the winds were from the east at 5 m/sec. The relationship of the dye drop positions to those of the sonobuoys is shown in Figure 21.

On 17 May, the aircraft flew a laser profilometer at 250 m altitude in two star patterns: one over the western front and the other over the eastern front (Fig. 21). The laser data from these star patterns, as well as from transect lines, quantify the variations in surface roughness inside and outside the cold water feature.

3. Discussion

To simplify discussion, this section is divided into three parts: (a) currents and frontal movement, (b) surface winds and sea stress, and (c) sea state. The conclusion section will coalesce the findings of these subsections.

A. Currents and Frontal Movement

Analyses of the 16-17 May sonobuoy data (Fig. 22) show that the cold water moved at a speed of 50-75 cm/sec in the active areas near the fronts and slowed to a null position in the center. These data, as well as measurements of cold water movement in the satellite imagery, indicate that the cold water currents were moving around the Ridge feature counter-clockwise. The currents in the warm water moved approximately 30% faster than the cold water and followed a similar counter-clockwise path around the periphery of the feature. The currents in the warmer water of the western front generally moved faster than those of the eastern front (>100 cm/sec as opposed to >50 cm/sec).

The photographic mosaic of the dyes dropped on 16 May (Fig. 23) show a smaller drift of the dyes on the cold side of the western front as compared with the warm side. Without the mosaic to examine, an analysis of the sonobuoy data in Figure 23 would indicate a gradual change in current speed as the aircraft approached the center of the frontal structure. However, the mosaic suggests that the apparent gradual change in current velocity may be a result of the comparatively wide spacing of the sonobuoys, and that the changes may instead be quite sharp, with zones of fairly uniform velocities lying between the regions of sharp change. No other measurements of shear were taken, although sharp thermal frontal patterns in the satellite infrared imagery suggest that shear zones probably existed within the Ridge feature.

Examination of satellite and aircraft data from 16-17 May, as well as for the rest of the New Look May, and July, and August surveys, indicates that the Ridge feature underwent little extrusive movement during these periods. In comparison, the previous years' data show that the Ridge feature, after being essentially static in position at the start of the Baseline survey, suddenly began extruding to the southeast at a rapid rate (140 km in 7 days). Data from the Baseline satellite-drifter buoy released on 22 June indicate current speeds in excess of 100 cm/sec were present in the cool water inside the eastern front. It is possible that the rapid extrusion after 17 June might have induced these speeds and that the 50 to 75 cm/sec found during New Look are the current speeds that might be normally expected when the feature is not being extruded.

An examination of the five years of satellite imagery shows similar instances of intermittent extension. These imagery indicate that the speed at which the front is extruded varies considerably, sometimes moving in spurts, while at other times moving extremely slowly.

In addition to the short-term sonobuoy measurements, satellite imagery show that frontal shear waves were active on both the western and eastern fronts. These moved at phase speeds of approximately 70 cm/sec, a period of approximately 0.83 days and a wavelength of 50 km. Movement during a 12-hour period is marked by the arrows in the images in Figure 27. A comparison of the speed of the frontal waves with the speed of the currents shows the waves were moving at close to the speed of the cold water currents. The imagery show that rapid

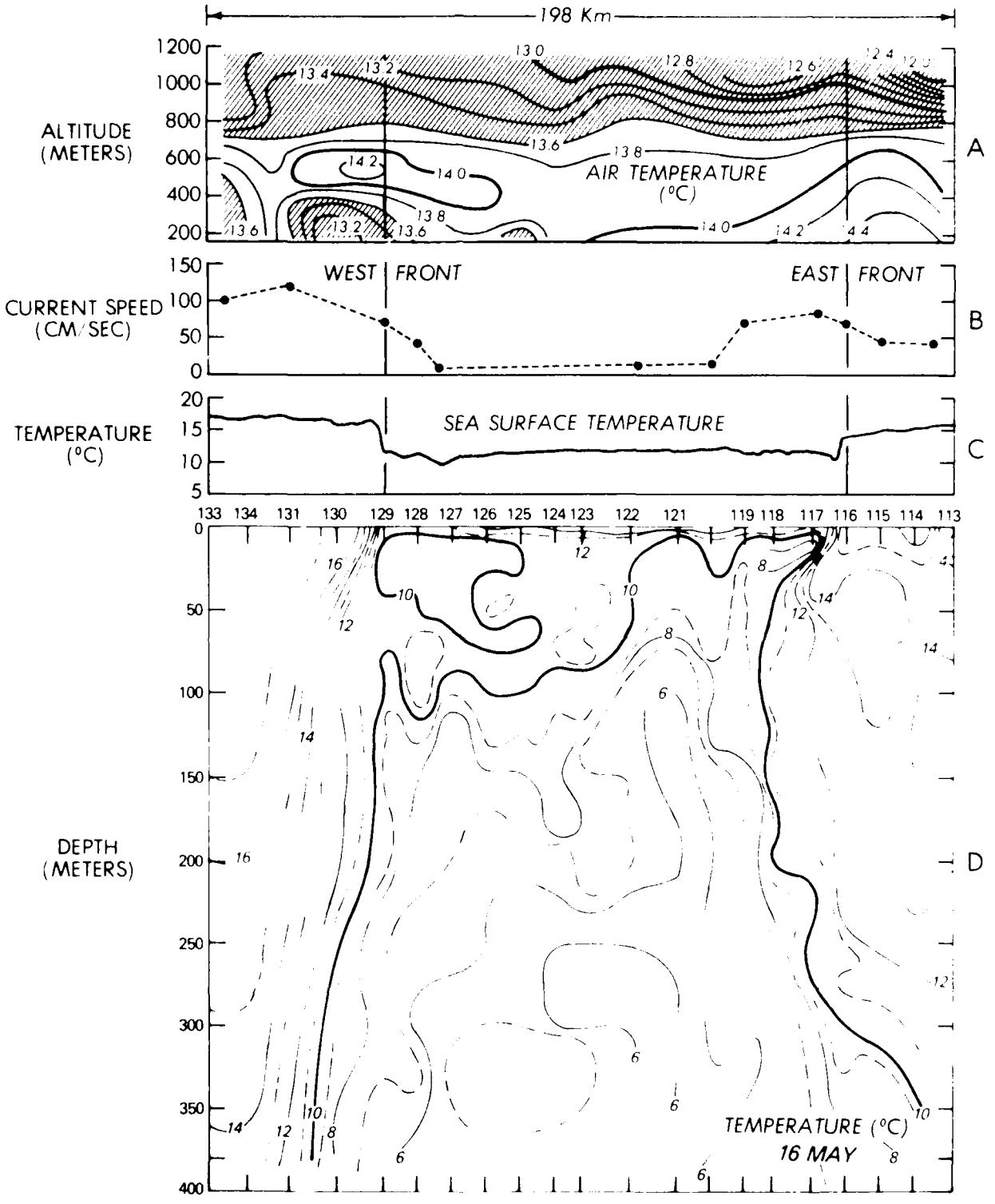

Figure 24. Environmental data for 16 May 1979

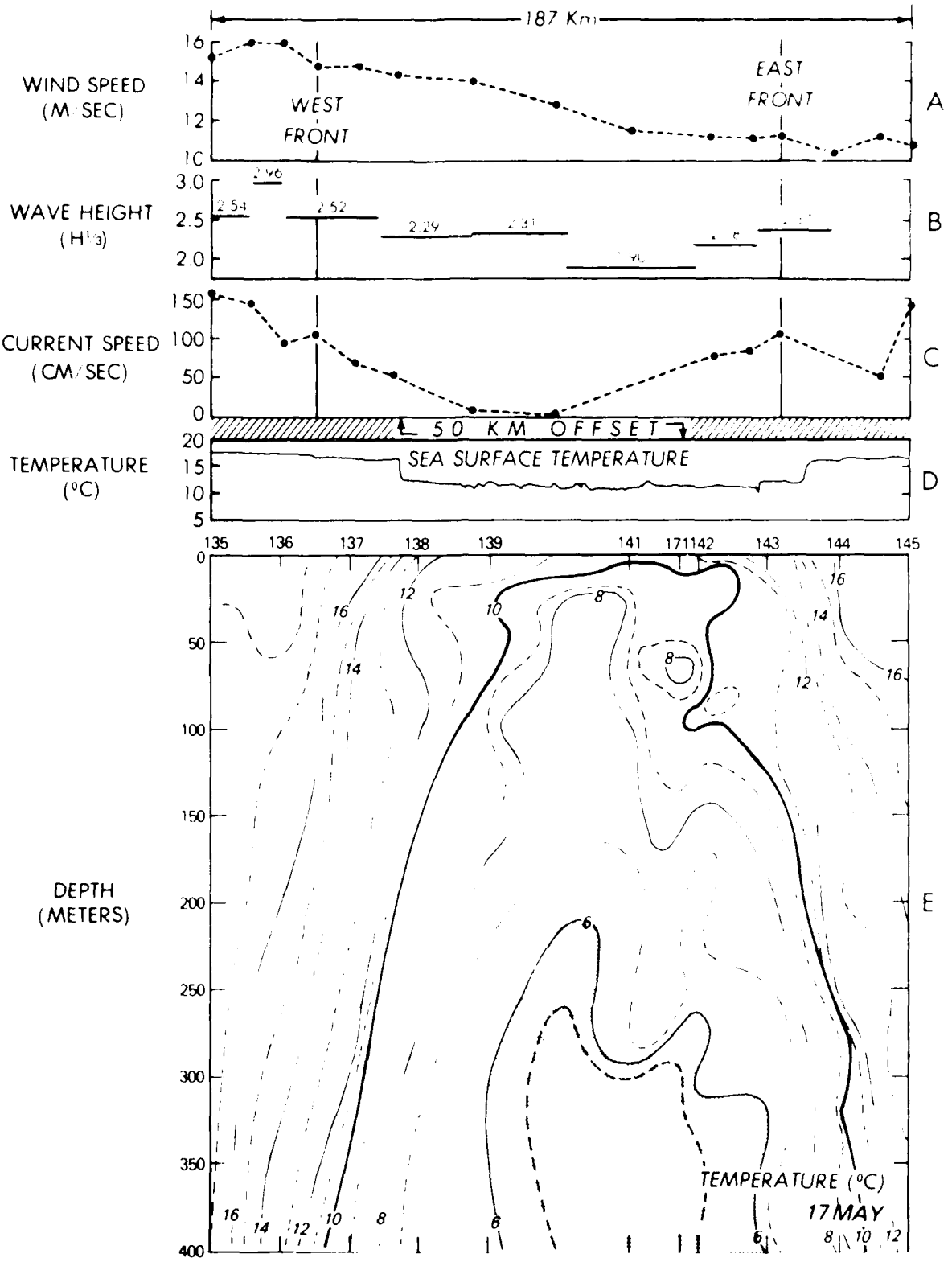

Figure 25. Environmental data for 17 May 1979

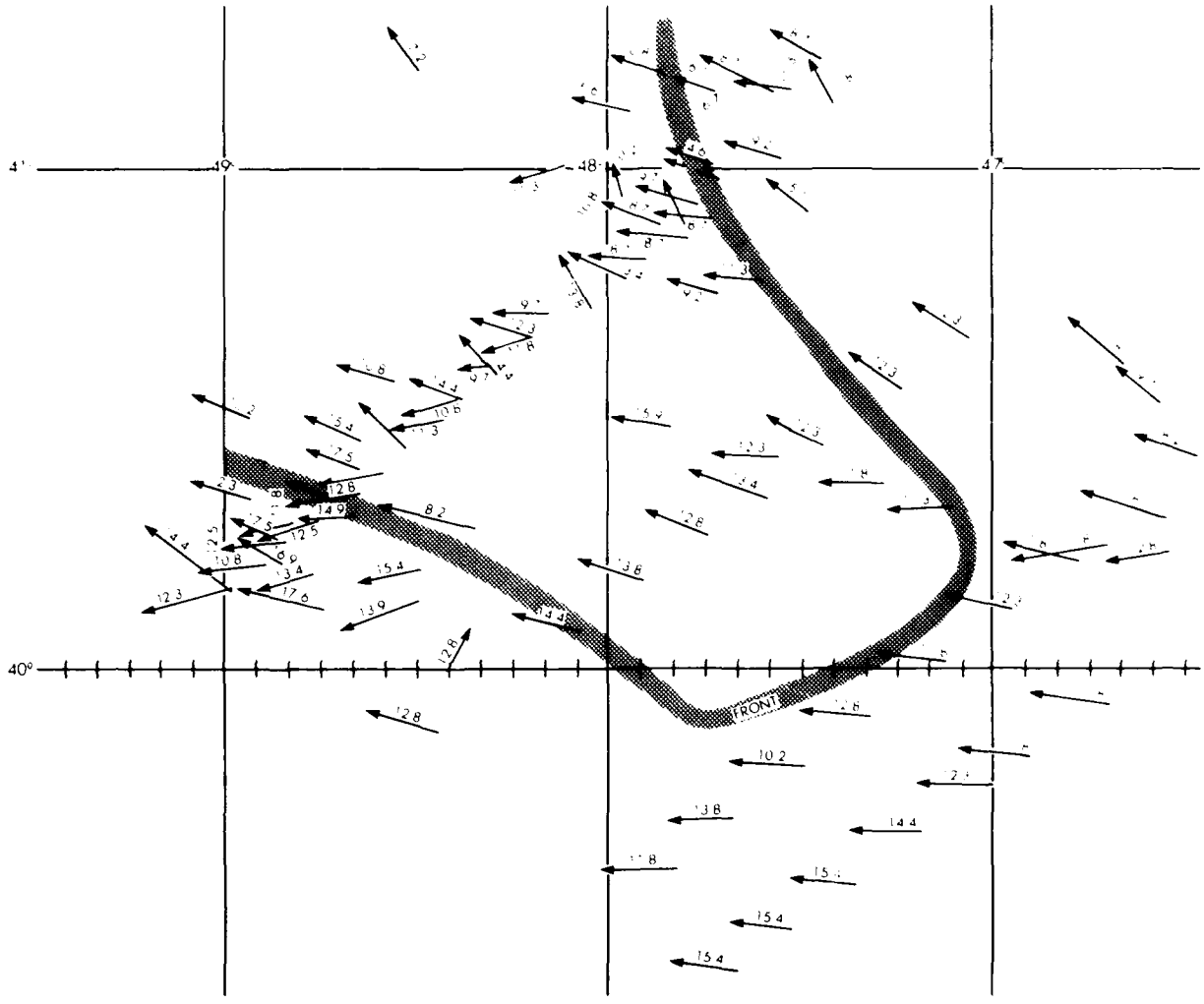

Figure 26. Wind directions and speeds (m/s) for 17 May 1979 derived from aircraft INS data. Values represent data collected for 75 through 300 m altitude over the area of the cross section and 250 m altitude for the rest of the area.

movement within the Ridge feature was also measurable. Tracking the displacement of several cold water features within the feature over several days shows they averaged 70 cm/sec. These displacements are similar to velocities measured during the short-term sonobuoy tracking.

Aircraft XBTs taken on 16-17 May (Figs. 24 and 25) show the vertical profile of the front to be extremely steep, i.e., with essentially no thermocline. This lack of thermocline plus the regularity of the shear waves would seem to indicate two possibilities: one is that wave movement along the front was causing lateral northeast/southwest displacement of the cold frontal edge; the second, and more likely, is that water was being transported in a southeast direction along the front in geostrophic balance with the pressure field across the front and was, therefore, an integral part of the current system.

The sonobuoy data did not show variations in direction that could be attributed to sinusoidal vector components of the frontal waves. The satellite and aircraft data, however, do show that a narrower portion of the Ridge feature was transected 17 May than 16 May. It may be surmised from this information that the trough of an eastern frontal wave had moved into the transect area. Although no satellite data are currently available for 17 May, an examination of the wave movement seen in the previous day's imagery may be used to show which trough may have been responsible for the narrowing of the transect area. This is probably the trough between the two southernmost arrows on the eastern front in Figure 27 and just south of the eastern lasar star in Figure 21.

B. Surface Winds and Wind Stress

As stated in the introduction to Part I, the speed and direction of local surface winds in the regions of an ocean front can be highly variable due to variations in the marine boundary layer. During the 16 crossings of the front made by the LYNCH during the Baseline survey of the previous year, wind speed was reported to increase on 11 occasions when going from the cold to the warm water. The mean increase of these 11 crossings was 34%. On the remaining occasions, the winds were the same across the front. On no occasion was the reverse noticed. Winds were generally 2-8 m/sec and wave conditions were low. (The Baseline meteorological data collected by the LYNCH are presented in detail in Part IV.)

Without the ships, the main source of wind data during the New Look (May) surveys was the aircraft INS. These data indicated that, at the altitude the aircraft was flying, there were no marked changes in horizontal wind speed or direction (Figs. 25 and 26). There were, however, sharp differences in atmospheric turbulence (as defined by INS vertical accelerometer data) as the aircraft crossed both the western and eastern fronts. On 17 May at an altitude of 250 m, the change in atmospheric turbulence was displaced 12 km from the surface location of the western thermal boundary (as marked by a 4°C jog in the PRT trace). It may be surmised that the reason for this displacement is the 10 to 15 m/sec winds from the southeast. What is difficult to determine is whether the atmospheric front extended vertically down to the surface or angled down in an eastward direction toward the surface location of the ocean front.

An examination of the difference in horizontal air temperatures for 16 May at various altitudes also shows the stability of the air column across the feature (Fig. 24). Unfortunately, the INS vertical accelerometer recorder was inoperative on 16 May when air temperature data was available. Perversely, when the INS vertical accelerometer was operative on 17 May, no air temperature data is available, thus the two data sets are not directly comparable. However, the air temperature for 75 m indicates that a westward displacement of the atmospheric front occurred on 16 May similar in extent to that shown by the INS data for 17 May. In addition, air

temperature data show the air over the entire western half of the cold water feature to be cooler than the air over the eastern section. The data show that a maximum change of 1.2°C occurred over the western frontal area while the change over the eastern frontal area was 0.3°C. Examination of the satellite infrared image for 16 May (Fig. 21) shows that within the cold water feature, the water is cooler in the western portion than in the eastern portion.

While not conclusive, data from the INS vertical accelerometer and the 250 m air temperatures indicate that atmospheric turbulence in the region of the western oceanic front was less than over the eastern oceanic front. Also, the generally cooler air over the western half of the cold water feature indicated that more stable atmospheric conditions were present in that region than in the eastern region of the feature.

The INS wind data indicate that while some modifications of wind speed and direction may have been taking place across the front at the surface, the winds at the various altitudes of the aircraft (75 to 3000 m) were generally constant, coming from the east at 5 m/sec on 16 May and increasing to greater than 10 m/sec from the southeast on 17 May. These winds seem reasonable when compared with surface weather charts of the area for 16-17 May. On 16 May, an atmospheric high was extended well over the area with gentle to moderate east to southeasterly winds prevailing. On 17 May, the high retreated to the northeast and the increased gradient flow caused a gradual increase in wind speeds and a shift to southeasterly winds.

The effect of these meteorological conditions on both days was to have a wind regime which reinforced the current on the eastern front and blew against the flow on the western front. Conversely, atmospheric turbulence was less over the cooler water of the western portion of the cold-water feature than over the eastern portion. The effects these conditions had on the sea state are detailed in the next subsection.

C. Sea State

The collection of detailed, synoptic wave data was basic to the success of the study. The proper method of collecting such data posed a difficult problem. During Baseline, a waverider buoy was released from the LYNCH and wave spectra collected across the feature. (These data are discussed in Part IV.) Unfortunately, the spectra from this single source do not give directionality. During New Look (May) an aircraft laser profilometer was included, in addition to the waverider buoy, as part of the wave spectra collection instrumentation. When the New Look (May) research vessels were forced to withdraw from the survey, the laser profilometer became the principal data source of quantitative wave information.

Laser profilometers have been used for wave studies by others (e.g., Ross et al., 1970; Schule et al., 1971; and Liu and Ross, 1980). In most of these studies, the wave fields were dominated by either swell or wind waves, and a single flight track in an appropriate direction was believed to be all that was needed. However, in the region of an ocean front where waves and swells are observed to change direction and where several wave sets can coexist, a single flight track line provides insufficient information for a competent wave study. In the study of these types of seas, a flight plan should be designed to handle not only multiple component seas but also wave refractions due to current gradients. A flight plan with these objectives was developed and used in the present study.

The flight plan consisted of flying the laser profilometer in a star pattern over both the eastern and western sides of the cold extrusion (Figs. 21 and 27). The significant wave height and the skewness values that resulted from the laser profilometer data along each flight track are given in Figure 28. In

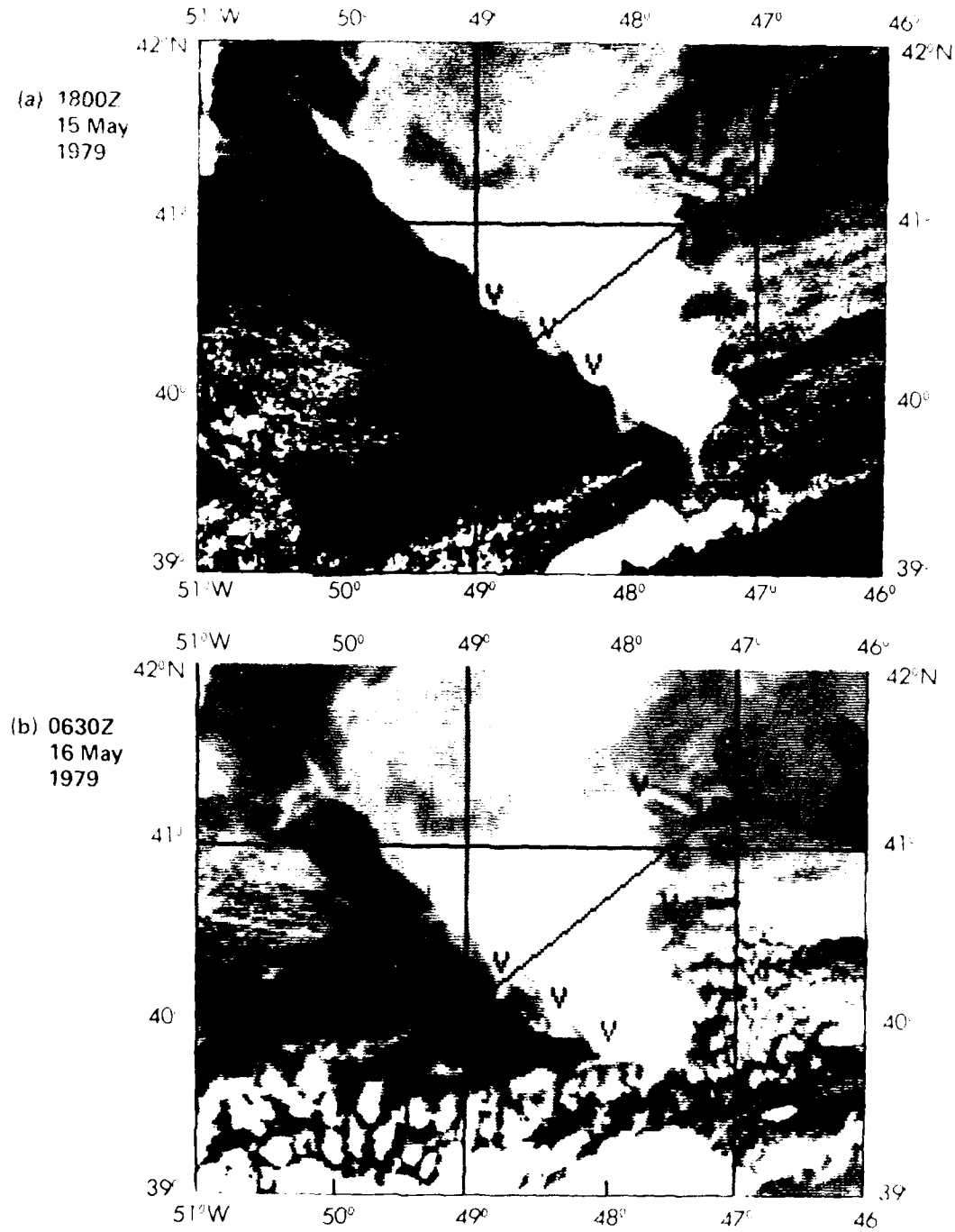

Figure 27. Infrared satellite image showing frontal wave movement for a twelve hour period between 15 and 16 May 1979

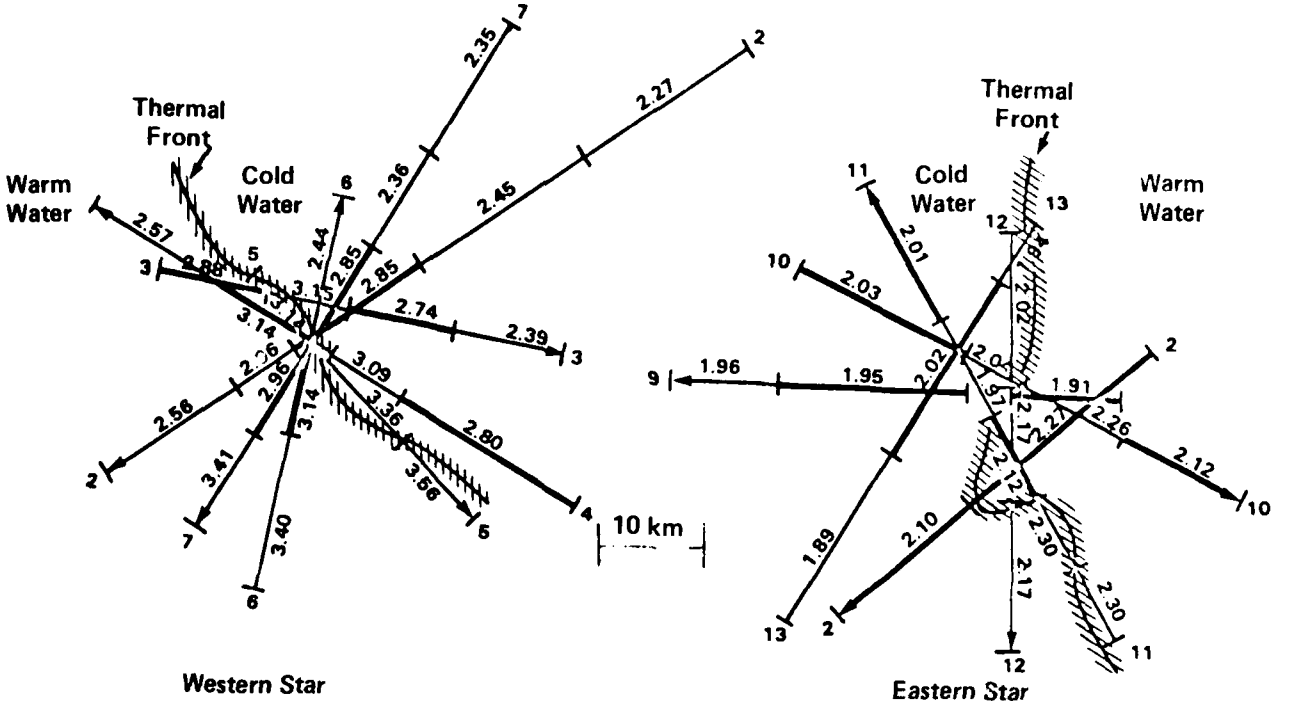

(a) Significant Wave Height (m)

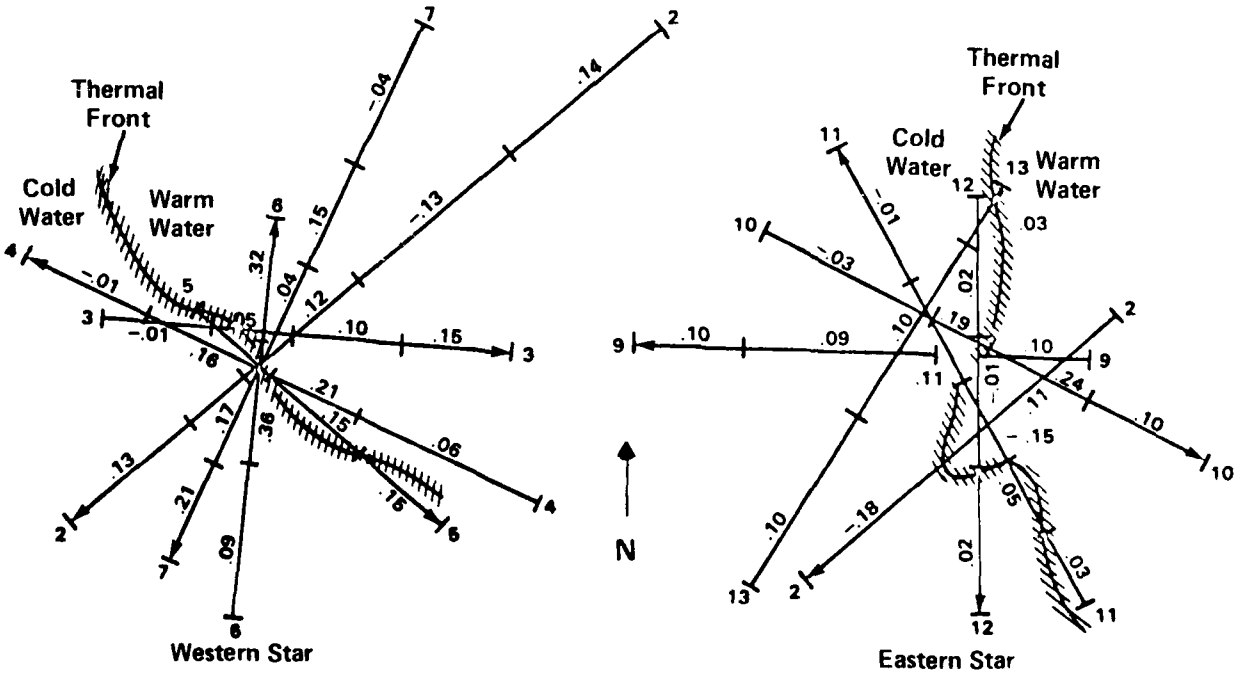

(b) Skewness Coefficient

Figure 28. Significant wave heights and skewness coefficients for 17 May 1979 derived from laser profilometer data (after McClain, et al., 1982).

Table B. Summary of wave systems data (after McClain et al., 1982)

Pattern	Wind Waves		Swell		
	Length (meters)	Direction (degrees)	Length (meters)	Direction (degrees)	INS Wind (Hdg/Spd) °/m/sec
Eastern Star (Warm Side)	160	291	205	244	285/8.5
Eastern Star (Cold Side)	135	281	188	232	265/10
Western Star (Cold Side)	157	270	180	208	259/12.5
Western Star (Warm Side)	111	255	205	232	263/12.5

order to have a tightly grouped track for determining the direction of the wave propagation only the spectra from the sections near the front are used. These sections are indicated by heavier lines in the wave height portion of the figure. McClain et al. (1982) devised a simple graphic method to process the data. Table B, above, shows the results of the McClain et al., analysis.

Based on these results, McClain et al. (1982) show that a general trend of wave variation can be detected. The data from one track which went across the entire cold feature (Fig. 29) show that the seas were higher in the area of the western star than the eastern star and that the local $H_{1/3}$ minimum of 1.90 m occurs just prior to the eastern star (unfortunately, the sonobuoy (9) dropped at this point failed, and no corresponding current field can be compared to the 1.90 m minimum). Given the essentially constant wind speed and direction, the wind waves should be fully developed across the feature. If this is true, then changes in sea state must be the result of the interaction of the current and an opposing or reinforcing wind. This effect is most marked in the area over the western front where the

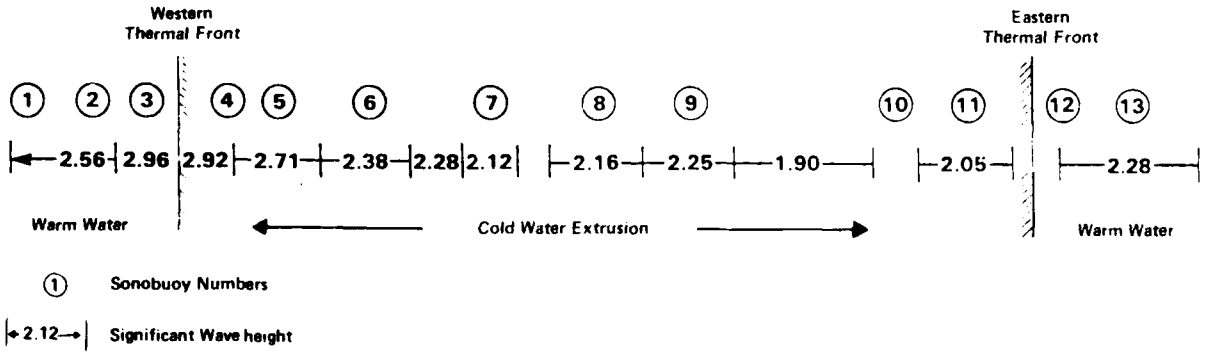

Figure 29. Significant wave heights in relation to sonobuoy positions along the cross section on 17 May 1979 (after McClain et al., 1982).

wind opposed the current and the highest $H_{1/3}$ was found. In the center of the cold feature where currents were minimal, the lowest $H_{1/3}$ were found. In the eastern front area where the winds and currents reinforced one another, $H_{1/3}$ again increased; but not to as great an extent as over the western front.

An examination of the significant wave height data along each flight track in the eastern star shows that no dramatic change took place in the significant wave height as the aircraft flew over the front. The situation in the western star, however, was quite different, as a marked increase in significant wave height across the frontal boundary can be seen. McClain et al. found that the mean skewness values determined for both the warm and the cold side of the star patterns (leg 5 excluded) indicate that the skewness was roughly 40% higher in the warm water region.

To illustrate the sea state change across the front, the apparent wavenumber spectra along flight track 7 are shown in Figure 30. (The word apparent is stressed here since the spectra are those collected along flight track 7 and do not represent lines orthogonal to the waves or swell.) As expected, all spectra show two prominent peaks at approximately the same location. Also, the lower of the apparent wavenumber peaks (hence, the longer wavelength) represents the wind waves and the higher wavenumber peaks represents swell due to the angle of encounter with the two wave trains. Along the track, the swell component ranges in peak value from 6 to 11 radians/m, but shows no systematic change. On the other hand, the wind wave component is very stable until the front is crossed. Once in the warm water, the peak value goes to 1.5 times the preceding value. Visual observations, on both 16-17 May, of increasing frequency of whitecapping in the warm water also support these changes. However, at the altitude of 250 m, no significant change in the mean horizontal wind speed or direction was recorded by aircraft INS in flights across the ocean frontal boundaries. McClain et al. suggest that two possibilities may be advanced to explain the changes in sea state that were observed across the fronts.

First, it must be remembered that definite variations in aircraft vertical motion were detected by the INS vertical accelerometer in flying across the fronts (Figs. 25-26). From this, it may be inferred that the variation in turbulence in the air-sea boundary layer may have been the chief cause for the changes in sea state.

There are, however, quantitative data that present problems with this explanation. Theory states that as wave energy grows, the wavelength associated with it should increase, or at least should not decrease. But the summary in Table B shows that the wavelength decreased from 157 m to 111 m across the frontal boundary. This discrepancy makes the second possibility, the effect of current-wave interaction seem to be more acceptable.

McClain et al. tabulated the surface currents for 17 May (Table C) into along-front and cross-front components with positive u in the down-stream direction and positive v to the right of u. Generally the u-component dominates and the flow is essentially a shear current similar to that used by Longuet-Higgins and Stewart (1960). McClain et al. shows that since the values of k and θ (the angle between the wave ray and the across-front axis) are measured directly on each side of the front, a comparison between theory and measurement is possible. They state that the expressions given by theory that can be most easily tested are for changes in energy, E, and wave number k. So that:

$$\frac{E_2}{E_1} = \frac{\sin^2(\theta_1)}{\sin^2(\theta_2)} \qquad (3.1)$$

and

$$\frac{k_2}{k_1} = \frac{\sin(\theta_1)}{\sin(\theta_2)} \qquad (3.2)$$

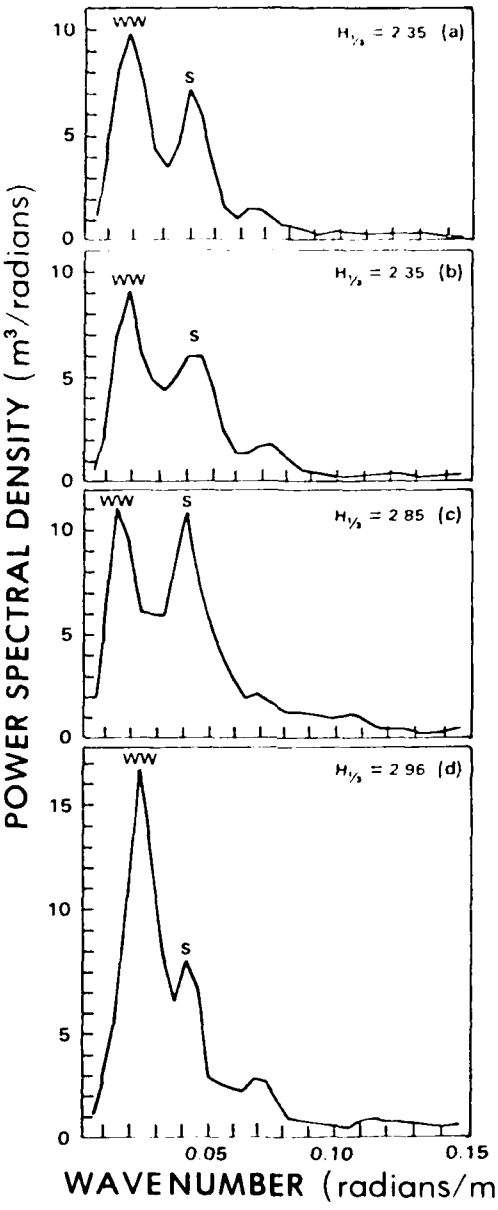

Figure 30. Variations of wavenumber spectra for laser profilometer tracks over the cross section on 17 May 1979 (after McClain, et al., 1982).

where the subscripts, 1 and 2, represent initial and final values, respectively.

In this case, for the wind waves at the western front, θ_1=48° and θ_2=33°, which result in E_2/E_1=1.09 as compared to 1.5 seen in track 7. From Equation 3.2, k_2/k_1=1.36 as compared to 1.41 from the graphic method of wavelength determination. In the theoretical result, equation 3.2 is a consequence of the irrotationality assumption coupled with the constraint that all variables are independent of the along-front coordinate. The latter condition seems reasonable since the currents are fairly

Table C. Decomposition of current components (after McClain et al., 1982)

		Heading	Along-Front		Cross-Front	
Sonobuoy #1	V(m/s)	(N)	θ'	u	v	
1	1.57	132	0	1.57	0	
2	1.44	132	0	1.44	0	
3	.83	143	-11	.91	-.18	Western
4	1.09	123	9	1.08	.17	Front
5	.73	107	25	.66	.31	
6	.54	116	16	.52	.15	
7	.09	SE	-	-	-	
8	.30	75	-	-	-	
10	.73	19	8	.72	.10	
11	.80	3	-8	.79	-.11	Eastern
12	1.07	0	-11	1.05	-.20	Front
14	.55	25	+14	.53	.13	
15	1.46	10	-1	1.46	0	

θ' is the angle between the current vector and the front.

unidirectional, the distance across the front is fairly small and 3.2 is approximately satisfied. However, since considerable wave breaking was occurring and the boundary layer did change, one would not expect equation 3.3 to be valid for the wind wave field.

McClain et al. used the mean current velocity of stations 1 and 2 and applied the expression

$$\theta_2 = \sin^{-1}|\sin\theta_1(1-v_2\sin\theta_1/c_1)^{-2}| \quad (3.3)$$

where $c_1=(g/k_1)^{1/2}$, $\lambda_1=157$ m, $\theta_1=48°$ and $v_2=1.5$ m/sec. The predicted change in direction should be 8°, but in this case 15° is observed. If equation 3.3 is applied to the swell, the result implies that the swell should not respond since θ_1 is only 14°. However, the measured value of θ_2 is -10° indicating a 24° refraction into the current which is unlikely and renders equation 3.2 unusable. The disagreement is probably due to uncertainty in the graphic method employed by McClain et al. in finding θ_1 and θ_2 for the swell in this instance. Actually, the value of swell propagation direction into the front, θ_1, appears low compared to the other three values.

McClain et al. apply a similar procedure to the wave components over the eastern front where the wind waves were propagating nearly perpendicular to the current direction. The refraction across the front was to the south (-12°). However, solving both 3.2 and 3.3 for θ_2 results in very small predicted changes in direction. Using 3.1, no change in the wind wave height is predicted. The swell offers a better comparison since it is traveling at a respectable angle to the current. Here $\theta_1=57°$ and $\theta_2=49°$ as measured. Application of equation 3.2 to each side results in $\sin(\theta/\lambda)$ equaling 0.00409 on the east and 0.00401 on the west. Using equation 3.3 with $\theta_1=57°$ and $v_2=0.92$ m/s (the mean of sonobuoys 11 and 12), $\theta_2=50°$ is in excellent agreement with the measured value of 49°. Thus, this last situation offers the best data/theory match.

McClain et al. also show that the change in significant wave height can be computed by taking the square root of equation 3.1 and using $\theta_1=57°$ and $\theta_2=49°$, a value of 0.96 is obtained for the swell. Using the $H_{1/3}$ values corresponding to the segments used in determining the θ's, the ratio of the mean values from each subpattern is also 0.96. This indicates that the change in sea state on the eastern side was probably due to a small modification of the swell by the current.

4. Conclusions

Analyses of the data derived from the sonobuoys across the cold feature show a

current field that decreases from the western and eastern front to a null point slightly east of the center of the structure. Dye markers dropped across the western front indicate that immediately at the front, a large horizontal shear existed with a 74 cm/sec current on the warm side existing less than 1500 m from water moving at 34 cm/sec on the cold side. No other measurements of shear were taken although patterns in the PRT analysis and satellite infrared imagery indicate that shear zones probably existed at the eastern front and in several areas within the cold feature.

A study of the satellite data show that frontal shear waves were moving along both sides of the cold feature at a period of approximately 18 hours. The study indicates that the movement of these waves through the current field should have induced a sinusoidal modulation to the velocity vectors of the current. However, since the sonobuoy data presented no such vector orientation, it is inferred that the data were collected for too short a period to measure these effects.

Wind speed and direction derived from aircraft INS show little variation across the feature (at least at the altitude of the aircraft). The gradual increase in wind speed that was found to the southwest is what may be expected from the gradient flow associated with the atmospheric high shown in the regional meteorological analysis. Those variations in wind speed seem small in comparison with the wave height variations found by the laser data at the western front and seem to be more aligned to variations in the current (although the change in wave direction does follow the change in wind direction). For example, the position of minimum roughness in the central portion of the cold feature matches the region of diminished currents. Also the roughness of the western frontal area, unaccountably diminishes southwest of the front. The aircraft winds for that region show no change and the difference may be due to the diminishing of the effects of current shear away from the zone of the frontal waves.

Examination of the INS vertical accelerometer data for 17 May indicate that at the 250 m altitude, the atmospheric turbulence front was slightly displaced from the ocean front. Although the displacement was most likely caused by the southeasterly winds, it is not known whether the displacement extended vertically to the surface or angled to the ocean fronts. Air temperature data for 16 May present a similar displacement occurring on this date at 50 m altitude. Visual observations showed a several kilometer wide zone of increased surface roughness on 17 May and a well-defined narrow (i.e., several meters) line 16 May. Whitecaps appeared in the warmer water on both days.

In summary, the analyses of data from intensive aircraft surveys 16-17 May 1979 indicate that well-defined regions of ocean surface roughness existed in the study area, that these roughness regions delineated the frontal boundaries of the cold feature and, in general, could be used to define the feature.

In addition, studies of the data indicate that while some roughness induced by air/sea thermal instability was present, the major cause of the measured variations in ocean roughness seemed to be the interaction of the wave field with the current.

It should be noted that the suite of instruments used in the two-day survey were incapable of measuring short period gravity waves. They were designed to measure larger scale ocean roughness such as long period gravity waves, current shear boundaries and thermal boundaries. As described, the instruments did this rather well. However, it is the shorter period waves that are detected by the synthetic- and real-aperture radars. The following portions of the study will show how these larger scale phenomena control the orientation of these short period waves and their detection by SAR and SLAR.

Table D. Characteristics of the NASA Lewis Research Center U.S. Coast Guard Side Looking Airborne Radar

- Motorola AN/APS-94D - Real Aperture
- Frequency: X-Band, Tunable - 9.10-9.40 GHz
- Pulse Width: 200 NS
- Pulse Repetition Frequency: 570 per sec, or randomly variable
- Polarization: H-H
- Antenna Length: 5.5M
- 3DB Antenna Beamwidth: 0.45DEG = 7.85 MRAD
- Range Resolution: 30M
- Minimum Detectable Signal: -97 DBM
- Mapping Swaths: 25, 50, 100 km with offset in 10 km steps, both sides of aircraft
- Image Outputs: Real time full resolution analog wet processed film
  Real time digitally dry silver process paper or film
- Digital Tape Output

Part IV. Side Looking Airborne Radar (SLAR)

1. Introduction

The previous portion of the study attempts to show that distinctive roughness variations are associated with the cold features extruded from the Labrador front. It also indicates that although the air-sea temperature difference was a factor on 16-17 May 1979, the major cause for the changes in roughness appeared to be the variations in current and wind stress. This portion of the report will document the detection of these roughness variations by specialized radars--in this case SLAR. The study will compare SLAR imagery to near-simultaneous environmental measurements taken by ship and aircraft.

The U.S. Coast Guard has experimented with the use of using SLAR-equipped C-130's to police oil spills in United States waterways and the open seas. The telltale modulation of sea state by oil pollutants is the basic rationale for their experiments. In addition to being useful in detecting oil spills, the U.S. Coast Guard has explored the use of SLAR as a device to monitor the movement of ice in shipping lanes. Experiments of this nature have been carried out in the Newfoundland/Labrador area as part of the U.S. Coast Guard's role as the operational unit of the International Ice Patrol. Thus, SLAR equipped C-130's were operating in the study area during the period of the Grand Banks Experiment and were made available on a time-available basis. The specifications of the SLAR aboard one of the two aircraft used during Baseline and New Look is given in Table D.

Since both SEASAT-A SAR and the ERIM SAR aboard the Canadian Convair 480 were not available during Baseline and New Look, the U.S. Coast Guard SLAR represents the only specialized radar data collected during the actual survey periods of the experiment.

2. The U. S. Coast Guard SLAR Data

SLAR-equipped C-130 flights were made over the experiment area on 11 and 19 June 1978 (Baseline) and on 10 and 16 May 1979 (New Look). The first three flights were taken by the Coast Guard AOS aircraft using a K-band SLAR horizontally polarized on the port side of the aircraft and vertically polarized on the starboard side. During the fourth flight, data was collected from an X-band SLAR belonging to NASA-Lewis Research Center and flown aboard a Coast Guard aircraft. This radar was horizontally polarized on both sides of the aircraft. Simultaneous to the collection of the SLAR data during these flights, infrared scanner data were collected and presented to the aircraft scientific crew on a realtime video display. This continuous display confirmed that the roughness features seen in the SLAR images were aligned with the thermal fronts in the area. Figure 31(a) and (b) shows examples of K-band SLAR imagery obtained during the two Baseline flights. Figure 31(c) shows a sample of X-band SLAR taken during the New Look flight. Real time optical SLAR imagery of this nature were the only products retained from the Coast Guard operational SLAR systems. Thus, no digital processing could be done with either the SLAR or the infrared scanner data.

The 11 June 1978 K-band SLAR imagery (Fig. 31(a)) shows feature roughness patterns associated with the front located at 44°10'N, 48°25'W in the satellite image for 12 June 1978 (Fig. 7). The higher radar reflectance (lighter tone) in the SLAR image occurs over the warmer water, implying a rougher water surface. The lower radar reflectance (dark tone)

(a) K-band SLAR-11 June 1978

(b) K-band SLAR-19 June 1978

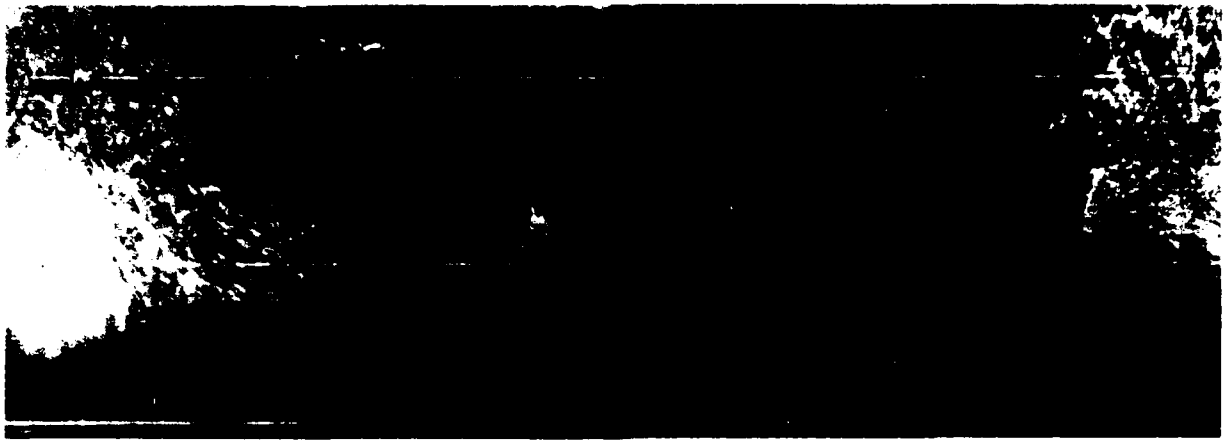

(c) X-band SLAR-16 May 1979

Figure 31. Samples of Coast Guard SLAR imagery collected during Baseline and New Look. The imagery in (a) and (b) were collected by the Coast Guard AOS and Aircraft 94D side-looking airborne radar on 11 June 1978 (a) and on 19 June 1978 (b). The nadir return from directly beneath the aircraft is shown along the top of each image. The range to the dashed line is 26 km, with each image segment being approximately 600 m. In (a), the aircraft was heading south (to the right) and took this image using the SLAR in a vertical polarization mode from the starboard side of the aircraft. In (b), the aircraft was heading west (to the left) and took this image in a horizontal polarization mode from the port side of the aircraft. The image in (c) was collected by the NASA Lewis Research center aboard the Coast Guard aircraft on 16 May 1979. The image was made from the starboard side of the aircraft as it flew east.

occurs over the cooler water and implies a smoother surface. Similar changes have been reported by others. For example, Weissman and Thompson (1977), after examining radar imagery of the Gulf Stream off Florida, interpreted similar variations in reflectance as variations in surface wind stress caused by changes in atmospheric stability and relative water velocity. In the SLAR image shown here, the wind direction and strength is not known nor is the exact relation to the thermal front (i.e., whether the SLAR defined front match or was several kilometers displaced from the thermal front).

The 19 June 1978 K-band SLAR image (Fig. 31(b)) shows surface patterns similar to patterns suggested to be associated with internal waves (Apel and Charnel, 1974; Fett et al., 1978; Fett and Rabe, 1977). These patterns again lay in the cold side of the front near 44°10'N, 48°25'W in the aircraft PRT analysis in Figure 17. As the aircraft data show surface temperature at this time was 8°C, heavy fog and low clouds were present. Winds were less then 3 m/sec. Seeing internal wave patterns of this type is predictable in this region both because of the greater water stratification and because they are more clearly visible due to the comparatively calm surface of the cold water.

On 16 May 1979, an X-band SLAR was flown across the front at an altitude of 600 m (Fig. 31(c)). On this occasion, frontal features similar to shear patterns were found that appeared to be aligned to the fronts at 40°15'N, 48°50'W and at 40°15'N, 47°30'W. The winds at this time were east to southeasterly (i.e., at right angles to the front) at less then 5 m/sec. While the match for these data

(a) Aircraft K-Band
SLAR image

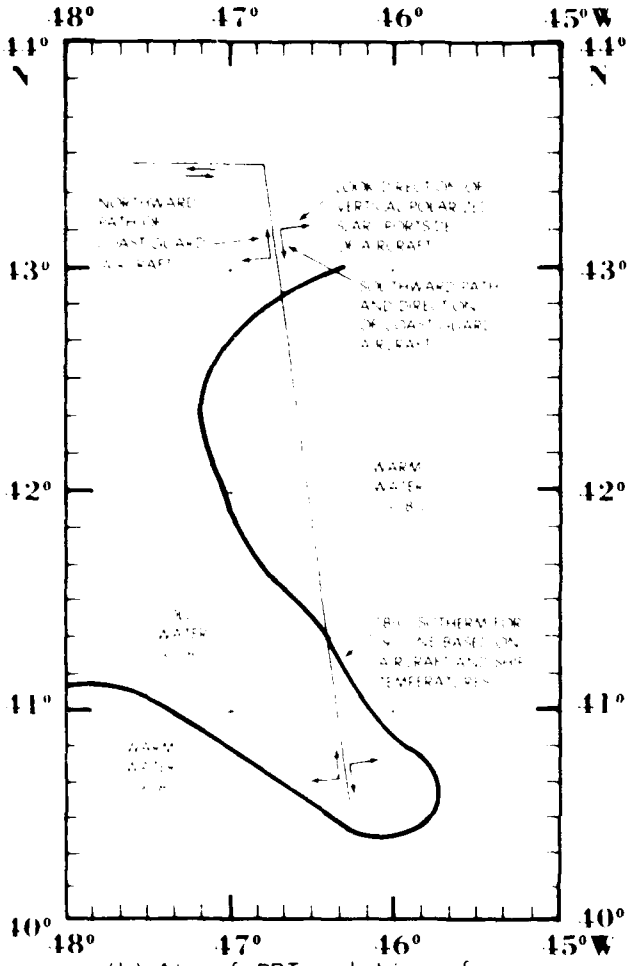

(b) Aircraft PRT and ship surface temperature analysis

(c) NOAA-5 infrared image

Figure 32 (opposite page and above). A comparison of (a) and aircraft K Band SLAR image, (b) aircraft PRT and ship temperature analysis, and (c) of NOAA 5 infrared image for a period centered on 19 June 1979. (Image enhancement by Atmospheric Environment Service, Canada.) The right side of the K Band SLAR image is hori zontally polarized. Note that the vertically polarized (left) portion of the SLAR image does not present as detailed delineation of the front as the horizontal polari zation (right) portion of the image. A return flight (north) over the same part gave similar results.

appear to be excellent, navigation errors in the notation of the imagery do not allow this data to be used except as an example of frontal pattern alignment.

3. The SLAR Image for 19 June 1978

The best example of features in the SLAR imagery matching features seen in the aircraft and satellite infrared data occurred in the southern portion of the Coast Guard flights 19 June 1979 (Fig. 32). Since several data sources are available near the time of this image, it is informative to compare these data and the SLAR image in detail.

Figure 32 presents a comparison of the 19 June SLAR image, the 19 June satellite infrared image and the 19 June

(a) Infrared

Figure 33. NOAA 5 infrared (a) and visible (b) imagery collected on 12 June [illegible] at 1245 GMT. (Image enhancement by Atmospheric Environment Service, Canada.)

(b) Visible

thermal front. (The 18°C isotherm representing the latter was constructed using ship surface temperature data for 17-19 June and aircraft PRT data for 17 and 23 June.) In the comparison, several features of similarity became evident. The most striking is the correlation of the curved features north of 42°N latitude found in the SLAR image and the arced thermal gradients shown in the frontal analysis and infrared image. In the SLAR image, the region separating these curved features and the mottled patterns to the south is in the same location as the thermal front in the infrared image. The mottled patterns in turn match the cold water region of the infrared image.

North of 42°50'N a similar phenomenon occurs. The striation area ends and a mottled pattern region begins. The mottled patterns in this instance appear to be composed of internal waves.

One feature to note in the SLAR image on Figure 32 is that the frontal region does not have a marked demarcation similar to the sharp gray tone delineation shown in the infrared imagery. This comparatively gradual change across ocean thermal fronts appears to be a normal feature of SLAR and SAR imagery and is discussed more thoroughly in the discussion section of this portion and in the portion dealing with SAR imagery.

No daytime satellite pass is available for 19 June. The infrared image shown in the figure is a late evening pass. Thus, no simultaneous visible image is available and no comparison of the sunglint patterns with similarly positioned SLAR patterns is possible. However, the visible image from a daytime satellite pass of one week earlier (12 June) may be used to derive an understanding of some of the roughness features shown in the SLAR image (LaViolette et al., 1980). The 12 June visible image and its companion infrared image are shown in Figure 33. Despite the offset of seven days, the sunglint in the visible image shows specular responses to regional ocean roughness that are similar in location to variations in σ_o shown in the 19 June SLAR imagery. In addition, the sunglint features in the visible satellite image have an obvious correlation with the thermal features shown in the companion infrared image. Although many of these features are caused by atmospheric conditions, in a number of instances they are caused by sea state. In the visible image, there are numerous areas that appear dark and are identifiable as cold water regions in the thermal image. For NOAA-5 satellite visible imagery, maximum sunglint for this time of year occurs along the eastern margin of each image. For the latitude of the Grand Banks Experiment, the eastern margin of the image requires facet slopes in the water of 0° to 2° to give specular reflections of the sun to the satellite. These slope requirements increase asymptotically westward. Where dark features begin to appear in the cold water areas of the 12 June visible image, slopes of 6° to 8° are required to provide specular response of the sun. The uniformity of the darkening in these regions is evidence that these ocean areas are relatively smooth and that fog is absent.

Weather charts for 12 June show a region of high pressure over the Grand Banks Experiment area with light easterly prevailing winds. Ship reports indicate 3° to 6°C air temperature to dewpoint difference over both the warmer and colder water. The light easterly winds, however, advect moist air from over the warm water to over the cold water. This could cause fog to be formed over the cold water side of a north-south ocean front. Such a fog could be the cause of the bright area at the end of the cold ridge feature.

The author feels that aside from the obvious cloud features, many of the variations in specular response in the 12 June visible image are due to variations in sea state. Unfortunately, correlating these variations to exact ocean events is impossible since there is no simultaneous ship or aircraft coverage. The image is presented only to give a spatial presentation of ocean

roughness that may be similar to sea state features at the time of the 19 June SLAR image.

Sea state conditions for 19 June 1978 reported by the meteorological team aboard the USNS LYNCH indicate that the dominant swells were coming from the south (180°-160°) with a mean height of 2 meters and a frequency of 1.4 Hz. Their reports (Table E) of (T_a-T_s) values indicate stable or close to neutral atmospheric conditions were present. In the area of the eastern front, the air was close to the same temperature as the sea on the warm water side of the front. On the cold water side of the front, the air was warmer than the sea by approximately 2.0°C. At the time of the overflight of the Coast Guard aircraft, the USNS LYNCH was in the cold water at 42°03'N, 48°32'W, with a (T_a-T_s) difference of 2.5°C, air-dewpoint temperature difference of 1.8°C, and southeasterly winds at 5 m/sec (the aircraft reported winds of 6.6 m/sec).

Table E also shows the winds to have been blowing parallel to the eastern front with a slight reduction in wind speed (8 to 6 m/s) on the cold water side of the front as compared to the warm water side. Not only did the air temperature decrease in going from the warm with the cold water but the dewpoint temperature decreased as well, signaling a drop rather than a rise in humidity. These data indicate that the location of a weak atmospheric front was coincident with that of the ocean front.

Waverider buoy data collected 18-19 June are shown in Figure 34. If these data can be considered synoptic, then the swells coming from the south behave as expected, decreasing in height and increasing in frequency as they progress northward. No marked change is visible in these data between the wind waves or swell on one side of the front than on the other.

The movement of the satellite drifter buoy dropped from the LYNCH several days later (22 June) may be used to get a general feel for the currents in the cold water on 19 June. Figure 14 shows the drifter moving at speeds of 100 cm/s 22 June near the eastern front. As mentioned in Part II, this speed may be the result of the sudden increase in the southeastward extension of the cold water feature on 18 June, thus the current speed on 19 June may have been slightly less then the 22 June measurement.

4. Discussion

Analysis of the Baseline data from the satellite drifter buoy, the waverider buoy, and the ship meteorological observations indicate that the thermal air-sea differences over both the cold and warm waters were not the major cause of the strong differences of σ_o in the 19 June SLAR image. Except for the weak atmospheric front aligned with the ocean front, there was little in the thermal air-sea interaction that would create the strong changes. The meteorological observations show (T_a-T_s) differences were close to neutral in the warm water and were positive in the cold water. On the other hand, as evidence that the currents played a major role in the variations of σ_o, the satellite drifter buoy data show a strong current was present inside the cold water feature and aligned with the shape of the front. Unfortunately, no current measurements were taken in the warm water outside the feature. However, the fact that an even faster current was present in the warm water may be inferred from the New Look sonobuoy data collected the following year (Fig. 22). During New Look, the warm water current on one side of the front was 30% faster then the current in the cold water on the other side of the front. Shear conditions would have been present between the core of the faster moving warm water and the cold water. The vertically polarized SLAR imagery during the southern run of the Coast Guard aircraft does show striation patterns in the area of the warm water which indicate shear conditions may have been present.

Table E. Meteorological and surface temperature data for 18 and 19 June 1978 - - USNS LYNCH

Date	Time (Z)	W_{Dir}	W_{Spd}	T_A	T_S	T_A-T_S	T_D	Wind Waves Per.[3]	Wind Waves Ht.[5]	Swell Waves Dir.	Swell Waves Per.[3]	Swell Waves Ht.[4]
18 June	Sta. A 1900-2030	160	9	21.1	20.6	0.5	18	2	1.5	170	6	2.0
	2100	160	9	20.0	20.5	0.5	17	2	1.5	180	6	2.0
	2200	170	9	20.2	20.5	-0.3	18	2	1.5	180	6	2.0
	2300	140	1.0	19.6	19.7	-0.1	18	2	1.5	180	6	2.0
19 June	0000	140	0.8	18.8	19.0	-0.2	18	2	1.5	180	7	2.0
	0100	160	0.7	18.7	18.8	-0.1	18	2	1.5	180	7	2.0
	0200	160	9	19.5	18.6	0.9	18	2	1.5	180	7	2.0
	0300	150	1.0	19.5	18.9	0.6	18	-	-	180	7	2.0
	0400	150	0.8	19.6	18.4	1.2	18	-	-	180	7	2.0
	0500	150	0.8	19.5	20.4	-0.9	18	-	-	180	7	2.5
	Sta. B 0600-0800	160	0.6	20.1 Frontal	20.1 Passage	0.0	18	-	-	160	7	2.5
	0900	160	0.6	17.9	17.2	0.7	17	-	-	160	5	2.5
	1000	160	0.5	17.0	15.7	1.3	16	-	-	160	5	2.5
	1100	150	0.6	16.9	14.8	2.1	15	3	1.0	160	5	1.5
	1200	140	0.7	17.6	15.4	2.2	16	2	0.5	160	5	1.5
	1300	140	0.7	17.4	15.4	2.0	16	2	0.5	160	5	1.5
	Sta. C 1330-1500	150	0.5	17.7	15.4	2.3	16	2	0.5	160	5	1.5
	1600	120	0.5	19.8	15.3	4.5	15	2	0.5	160	5	1.5
	1700	130	0.5	17.8	15.3	2.5	15	2	0.5	160	5	1.5
	1800	140	0.7	17.7	15.5	2.2	15	2	0.5	160	5	1.5
	1900	170	0.7	19.1	16.2	2.9	17	3	1.0	160	5	1.5
	Sta. D 1930-2100	140	0.7	16.1	15.3	0.8	16	3	1.0	160	5	1.5

1. Wind speed in meters/sec
2. All temperatures in °C
3. Wave periods in seconds
4. Wave heights in meters

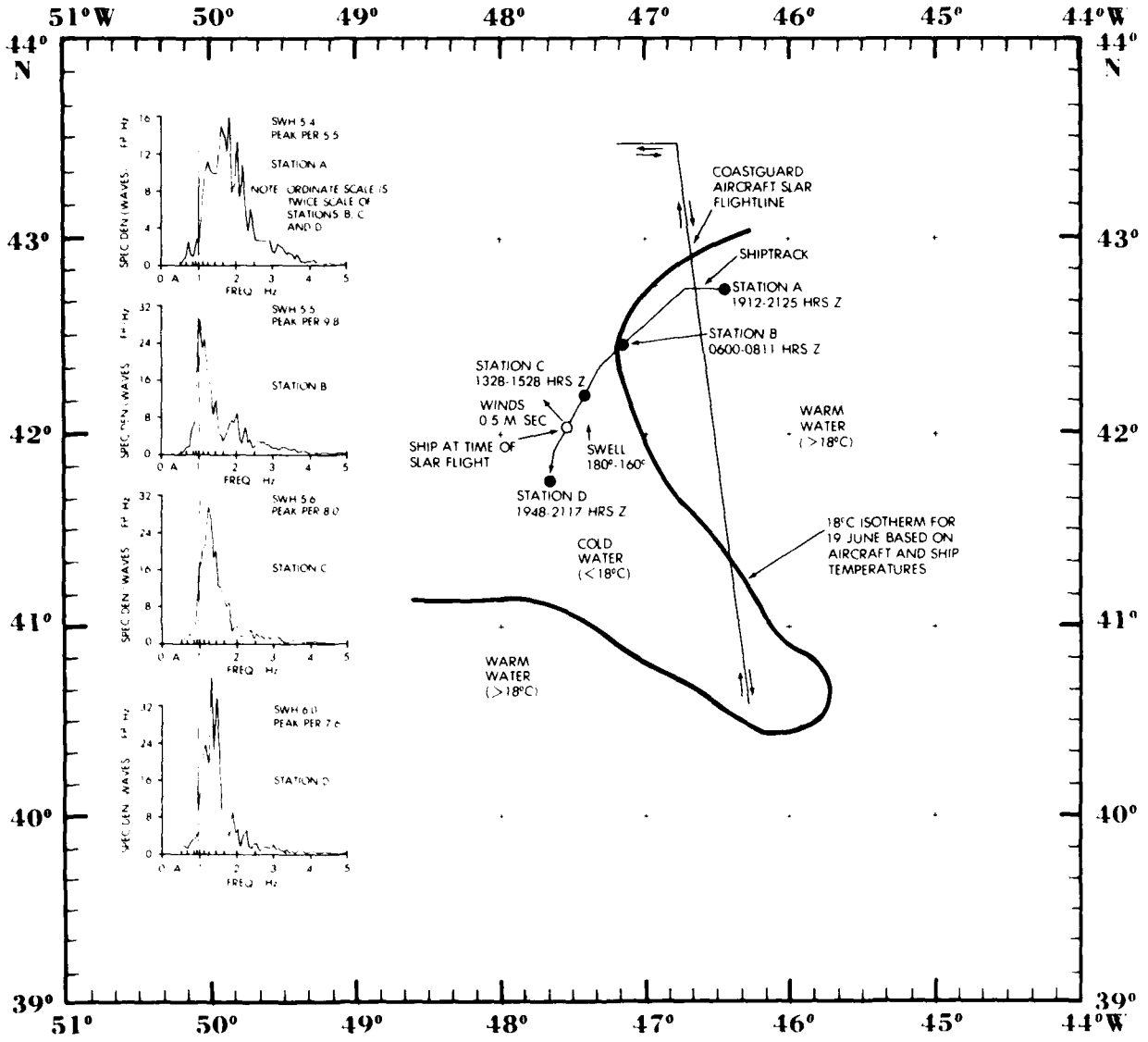

Figure 34. Canadian waverider buoy data taken across the eastern front on 18 and 19 June 1979. The direction of swell is that observed by the shipboard meteorological team (see Table E).

Although a sharp gradient marks the ocean front in the temperature data, the 19 June SLAR image does not show a similarly sharp boundary. The change in σ_o across the front, while definite, is gradual. This gradual change is also indicative of the current influence on the variation in σ_o because of frictional effects, the strongest currents are not found immediately at the front but are normally displaced to one side.

The mottled pattern of the cold water in the 19 June SLAR image is similar to patterns found in SAR imagery taken during the life of SEASAT-A. The generally darker appearance of these cold water patterns in comparison with the more specular response of the warm water seems to denote a quieter sea state. The mottled patterns themselves are unusual, however, in that they do not resemble the sunglint patterns seen in either satellite visible imagery or manned spacecraft photography. This variation may be due to a phenomenon not present in the specular return of incoherent sunlight: Bragg scattering. In the case of the specialized radars, the coherent signals returned from short-period waves are either reinforced or destroyed according to the spacing of these ocean reflectors in relation to the radar frequency.

One reason advanced, therefore, to explain the cause of these mottled patterns is that they are the returns from long-period, low-elevation swells that had capillary waves of the same wavelengths as the radar, but only a portion of which were tilted at the correct angle to provide resonant backscatter. The result is that in the relatively calm seas of the cold feature, the only backscatter was from the capillary waves aligned at the proper angles along these long period swells. These long-period, low elevation swells may have continued unchanged into the warm water; however, the increased specularity of the more chaotic warm water was so great that their σ_o is essentially masked in the SLAR image. Figure 35 shows a sea condition on the lee side of the USNS LYNCH with a similar effect. Here, the hull of the vessel blocks the near-surface wind for a short distance and the swell field is visible in the water. Beyond this lee effect, the ocean becomes highly reflective and the swells in that area are comparatively hidden in the speckle.

The mottled patterns of the SLAR image have different orientation and wavelength from the southerly swells reported by the meteorological team aboard the LYNCH. The waves associated with the SLAR patterns may have low frequencies and amplitudes which are undetectable in the presence of the higher frequencies and amplitudes of the swell set from the south identified by the meteorological team. In the aggregate, however, the broader area of these lower frequency waves provide the greater resonant backscatter and this area is what was detected by the radar. The lack of visual detection of these low frequency, low amplitude waves by shipboard observers is an observational phenomenon often noticed in coordinated operations between aircraft and ships. Roughness features in the ocean, plainly visible to observers aboard the aircraft, cannot be seen by observers looking at the same stretch of water from the low elevation angle of the ship; and increased altitude heightens the visibility of these roughness features.

Whether the north-south orientation of the mottled patterns is actively independent or is aligned to the shape of the cold feature can not be determined from the 19 June data. Since the aircraft did not cross the cold feature's southern front, a curved alignment parallel to the southern terminus could not be proved or disproved.

5. Conclusions

U. S. Coast Guard SLAR imagery collected during both Baseline and New Look does show roughness patterns that are associated with the location of thermal fronts. In the imagery of the vertically/horizontally polarized K-Band SLAR, the horizontally polarized imagery pro-

Figure 35. Variations in the wave field on the lee side of the USNS LYNCH. Photo graph was taken from the main deck. The wave field change is 30 m from ship (photo by R. A. Orioli).

vided the most information. The data from one flight during New Look are all of the X-band imagery that are available for examination; these appear to have navigation errors which limit their usefulness. This sampling is insufficient to tell whether the K-Band SLAR is superior to the X-Band in detecting fronts.

Although the U.S. Coast Guard SLAR imagery do present pattern changes in the regions of ocean fronts similar to the changes seen in satellite visible imagery, there are obvious differences. In both the Baseline and New Look SLAR imagery, the image area coincident to the cold ridge waters has a distinct mottled appearance. On the other hand, the areas of the warmer waters outside the cold feature show a more specular response. The author feels that differences are a result of Bragg scattering and that the mottled patterns are caused by backscatter from extremely short period, low elevation waves having the proper angle and spacing for a resonant return to the aircraft radar. While these effects are plainly visible in the calmer, cold waters inside the ridge feature, they are lost in the specular warm water outside.

In addition, there are striations patterns apparent in the horizontal polarized portion of the SLAR imagery that run parallel to the front on the warm water side of the normal boundary. These features may be shear lines created by the faster moving warm water and accented by the opposition of the wind to the current flow.

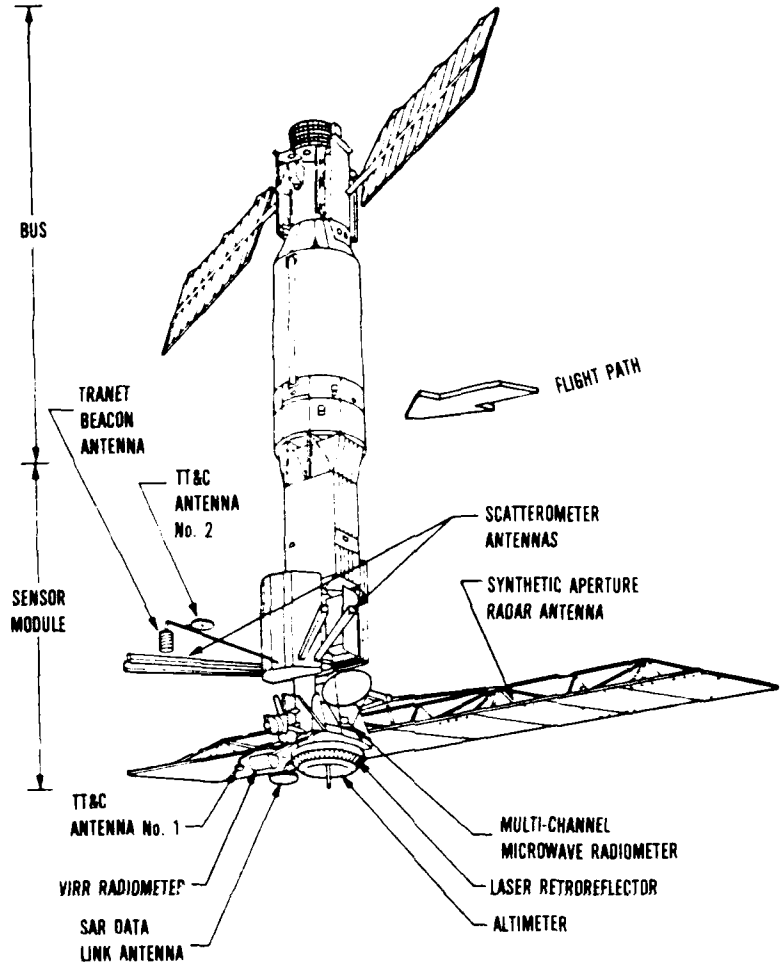

TECHNICAL CHARACTERISTICS

- CENTER FREQUENCY - 1274.8 GHz
- BANDWIDTH - 19 MHz
- TRANSMIT TIME TOTAL TIME - 0.35
- PULSE WIDTH - 33.8 μ sec
- CHIRP RATE - 0.562 MHz/μ sec
- PULSE COMPRESSION RATIO (TIME BANDWIDTH PRODUCT 1 - 642
- EFFECTIVE PULSE WIDTH - 53 nsec
- PEAK TRANSMITTED POWER - 1125 w nom
- PRF'S - 1404 1540 1580 1647 Pulses/sec
- AVERAGE TRANSMITTED POWER - 55w
- SYSTEM NOISE TEMP $\leq$ 600° K
- RECEIVER GAIN+ 77 TO 98 dB
- GAIN - STC. AUTO. COMMANDABLE
- AVERAGE BACKSCATTER - 13 dB at 20°
- BACKSCATTER RANGE - 26 TO 0 dB
- RECEIVER POWER RANGE - 97 TO 71 dBm
- ANTENNA PEAK GAIN - 34.5 dB
- ANTENNA POLARIZATION - HORIZONTAL
- ENG DATA RATE -494 cps
- SIZE 122 x 86 x 33 cm
- WEIGHT - 125 kg

Figure 36. SEASAT-A SAR technical characteristics

Part V. SEASAT-A SAR

1. Introduction

On 29 June 1978 the National Aeronautics and Space Administration launched SEASAT-A, the first satellite dedicated to the exploration of the oceans (Fig. 36). SEASAT-A contained active and passive microwave instruments designed to measure large scale ocean and atmospheric processes. On 10 October 1978 after 100 days of operation, a massive short circuit caused the spacecraft and all its sensors to permanently shut down.

Prior to the failure, SEASAT-A SAR data were collected during the period 21 September and 10 October from seven satellite passes over the Grand Banks Experiment area. As mentioned in Part I, no survey platforms were in the study area during that time. Thus, the comparison of SEASAT-A SAR data with real time ocean events as measured by other sources is limited to NOAA-5 infrared data and regional weather analyses. No NOAA visible image is included in the study, since the combination of the lateness of the year and the high latitude of the study region preclude any sunglint being detectable by the NOAA-5 visible sensors. The results of comparing SEASAT-A SAR with NOAA-5 thermal imagery and regional weather analyses are the subject of this section of the study.

2. The SEASAT-A SAR Data

SAR data represent the reflectivity of a surface at the opening frequency in the backscatter direction (σ_o). The values of σ_o obtained are directly proportional to the surface backscatter cross section and are represented in the SAR imagery as variations in brightness. In the decimeter spectral region (the wavelength of the SEASAT-A SAR was 23.5 cm), the backscatter energy is dependent primarily on the physical properties of the reflecting surface (i.e., average slope and small-scale roughness), and the dielectric constant of the reflecting surface.

The SEASAT-A SAR was able to sense only the spatial distribution of 30 cm to 40 cm waves on the ocean surface--in essence, short-period gravity waves. This was done through a Bragg resonance of the radar backscatter of the ocean surface. Experience has shown that the distribution of these short period waves is correlated with larger scale ocean roughness phenomena such as long gravity waves, current shear boundaries, thermal boundaries, and regional bathymetry. The ability of the SEASAT-A SAR to detect and monitor these large scale oceanic processes is dependent upon the modulations of the short period waves by these larger scale phenomena.

The image format of the SEASAT-A SAR system contains distortions that result from the spacecraft's movement to the Earth, as well as to the imaging geometry. Distortions, in the first instance, arise from the effects of the Earth's rotation and curvature and from differences in pixel dimensions in the along-track (azimuth) and across-track (range) directions. In the along-track direction pixel size varies with the velocity of the spacecraft relative to the image target on Earth at any particular Earth latitude. In the across-track direction, pixel size varies with the range distance between the spacecraft nadir and the target. Pixel sizes of the images in this study are approximately 16 m in the along-track direction and vary across-track from about 19.4 m in the near range to about 14.8 m in the far range.

Since SAR nadir-image format basically represents the slant range, or distance from nadir to each of the respective surface elements in the scene, the SEASAT-A SAR imagery normally contains distortions due to the imaging geometry that are inherent in all SAR imaging systems. In the SEASAT-A SAR imagery presented in this study, this distortion has been partially corrected during processing. This correction allows the range azimuth aspect ratio to be each maintained at unity at the center of subswath.

All of the SEASAT-A SAR data used in this study are optically processed imagery. The processing was done by the Jet Propulsion Laboratory (JPL) in Pasadena, California. Although digital processed SAR data have some advantages over optical processed data, time and funding constraints prevented the SAR data from being digitally processed into imagery for use in the present study (Fig. 37 shows an example of an optical SAR image and the same SAR data digitally processed). In the optical image, the SEASAT-A SAR 100 km swath was divided into four subswaths to accommodate processing limitations. The data for each subswath were processed separately and recorded on 70 mm film. Each subswath film strip covers an area about 30 km wide and overlaps the adjacent subswath by 6 to 7 km. An across-track gradient of image brightness resulting from processor peculiarities is present in each subswath. This creates a discontinuity in image brightness across the subswaths. The dots at the edges of each strip are timing marks representing a one-second flight distance on the ground (about 6.67 km).

The location of an ocean feature in an optical image filmstrip that includes landmarks can be estimated with an error of about 2 km by using maps and spacecraft ephemeris data. However, an optical image filmstrip without landmarks can easily suffer a location error of more than 10 km The magnitude of location error becomes important in a region as far from land as the Grand Banks experiment area. Two of the ascending SAR data passes--2 and 5 October--went over land and these had respective location errors of 13 and 17 km to the southwest (i.e., the images would have to be repositioned by these distances easterly at right angles to the track line to be geographically correct). None of the film strips of the descending passes included land, thus, their location error cannot be defined.

All of the SEASAT-A SAR data collected over the Grand Banks area were collected during the period of the "frozen orbit" (i.e., the orbit of the satellite was such that it passed over essentially the same area every three days). The convergence of the ascending and descending paths of the frozen orbit form a diamond-shaped region in the northern portion of the study area which was viewed by the satellite for two of every three days. This cross-over region is of particular interest in that the SEASAT SAR had a right-side look and was in an orbit inclination of 108°. Thus, the convergence of the two orbits provides an opportunity to examine the variability of σ_o data for the same region at different satellite orientations. Figure 38 shows where this diamond-shaped region fell in the Grand Banks experiment area.

3. September-October Data

The Canadian Shoe Cove satellite data receiving station did not begin to operationally receive SEASAT-A SAR data until late September 1978. Of the SAR passes that the station recorded, seven covered the Grand Banks Experiment area, five descending and two ascending. Only eleven NOAA-5 passes are available for the 20-day period when the SAR data were collected. Of these, five are sufficiently cloud free to use in this study and four are close enough in time to use for comparison with the SAR data. Table F presents the times and orbit numbers of the SEASAT-A and NOAA-5 data used in this study.

In general, The NOAA-5 infrared imagery showed that for the period September 21 through October 4, three cold-water features extended from the Labrador Front. Two of these formed a bifurcated feature lying over the Newfoundland Ridge, whereas the third was located over the Newfoundland Seamounts. In the text that follows these are discussed as the Newfoundland Ridge-East feature, the Newfoundland Ridge-West feature, and the Newfoundland Seamount feature. A schematic presentation representing the overall general positions of these thermal features derived from all five NOAA-5 passes is given in Figure 38. However, some movements in the individual features are observable in the day-to-day infrared imagery. These are also presented in Figure 38. The NOAA-5 image for 29 September is presented in Figure 39 to show the relationship of the various features to one another in a single image.

The NOAA-5 imagery, as stated in Appendix A, are difficult to register into a mercator projection with an accuracy greater than ±20 km. This is especially true for the imagery used in this comparison; most of which lie outside the satellite synch line. However, the persistence of the relative geographic positions of the three thermal features from image to image is strong evidence that computer generated registrations are well within the given accuracy. This persistence is especially noticeable in the four overlays of the Newfoundland Ridge-East feature shown in Figure 38.

Table F shows that on the morning of 21 September, NOAA-5 and SEASAT-A passes over the study area were approximately two hours apart. There is no companion SEASAT-A SAR image for 26 September. However, the NOAA-5 IR image listed for that day is invaluable in showing the

Table F. SEASAT-A related NOAA-5 passes over the Grand Banks experiment area

	SEASAT-A		NOAA-5*	
Date (1978)	Pass Number	Time (Z)	Pass Number	Time (Z)
21 September	1231 (Descending)	02:25 hrs	9702	00:20 hrs
26 September	----------	----------	9788	12:45 hrs
29 September	----------	----------	9801	12:28 hrs
30 September	1360 (Descending)	03:20 hrs	---	----------
2 October	1395 (Ascending)	13:22 hrs	9838	23:22 hrs
3 October	1403 (Descending)	03:14 hrs	---	----------
4 October			9888	12:42 hrs
5 October	1438 (Ascending)	13:35 hrs	---	----------
6 October	1446 (Descending)	03:27 hrs	---	----------
9 October	1489 (Descending)	03:42 hrs	---	----------

* Of the eleven NOAA-5 passes saved by NOAA NESS, only the five presented here are usable because of either clouds or poor data tapes.

(a) Optical processed
SAR image
21 September 1978

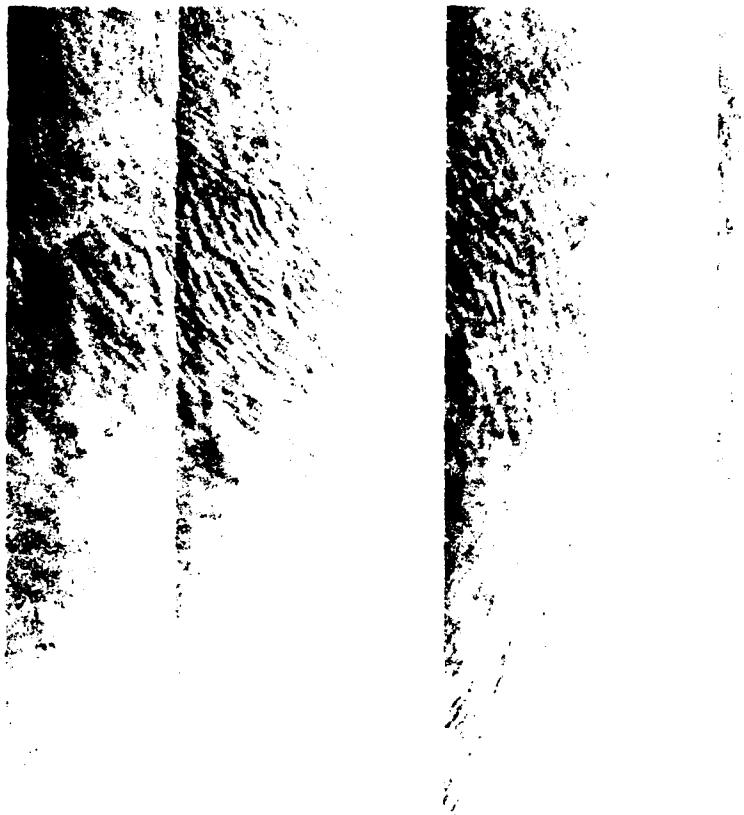

(b) Digital processed
image
21 September 1978

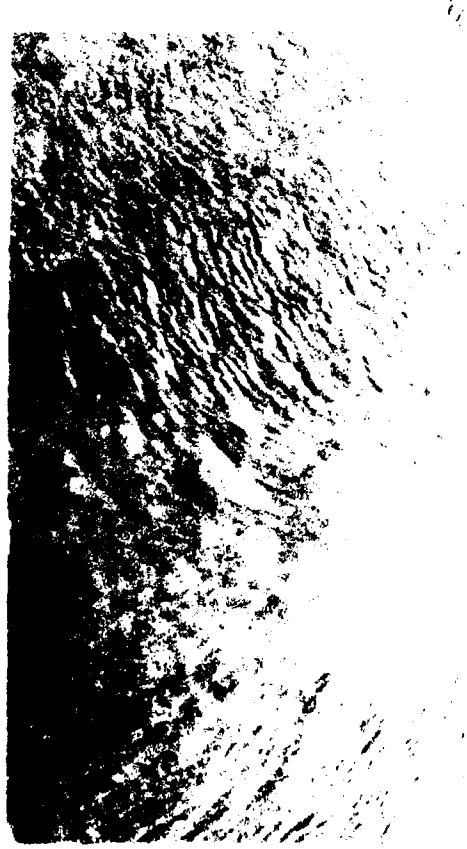

Figure 37. An example of an optical and digitized processed SAR image of an area over the Newfoundland Ridge

continuity of the imagery over Newfoundland Ridge for the period between 21-29 September. The remainder of the related NOAA-5 and SEASAT-A passes in the table vary in time apart; ranging from 4 to 23 hours. Because of the large time differentials between 6 and 9 October SEASAT passes and their nearest NOAA pass, their SAR/IR comparisons must be used with discretion.

The time differences, while sufficient for comparisons of purely oceanographic features, are insufficient for comparisons that involve the critical relationship of wind to current. Figure 40 shows surface weather analysis of the general region of the Grand Banks for 0000 hours (Z) for 21 September and for each day for the period 29 September-9 October. The figure is presented to show the general weather conditions present during the study period, as well as to demonstrate the rapid movement of atmospheric fronts through the area. In the analyses that follow, information on general wind conditions for the times of SEASAT-A SAR passage are derived from interpetative analysis of the six-hour synoptic surface weather charts and ship reports. The winds thus derived are given in Table G for each of the thermal features for the seven days of SAR coverage.

During the period of 21 September-9 October, no ship reports were available close to the fronts. Those reports which are available are from ships well into the warm or cold water areas. Temperature and wind conditions derived from these reports, therefore, should be considered to represent the general warm or cold water regions rather than conditions immediately at the fronts. The reports show the temperatures of the warm waters were in the low 20's(°C) whereas the cold waters of the ridge features averaged 15°C. The lowest temperatures were reported by ships operating in the area of the Newfoundland Seamounts, where water temperatures of 8°C were reported.

For clarity, the three main features are discussed separately starting with the most stable of the features: The Newfoundland Ridge-East feature. The discussion section immediately following will coalesce the findings of these subsections.

A. The Newfoundland Ridge-East Feature

The eastern portion of the bifurcated thermal feature lying over the Newfoundland Ridge remained remarkably stable during 21 September-4 October 1978. The minor movement shown in the schematic overlay in Figure 38 may be due to accuracy variances in the computer-registered imagery.

Table G. General speed (m/sec) and direction of winds over the three main ocean features*

	--21 Sept--		--30 Sept--		---2 Oct---		---3 Oct---		---5 Oct---		---6 Oct---		---9 Oct---	
	SPEED m/sec	DIR.	SPEED m/sec	DIR.	SPEED m/sec	DIR.	SPEED m/sec	DIR.	SPEED m/sec	DIR.	SPEED m/sec	DIR.	SPEED m/sec	DIR.
Newfoundland Ridge - East Feature	10	NW	10	SW	10	E	5	SE	14	NW	13	N	7	SSE
Newfoundland Ridge - West Feature	10	NNW	10	SW	7	ESE	5	S	13	NNW	10	NE	6	SE
Newfoundland Seamount Feature	10	W	10	SW	10	ENE	7	SE	16	NW	15	NNW	8	S

*Data obtained from surface weather charts and ship reports.

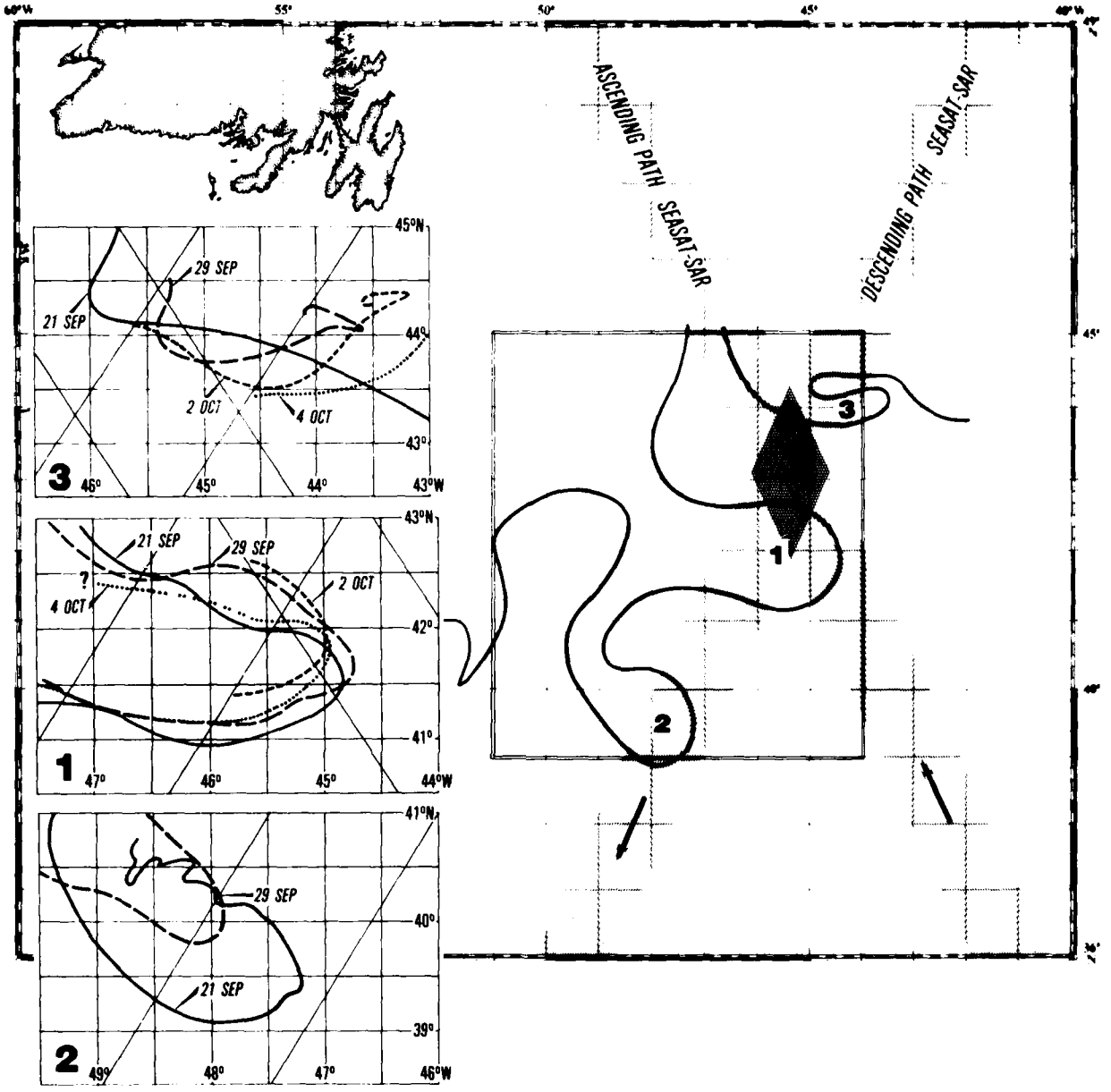

Figure 38. The general positions and movement of the cold water features during the period 21 September through 4 October 1978. The presentations were derived from the five NOAA-5 infrared images listed in Table F.

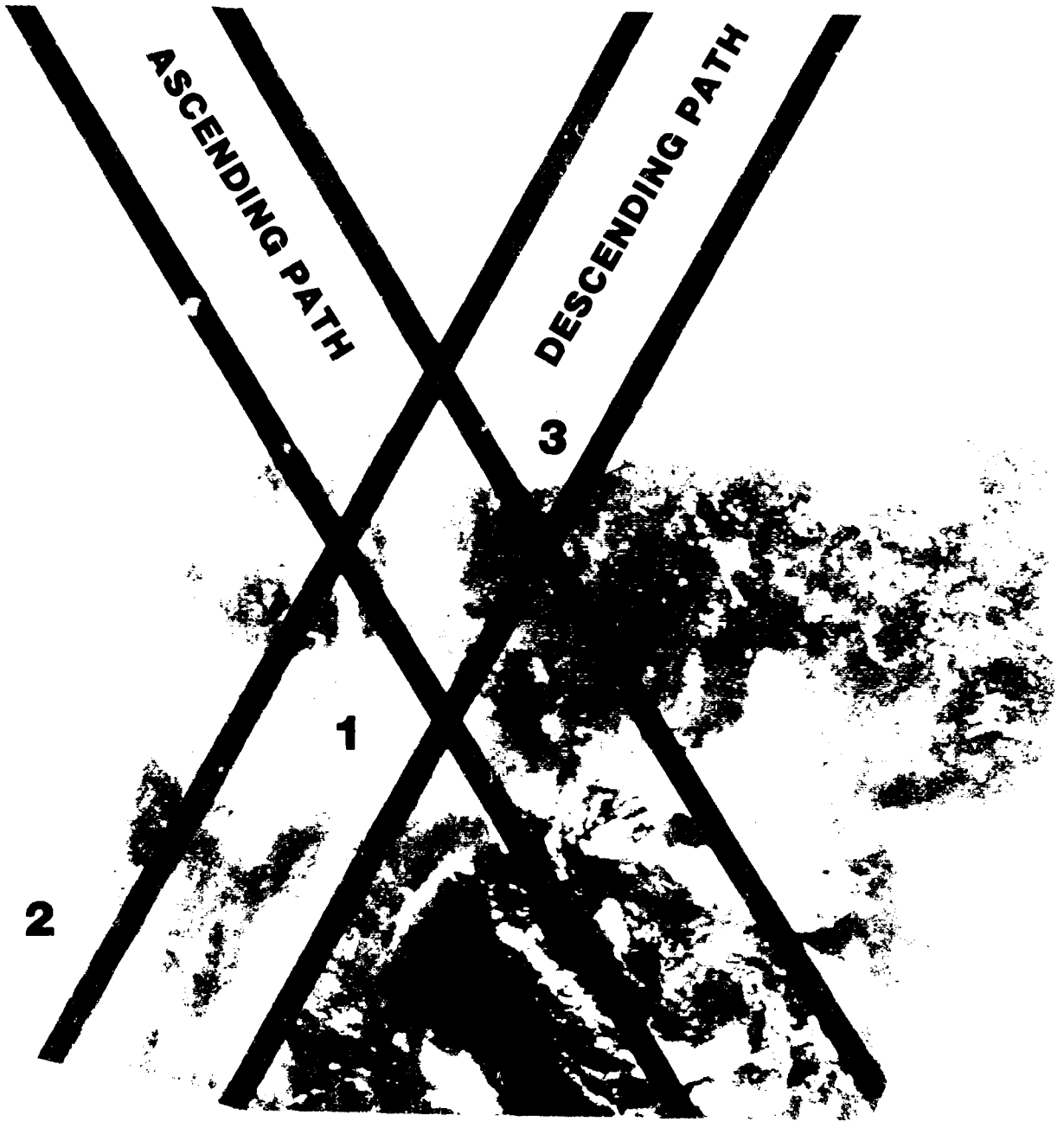

Figure 39. The three cold water features on 29 September 1978. The overlay is the descending and ascending swaths of the SEASAT A SAR.

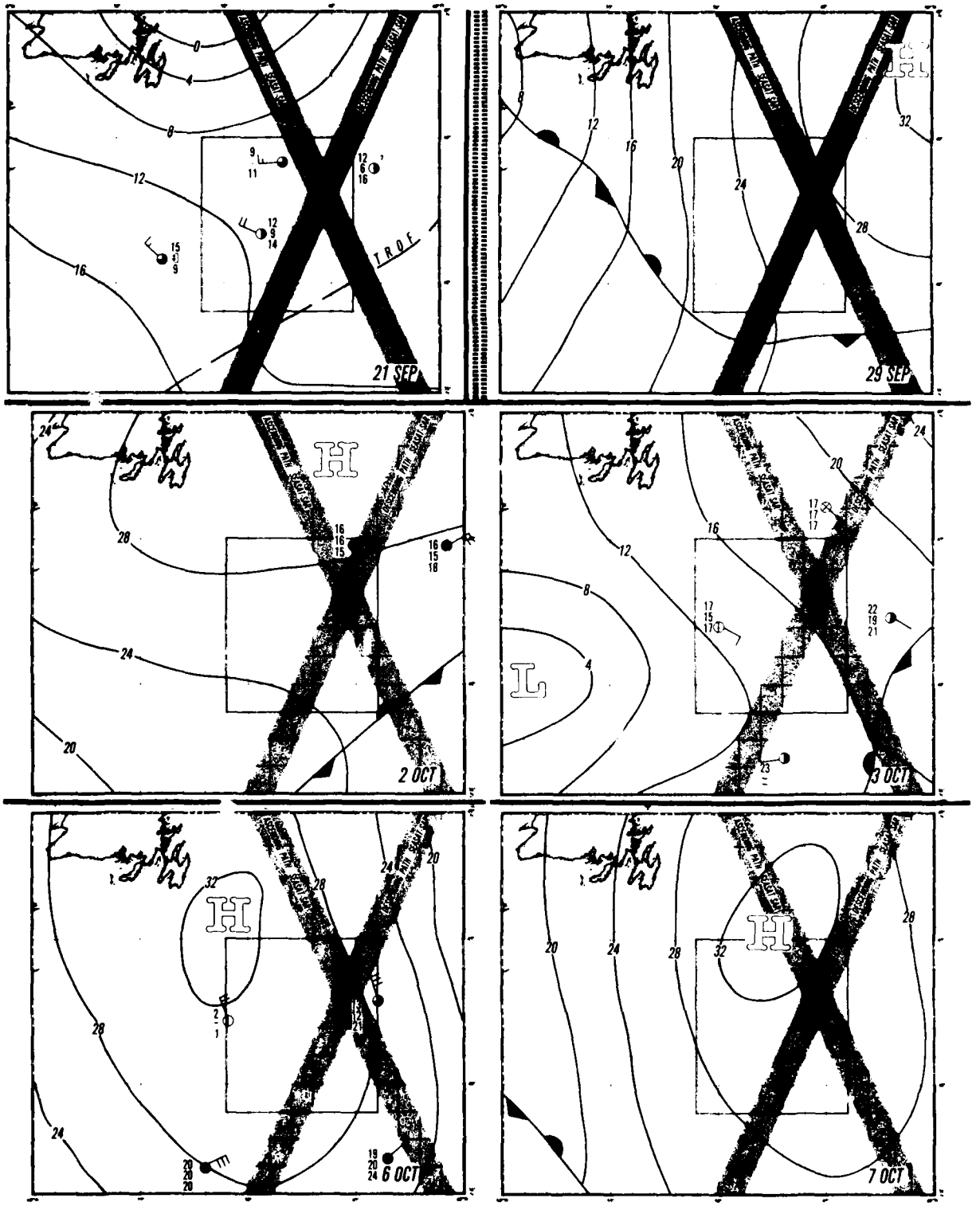

Figure 40. Surface weather analyses for 21 September and the period 29 September through 4 October 1978. Ship observations are shown on those days having SEASAT-A SAR data.

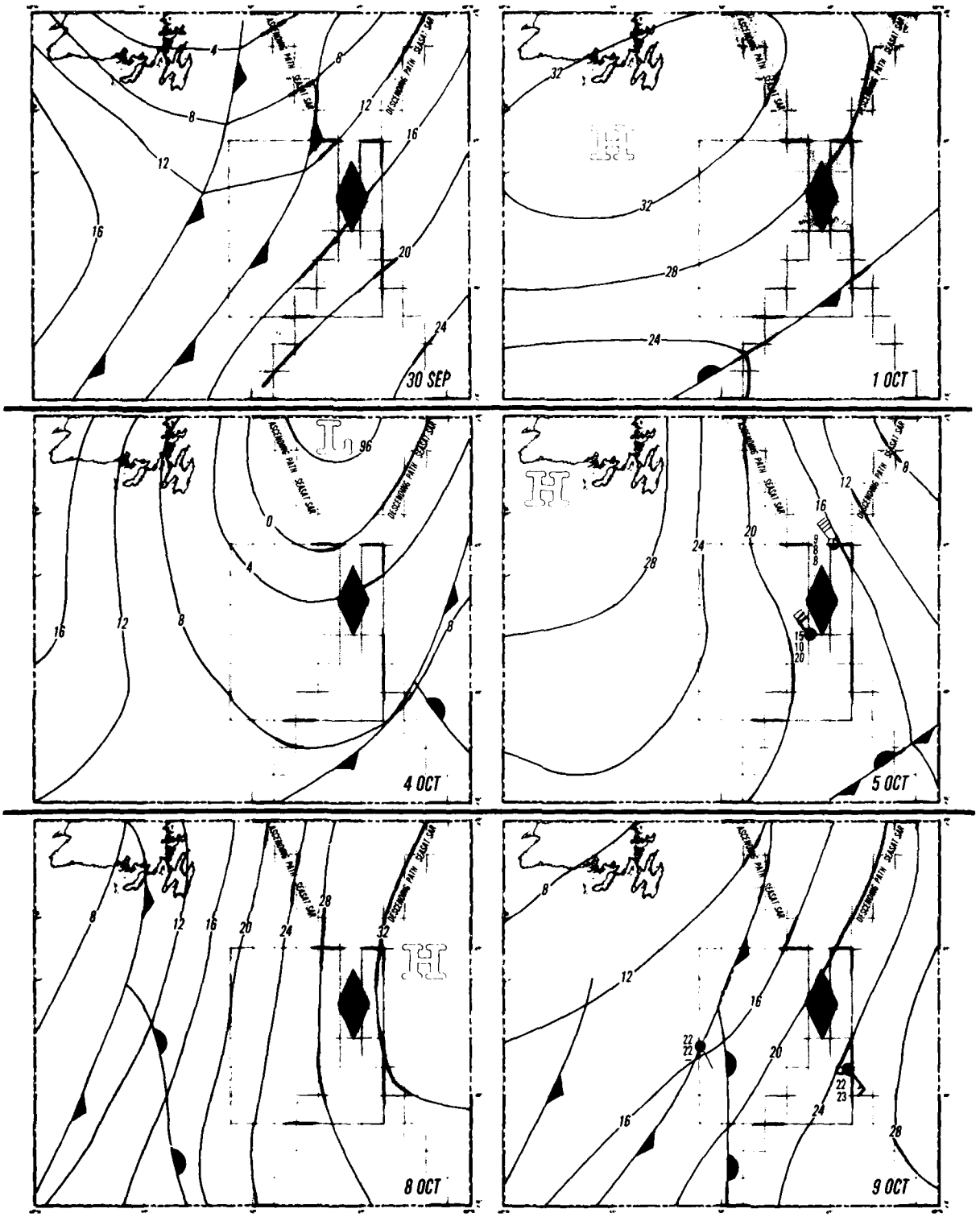
30 SEP
1 OCT
4 OCT
5 OCT
8 OCT
9 OCT
ASCENDING PATH SEASAT SAR
DESCENDING PATH SEASAT SAR

In comparing the descending SAR imagery with the IR imagery of this feature (Figs. 41-43), the correlation of obvious frontal features in the two data sets is usually very good. The average displacement of the SAR with the IR (approximately 25 km) is well within the data location accuracy of the two satellites. The exception occurs in comparing the 4 October IR image to the 3 October SAR image. Here, the southern front in the SAR image for this date is extremely poorly defined; thus, the relation with the corresponding feature in the IR image must also be considered poor. Since the southern front is comparatively well displayed in the next available SAR image--6 October (Fig. 44), it may be inferred that the absence of an obvious frontal demarcation is due to some variation in the current or wind regime.

In comparing the ascending SAR imagery (2 and 5 October) with the IR imagery, no corresponding frontal feature is visible. Indeed, the ascending SAR imagery show no indication of any structure in the area of the Newfoundland Ridge, and the imagery are uniformly specular (although as will be shown the ascending SAR imagery do show frontal features in the area of the Newfoundland Seamounts). This discrepancy is probably due to location errors in the two data sets--an east-west displacement of less than 30 km would allow this to occur. As mentioned earlier, the 2 and 5 October swaths have a proven location error of 13 and 17 km, respectively. Similar errors in the other data sets are probably present.

Although only the SAR imagery for 21 and 30 September and 3 and 6 October are close enough in time to allow direct comparison with the IR imagery, the constant position of the feature allows a limited comparison between the 6 and 9 October SAR image with the 4 October IR image (Fig. 44). This shows a match of location of the northern front in the 9 October image that is similar to the match of the previous SAR-IR imagery. However, approximately 25 km south of the northern front, a sharp variation in σ_o is found that lies in an almost east-west direction. No corresponding feature is shown in the 4 October IR image; since this IR image is the most current available, identification of a possible corresponding thermal feature is impossible. South of this sharp variation is a poorly defined pattern whose southernmost portion matches the location of the southern front in the 4 October IR image.

The direction of the winds were variable during the four days that allow direct SAR-IR comparison. In the area of the Newfoundland Ridge-East feature, the winds were parallel to the northern and southern fronts on two occasions (21 September and 3 October). On 30 September and 6 October, the winds blew essentially across the fronts. The wind speeds were generally greater than 10 m/sec with an exception on 3 October when wind speeds are estimated at 5 m/sec.

B. Newfoundland Ridge-West Feature

The westernmost Newfoundland Ridge feature is visible only in the 21, 26 and 29 September IR imagery (Figs. 45 and 46). The 26 September IR image (not presented) shows the feature still in position, thus providing continuity between the 21 and 29 September IR imagery. However, the 29 September IR image shows a definite weakening of the thermal gradients associated with the feature. The region was cloud-covered on 2 October. On 4 October, when the region became comparatively less cloudy, the IR image shows no indication of a cold feature.

For comparison with these IR imagery, the best of the SAR imagery is that of 21 September. The location correlation for this SAR image and the IR image is very good (Fig. 45). On the other hand, the location correlation of the 29 and 30 September SAR and IR imagery is very poor (Fig. 46). In this latter comparison the tip of the main feature in the SAR-IR imagery matches well, but the SAR image shows a poorly delineated area of

roughness in the southern portion of the image that does not match a corresponding thermal feature in the 29 September IR image. However, the area of roughness does match the IR feature in the 21 September IR image. In fact, the SAR imagery for the western ridge feature for 3 6, and 9 October also show roughness patterns that correspond in general location with the cold IR feature on 21 September. All these SAR imagery show roughness patterns similar to that of 30 September, and it is difficult to draw a line on any image that denotes exactly where the thermal feature begins. However, the general region in each SAR imagery that corresponds to the location of the thermal feature of 21 September are areas of obvious σ_0 change.

The wind speed for both 21 and 30 September was 10 m/sec. The direction in relation to the thermal fronts of the feature is interesting. Unlike the linear features shown in the SAR imagery of the Newfoundland Ridge-East feature, the frontal features in these two SAR imagery are curved. Thus, the effects of essentially constant winds blowing at different angles to the front can be observed.

C. New Foundland Seamount Feature

During 21 September-4 October, the thermal feature lying over the Newfoundland Seamounts had the most horizontal movement of the three ocean features (Fig. 38). The IR images for the period 29 September-4 October are spaced closely enough in time so that the relative movement of the feature can be measured. These measurements show that a relative translation of 100 km took place toward the east in the six-day period. In addition, the relative displacement of the feature appears to have been 30 km to the south between 29 September and 2 October. Examination of the cold features located in the IR image for 21 and 29 September show that the general movement was too great to do more than generally indicate that the thermal structure on 21 September is genetically related to the thermal structure on 29 September. (The 26 September IR image was cloud covered in the region of the Seamounts and could not provide continuity between the 21 and 29 September images.)

In comparing the SAR imagery and IR imagery, the most unusual match is that shown for 21 September (Fig. 47). In all the SAR/IR comparisons made for this study, this is the one occasion that does not appear to relate to another. This data set is further discussed in the discussion section.

The remaining SAR imagery of the Newfoundland Seamounts area show good correlation with the IR imagery, with the best defined front displayed in the SAR image for 30 September (Fig. 48). The SAR imagery for 2 and 3 October show a general frontal region rather than a well-defined front (Fig. 49). The SAR imagery for 5 and 6 October show only a very general correlation with the IR image for 2 and 4 October (Fig. 50). The 5 and 6 October imagery have linear features which, because of their location, may be regarded as resulting from shear action at the front. Since the 4 October IR image is cloud covered in the area of the SAR data swath, features in the SAR imagery for 5 and 6 October must be compared to thermal features in the 2 October IR image. Figure 50 shows both locations in the drawing while presenting only the 4 October IR image. The apparent offset of the SAR delineations of the thermal front in Figures 49 and 50 are easily corrected with an error of less than 5 km by moving the SAR swath to the east using the location corrections mentioned earlier.

Wind conditions derived from the weather charts and ship reports show that winds were normally strong--10 m/sec or greater. The exception was 3 October when the wind speed in the area of the Seamounts averaged 7 m/sec.

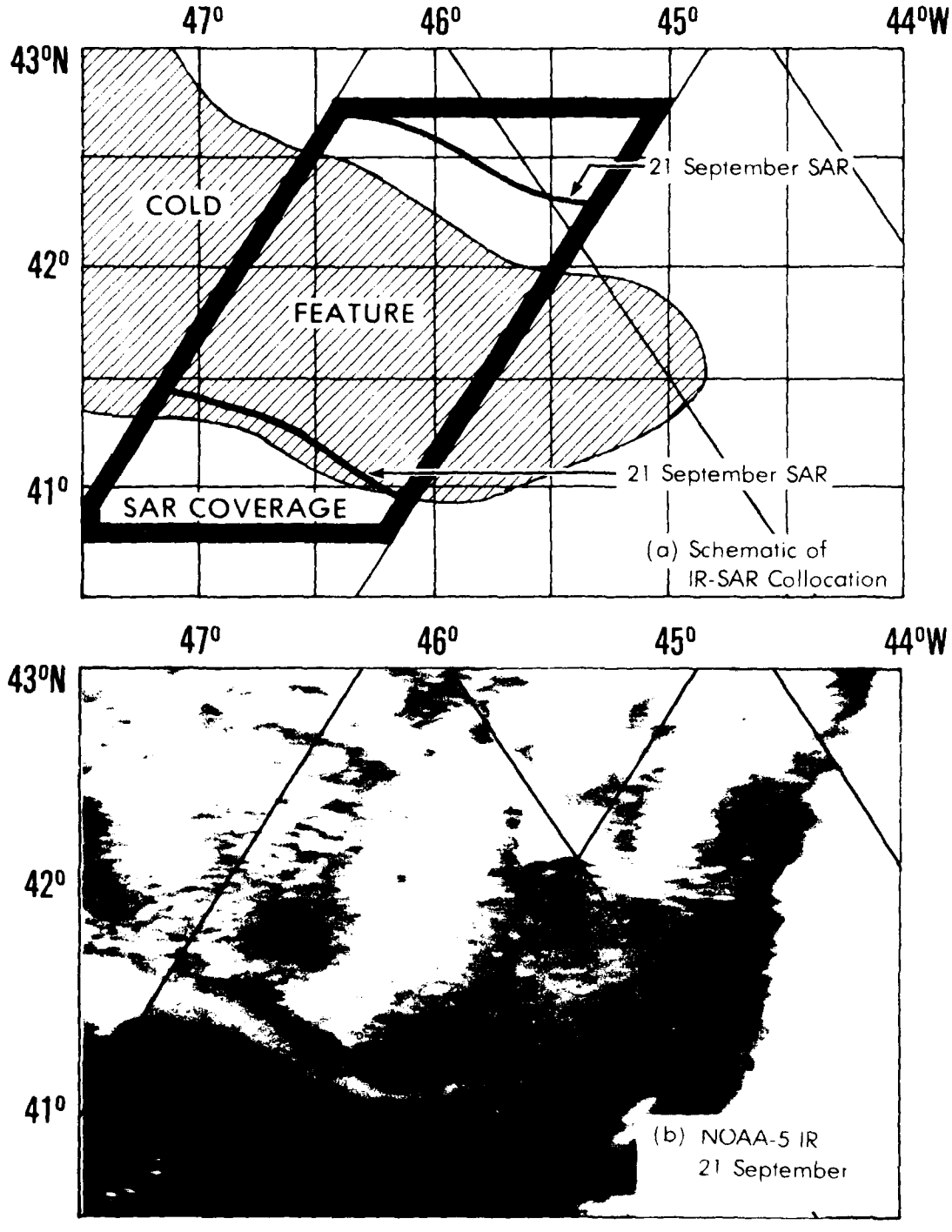

Figure 41. The SAR and infrared imagery for the Newfoundland Ridge-East feature for 21 September 1978. The schematic shows the SAR frontal definition (heavy line) for 21 September overlain on the area of the cold water (zipped pattern) for 21 September.

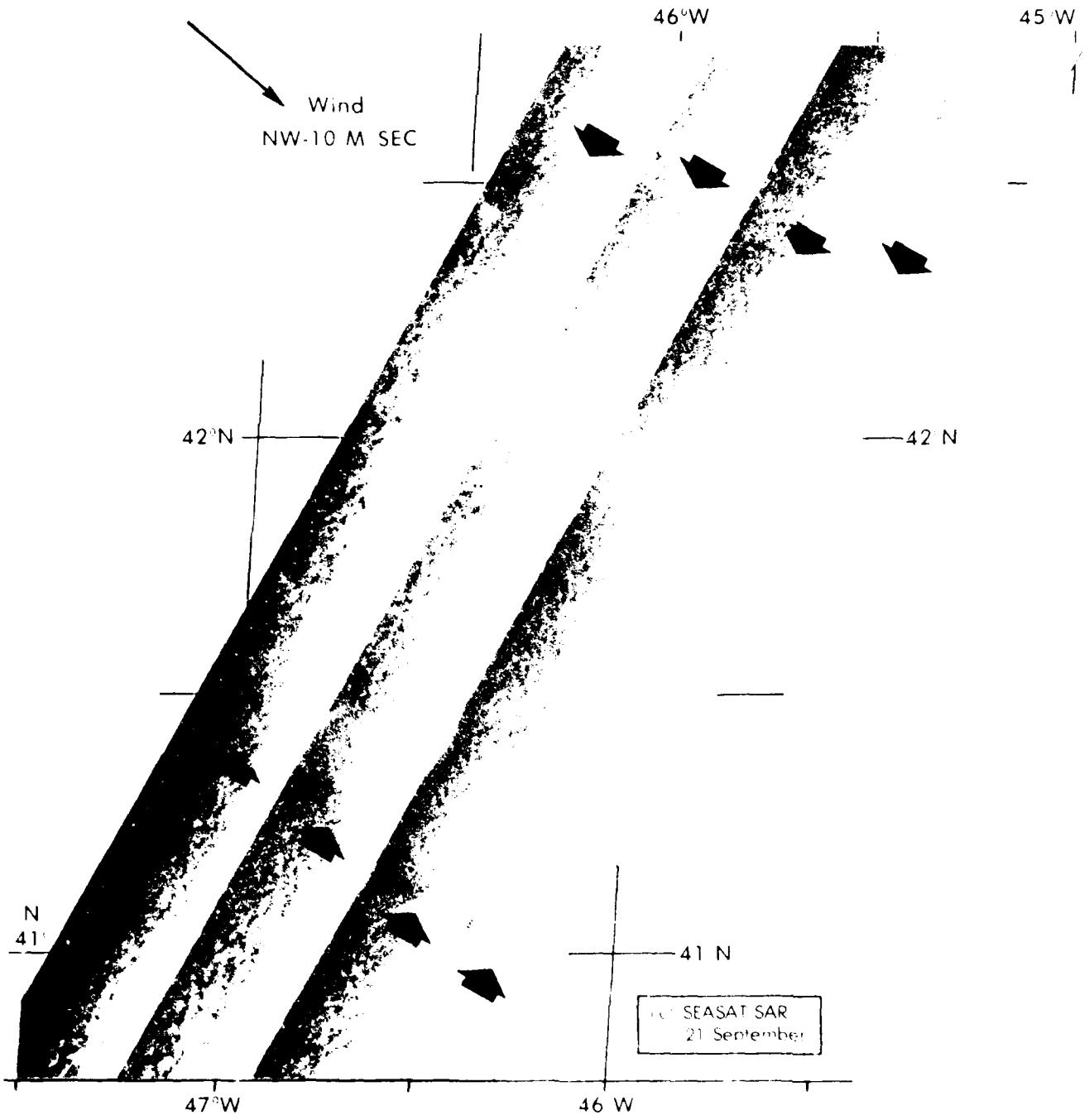
46°W
45°W
Wind
NW-10 M SEC
42°N
42 N
41 N
47°W
46 W
SEASAT SAR
21 September

AD-A136 181 THE GRAND BANKS EXPERIMENT: A SATELLITE/AIRCRAFT/SHIP EXPERIMENT TO EXPLO..(U) NAVAL OCEAN RESEARCH AND DEVELOPMENT ACTIVITY NSTL STATION MS.. P E LA VIOLETTE

2/2

UNCLASSIFIED JUL 83 NORDA-49 F/G 17/9 NL

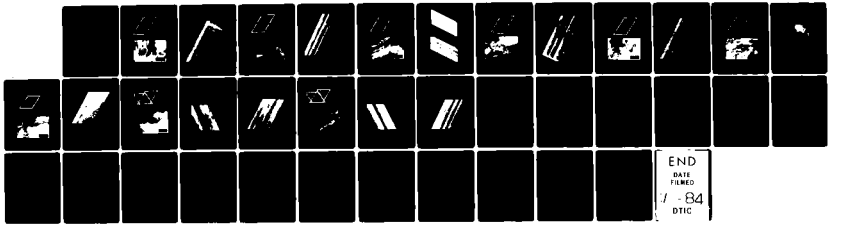

END
DATE FILMED
1-84
DTIC

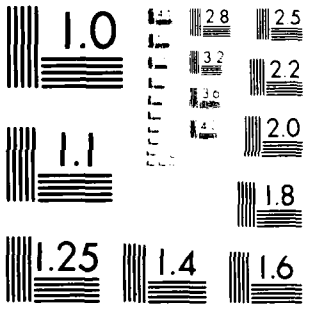

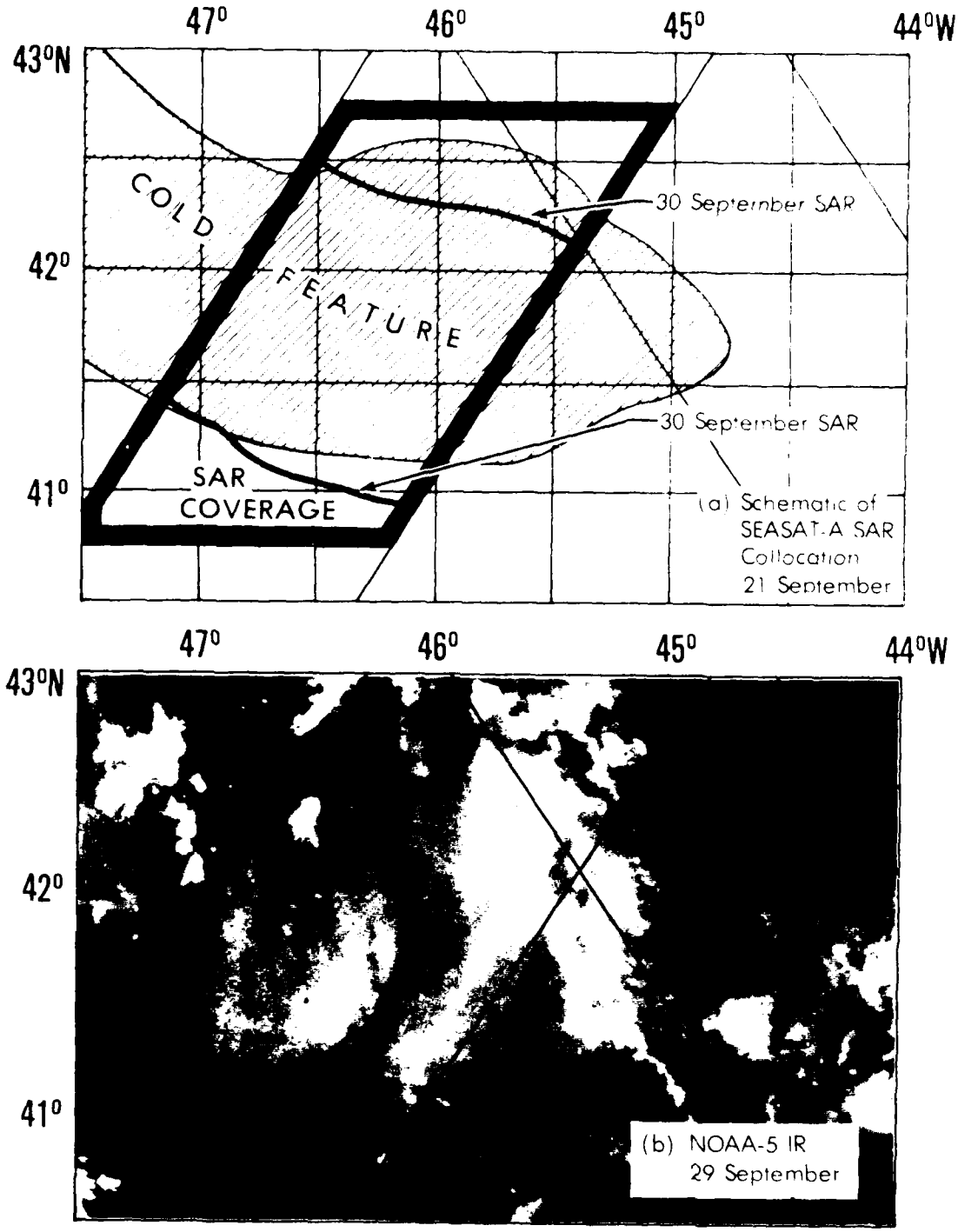

Figure 42. The SAR and infrared imagery for the Newfoundland Ridge East feature for 21 September 1978.

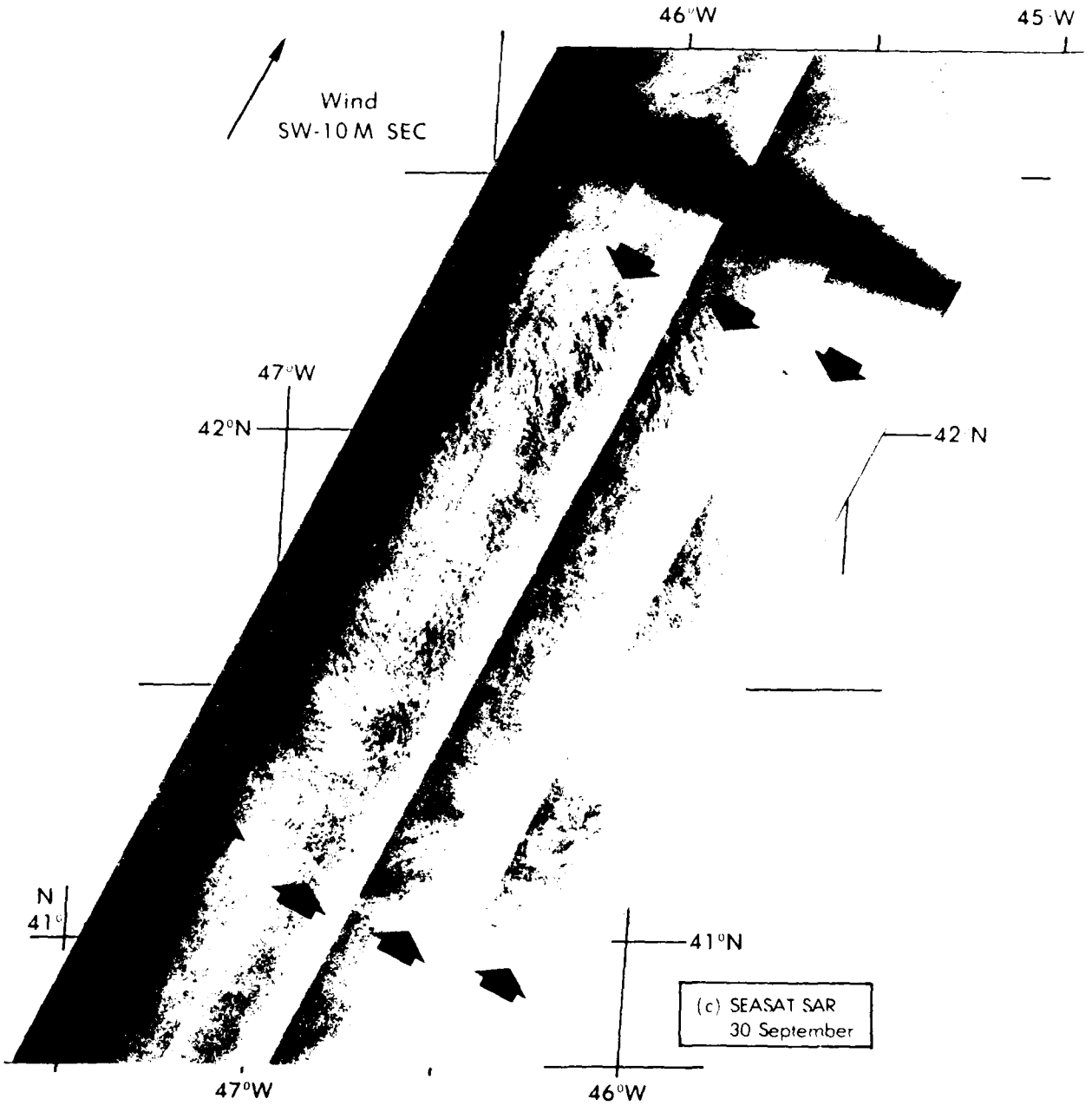
46°W
45 W
Wind
SW-10 M SEC
47°W
42°N
42 N
N
41°
41°N
(c) SEASAT SAR
30 September
47°W
46°W

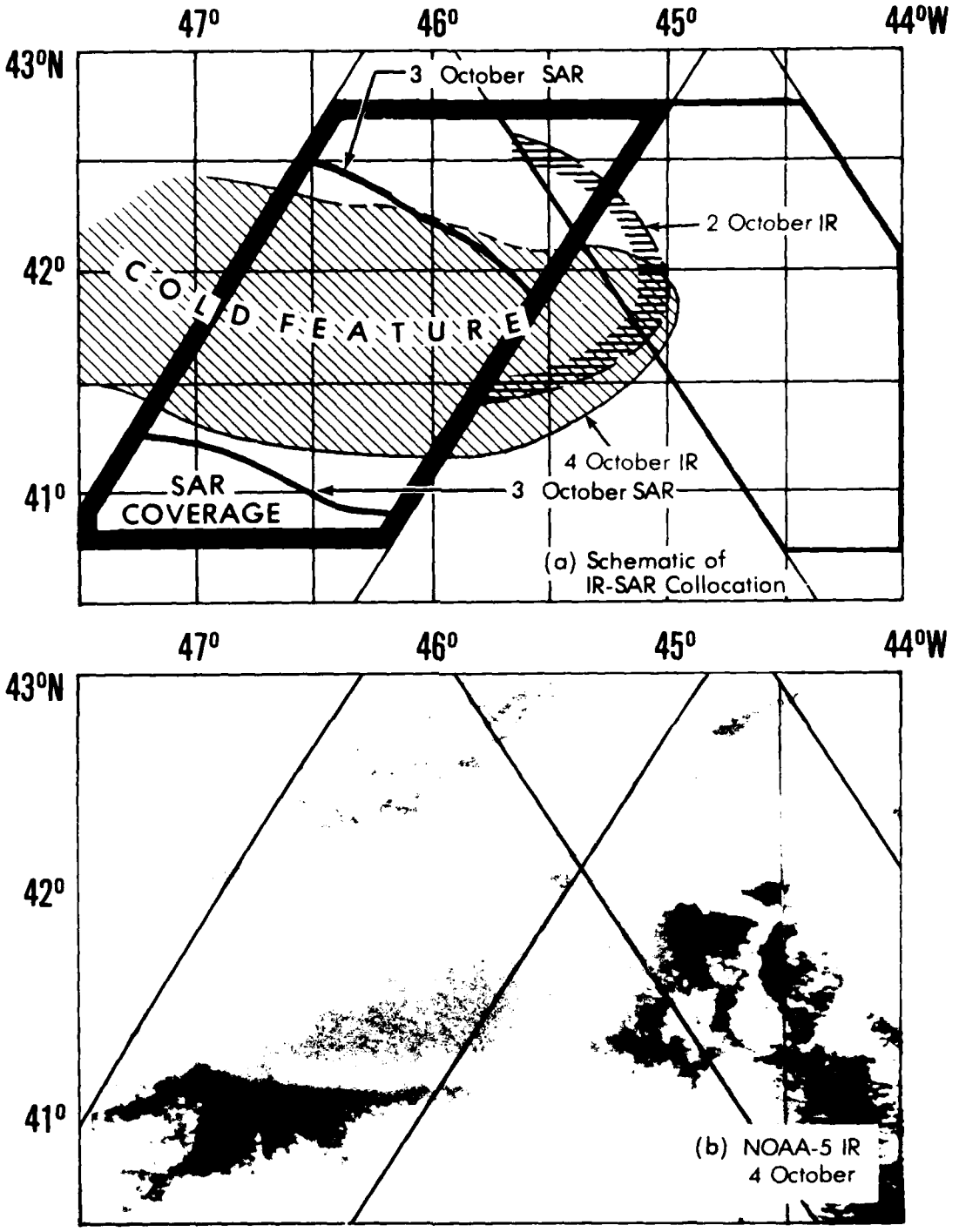

Figure 43. The SAR and infrared imagery for the Newfoundland Ridge-East feature for 2-4 October 1978. The schematic shows the SAR frontal definition (heavy line) for 3 October overlain on the area of the cold water (zipped patterns) for 2 and 4 October. Since the swath area of the SAR was cloud-covered on 2 October only the IR image for 4 October is shown.

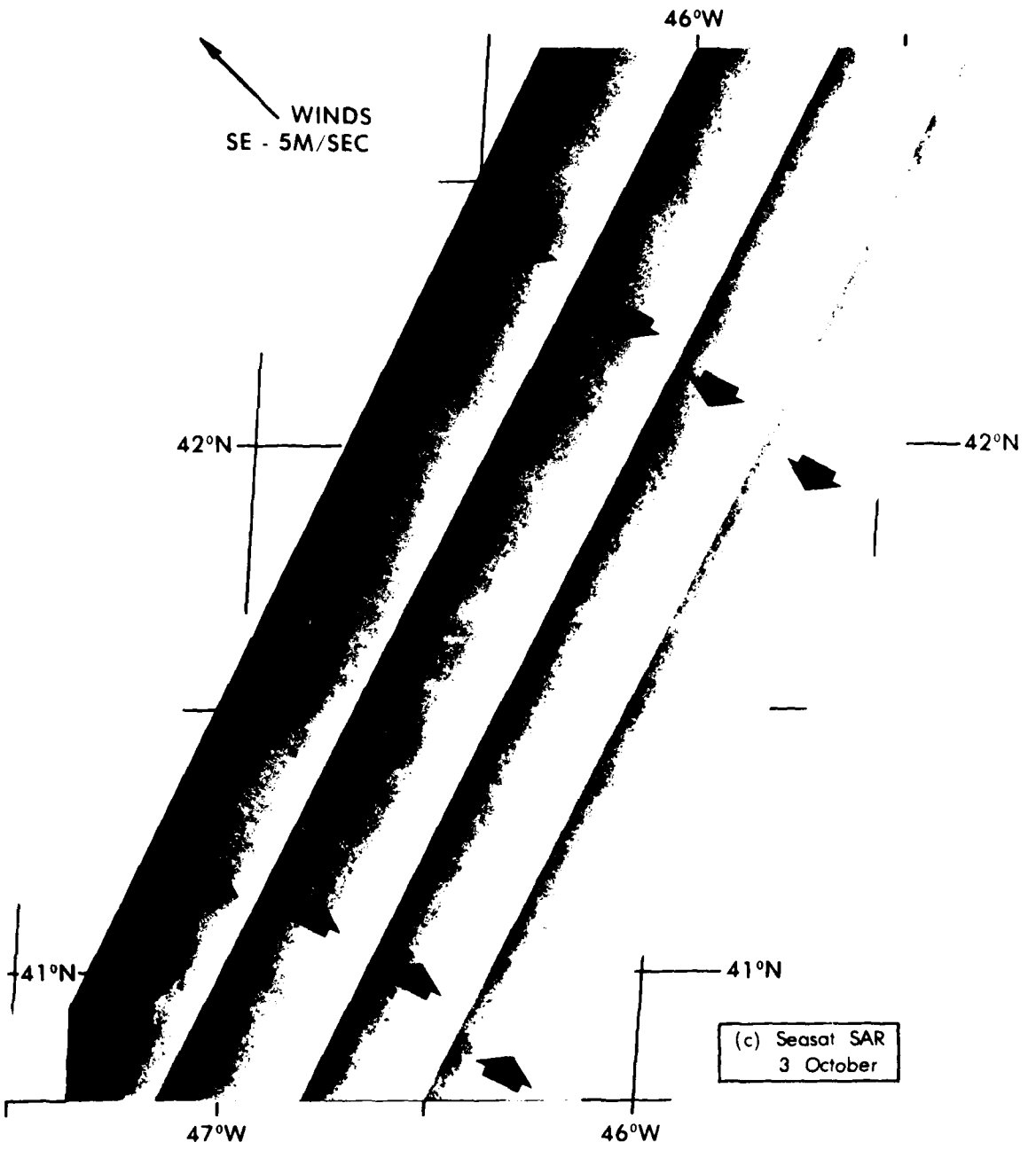
46°W
45°W
WINDS
SE - 5M/SEC
42°N
42°N
41°N
41°N
47°W
46°W
(c) Seasat SAR
3 October

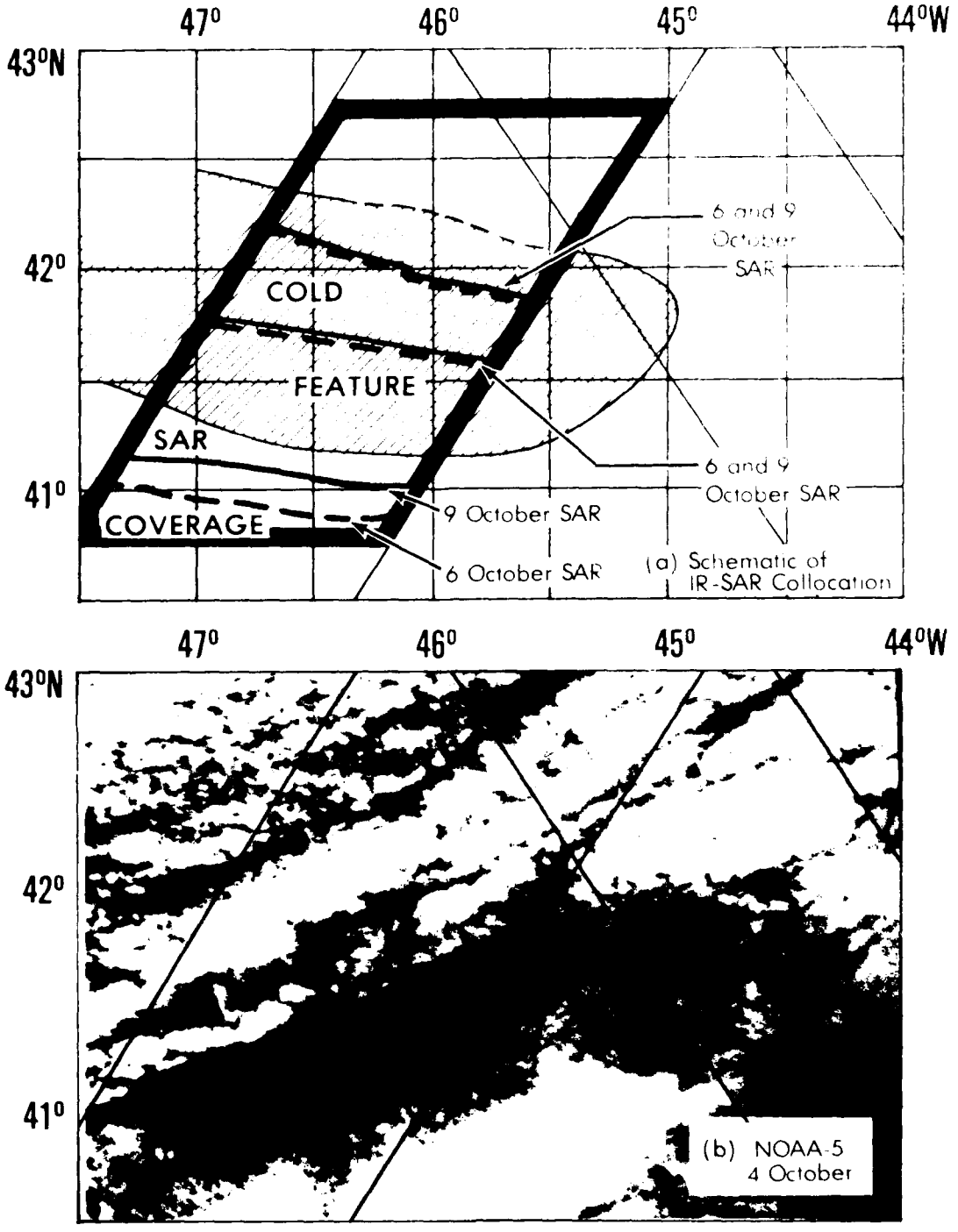

Figure 44. The SAR and infrared imagery for the Newfoundland Ridge East feature for 4, 6, and 9 October 1978. The schematic shows the SAR frontal definitions (heavy line) for 6 and 9 October overlain on the area of the cold water (zipped pattern) for 4 October.

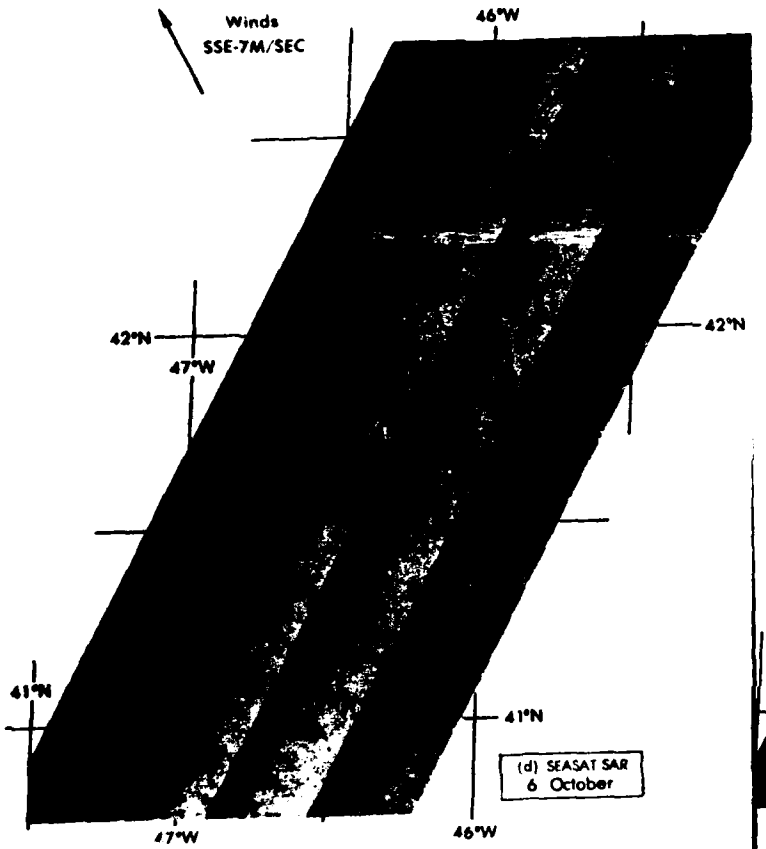
Winds
SSE-7M/SEC
46°W
42°N
47°W
42°N
41°N
41°N
47°W
46°W
(d) SEASAT SAR
6 October

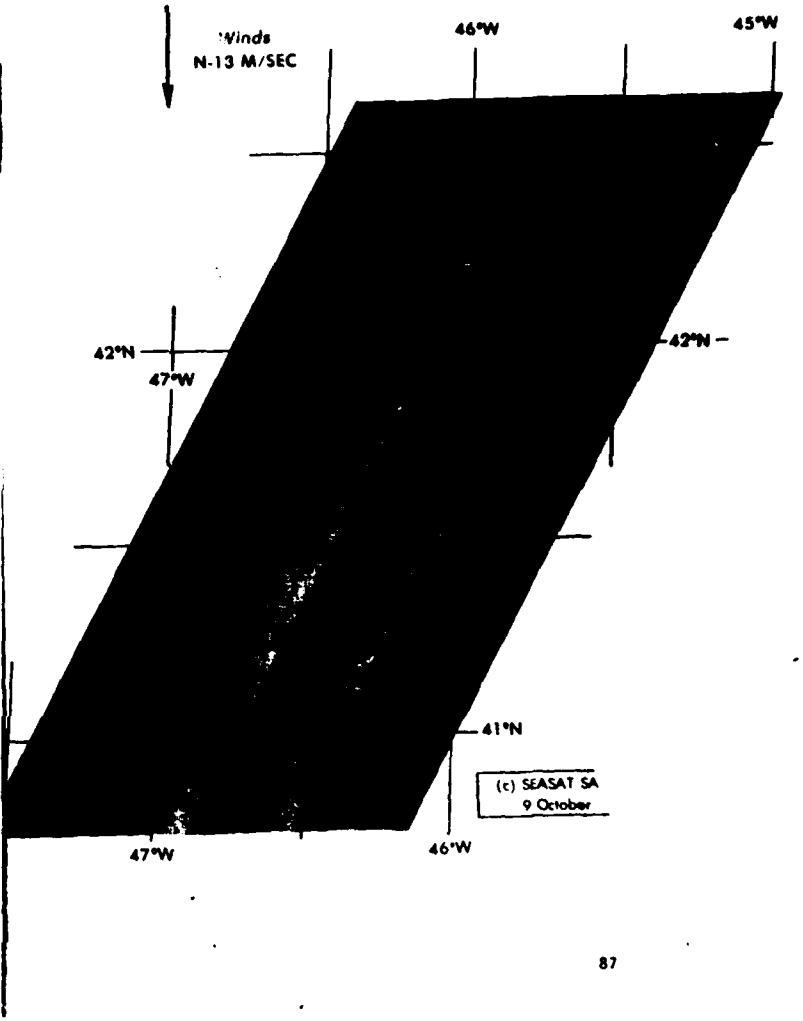
Winds
N-13 M/SEC
46°W
45°W
42°N
47°W
42°N
41°N
47°W
46°W
(c) SEASAT SA
9 October

Pg. 87

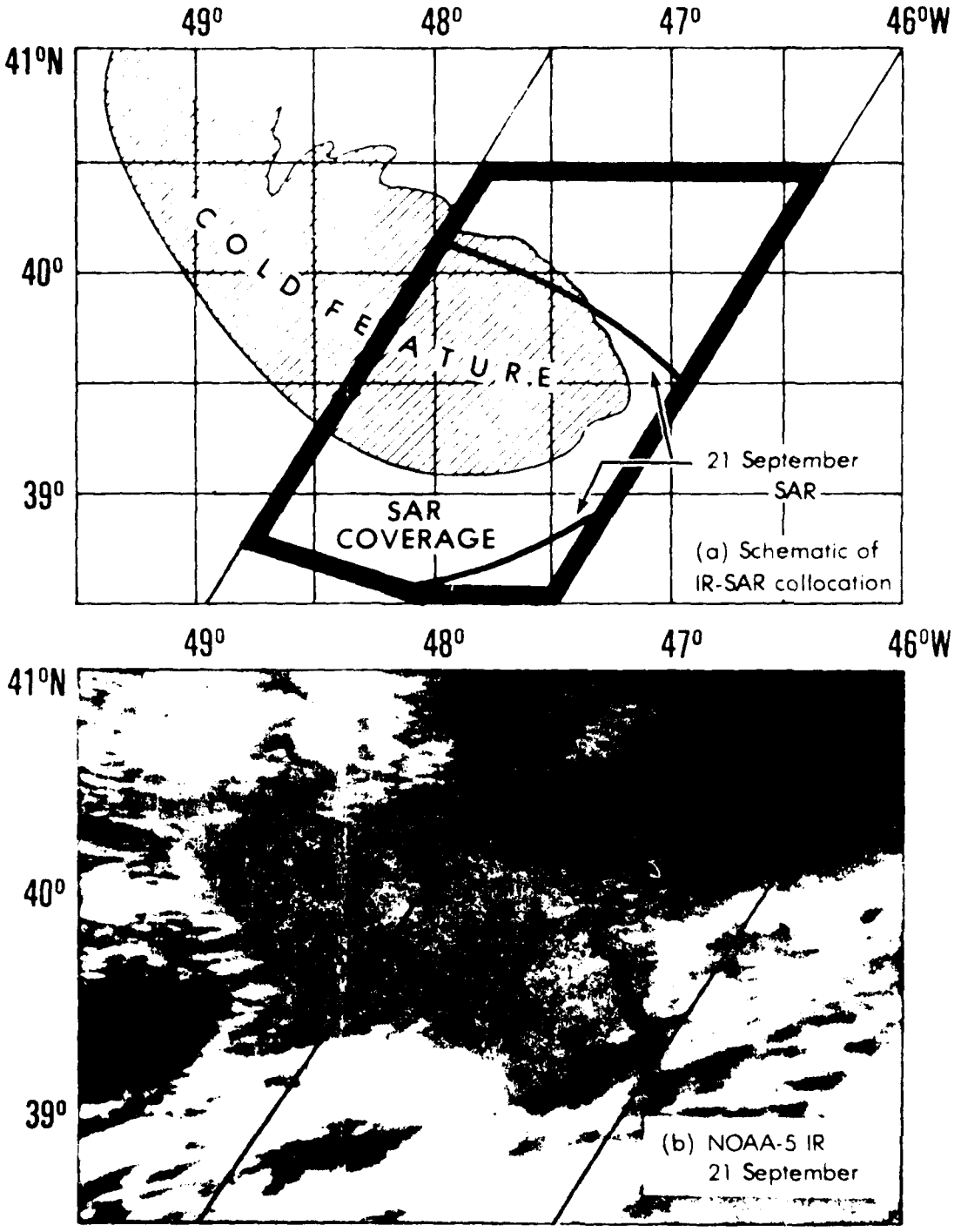

Figure 45. The SAR and infrared imagery for the Newfoundland Ridge-West feature for 21 September 1978. The schematic shows the SAR frontal definition (heavy line) for 21 September overlain on the area of the cold water (zipped pattern) for 21 September.

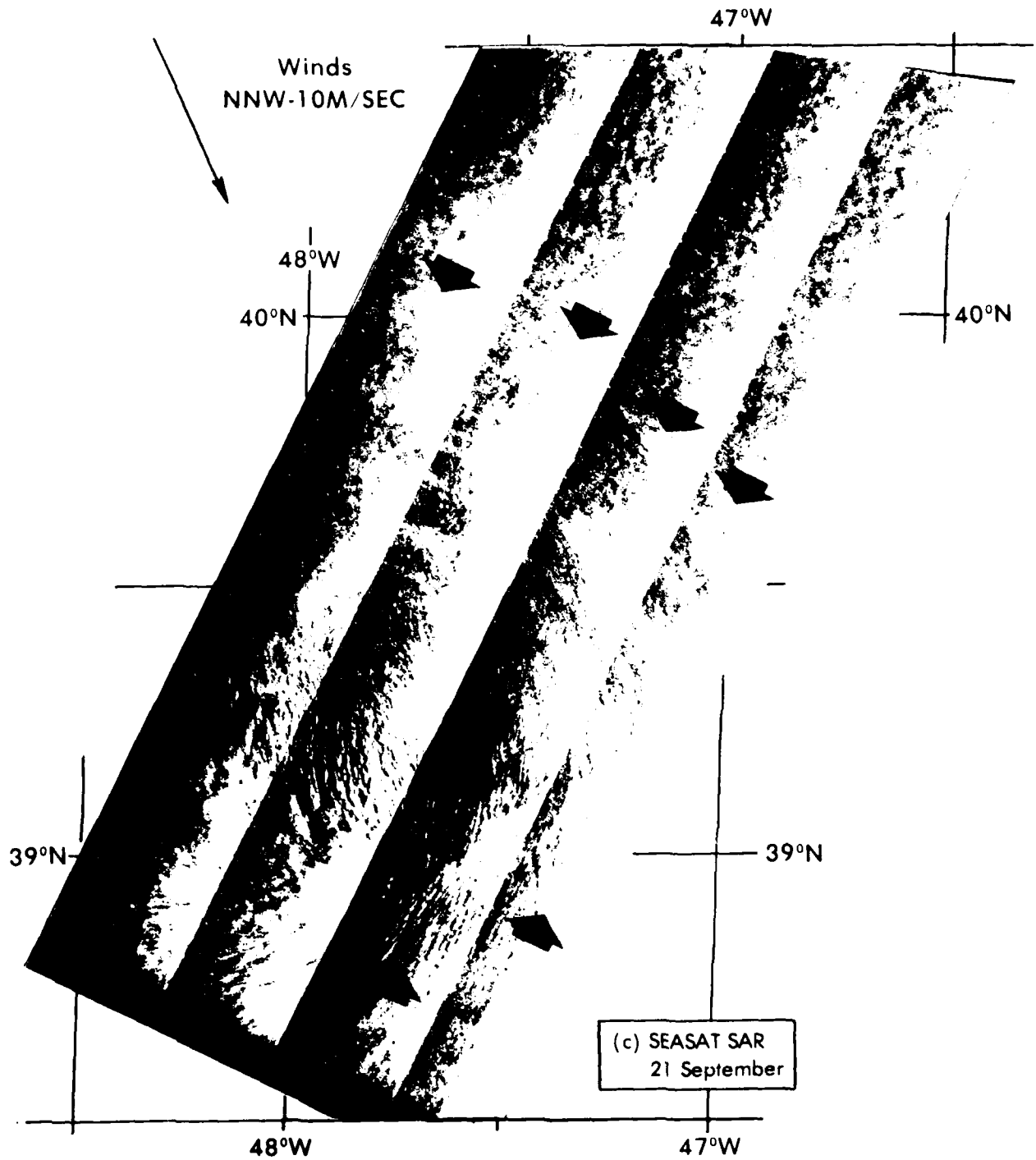
47°W
Winds
NNW-10M/SEC
48°W
40°N
40°N
39°N
39°N
(c) SEASAT SAR
21 September
48°W
47°W

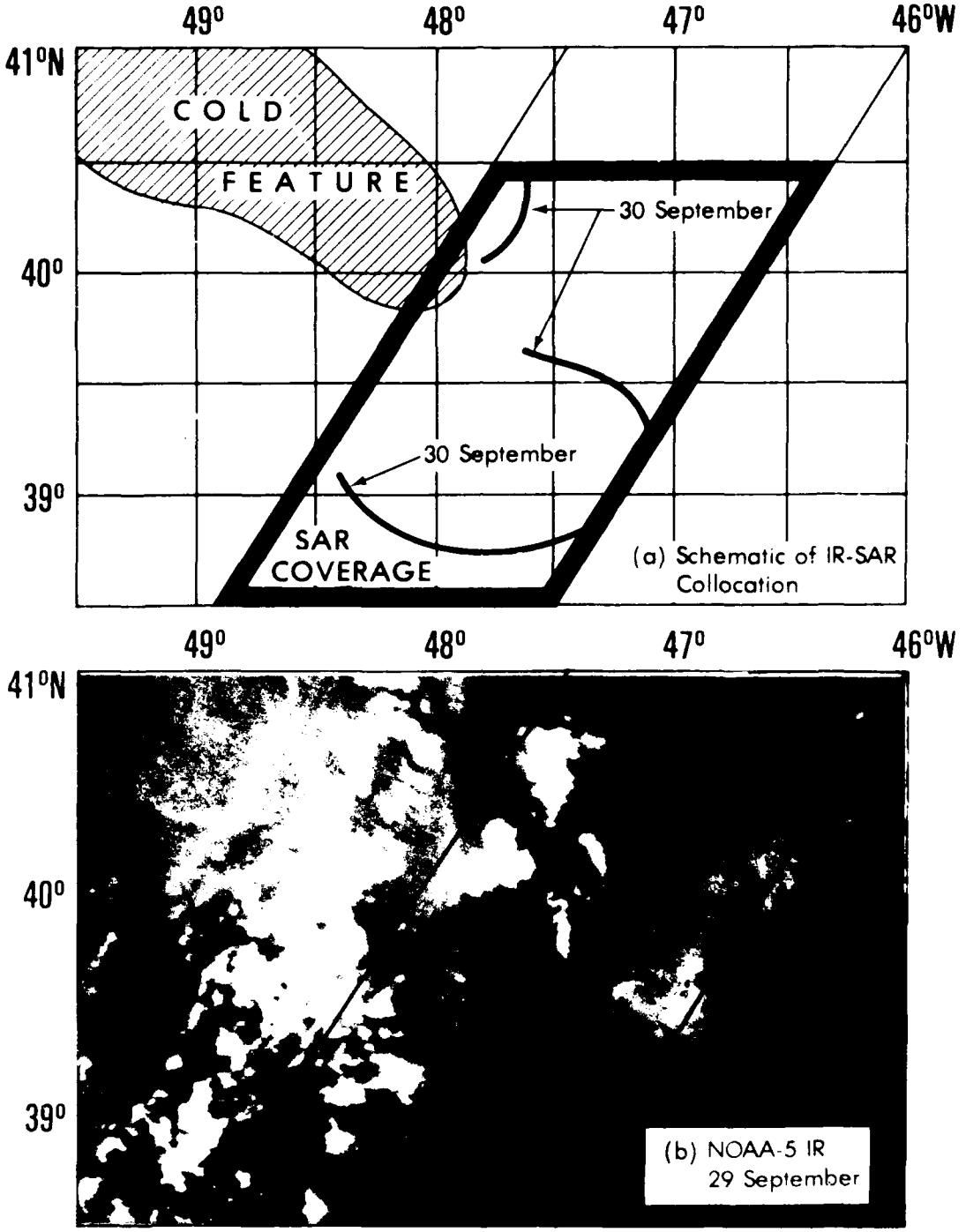

Figure 46. The SAR and infrared imagery for the Newfoundland-West feature for 29 and 30 September 1978. The schematic shows the SAR frontal definition (heavy line) for 30 September overlain on the area of the cold water (zipped pattern) for 29 September.

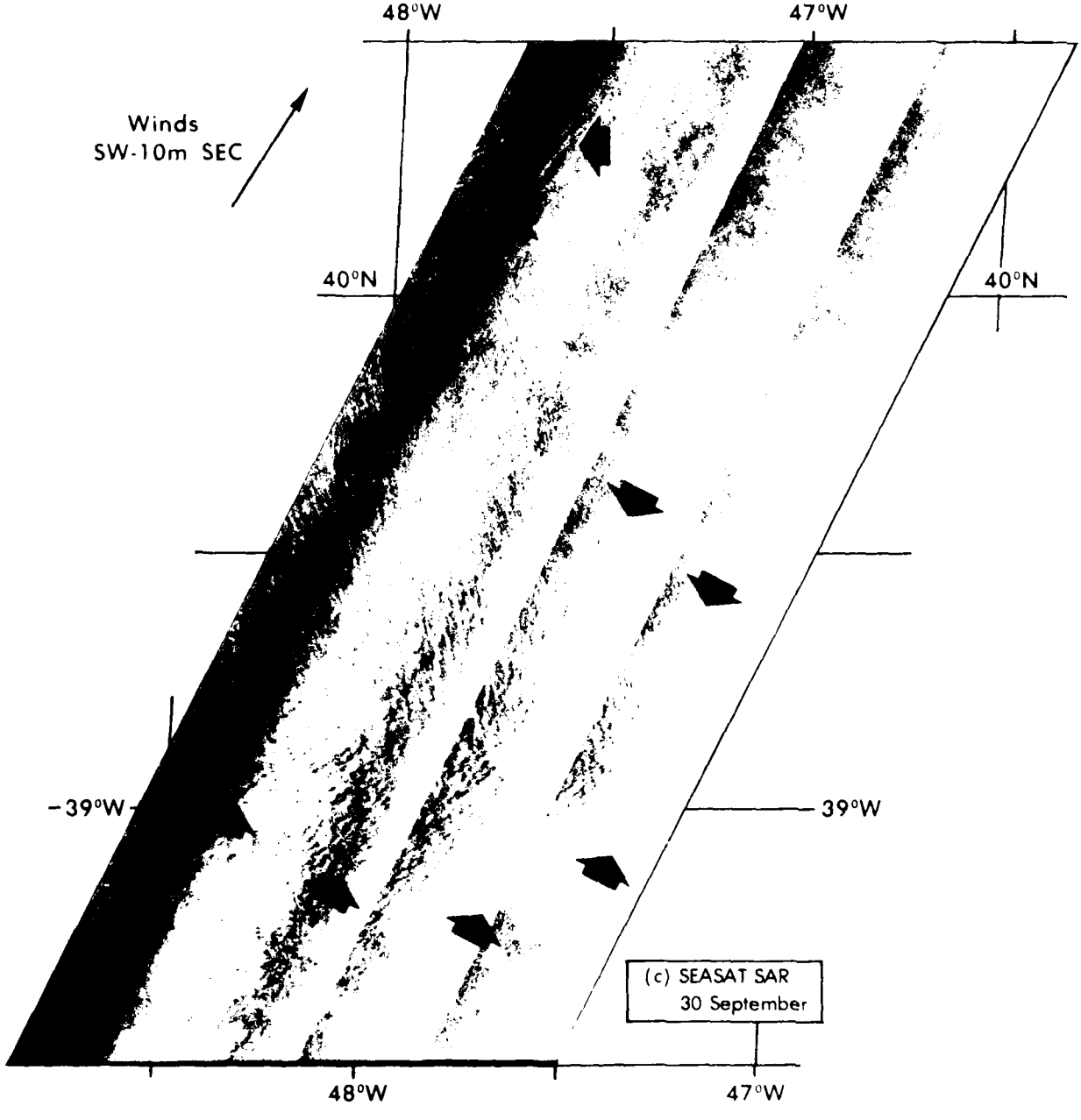
48°W
47°W
Winds
SW-10m SEC
40°N
40°N
39°W
39°W
(c) SEASAT SAR
30 September
48°W
47°W

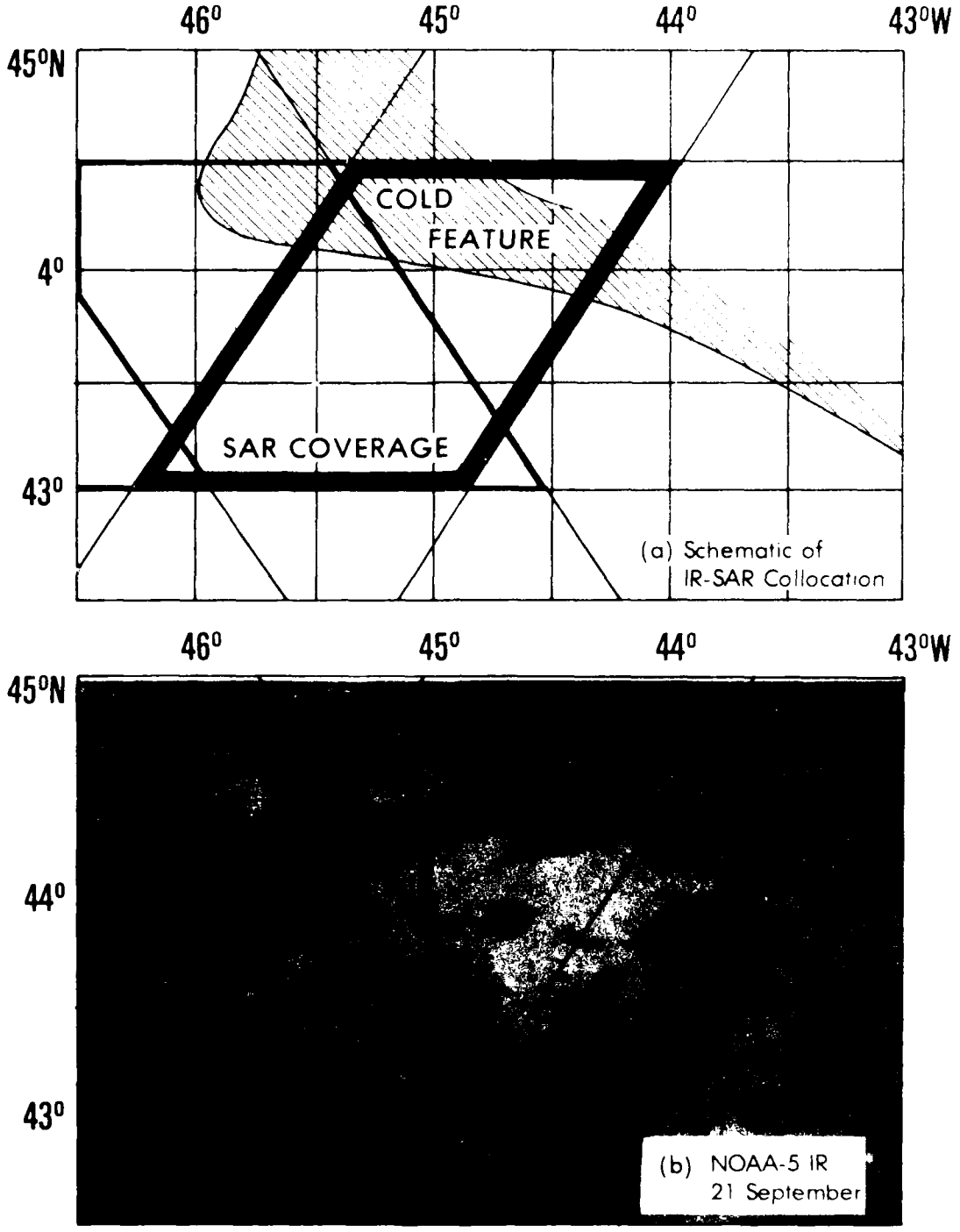

Figure 47. The SAR and infrared imagery for the Newfoundland Seamounts for 21 September 1978. The schematic shows the area of the cold water only. No definable structure (such as seen in the other SAR imagery) is visible in the SAR image of this area.

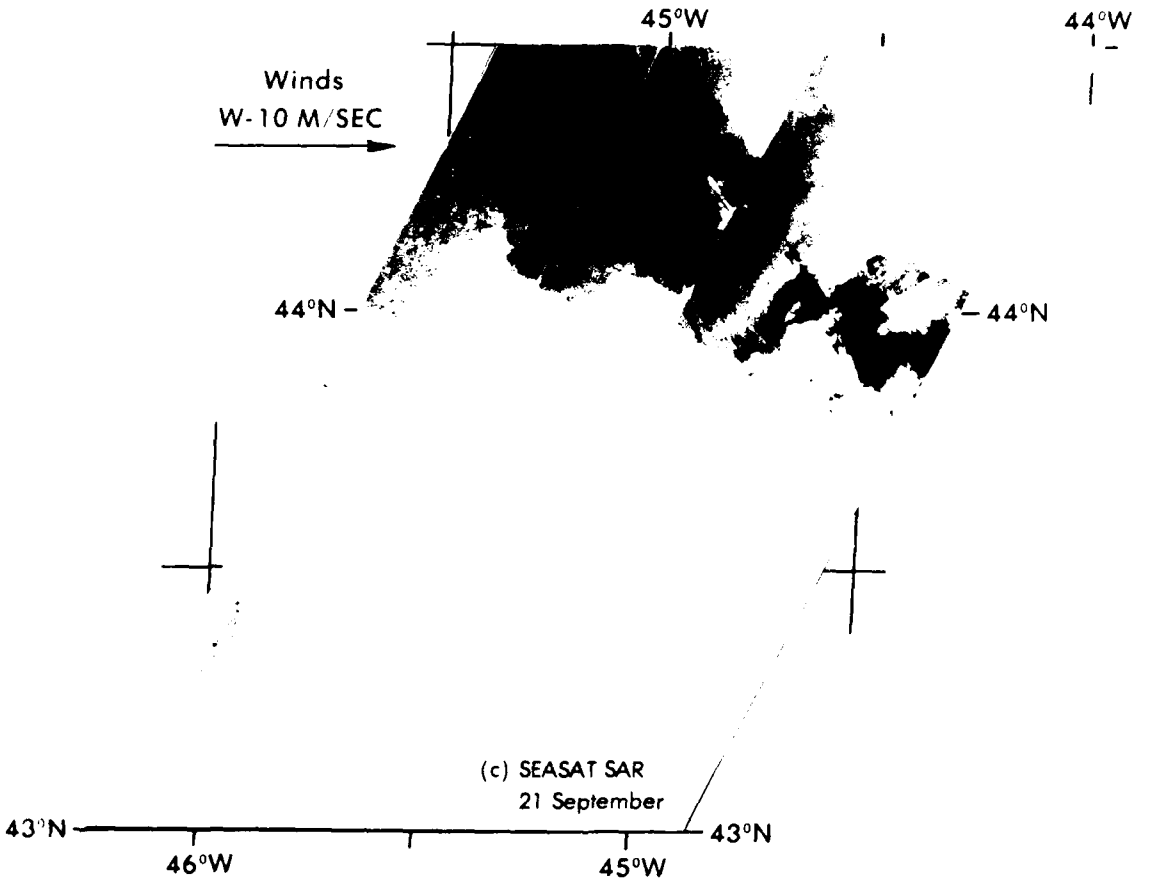
45°W
44°W
Winds
W-10 M/SEC
44°N
44°N
(c) SEASAT SAR
21 September
43°N
43°N
46°W
45°W

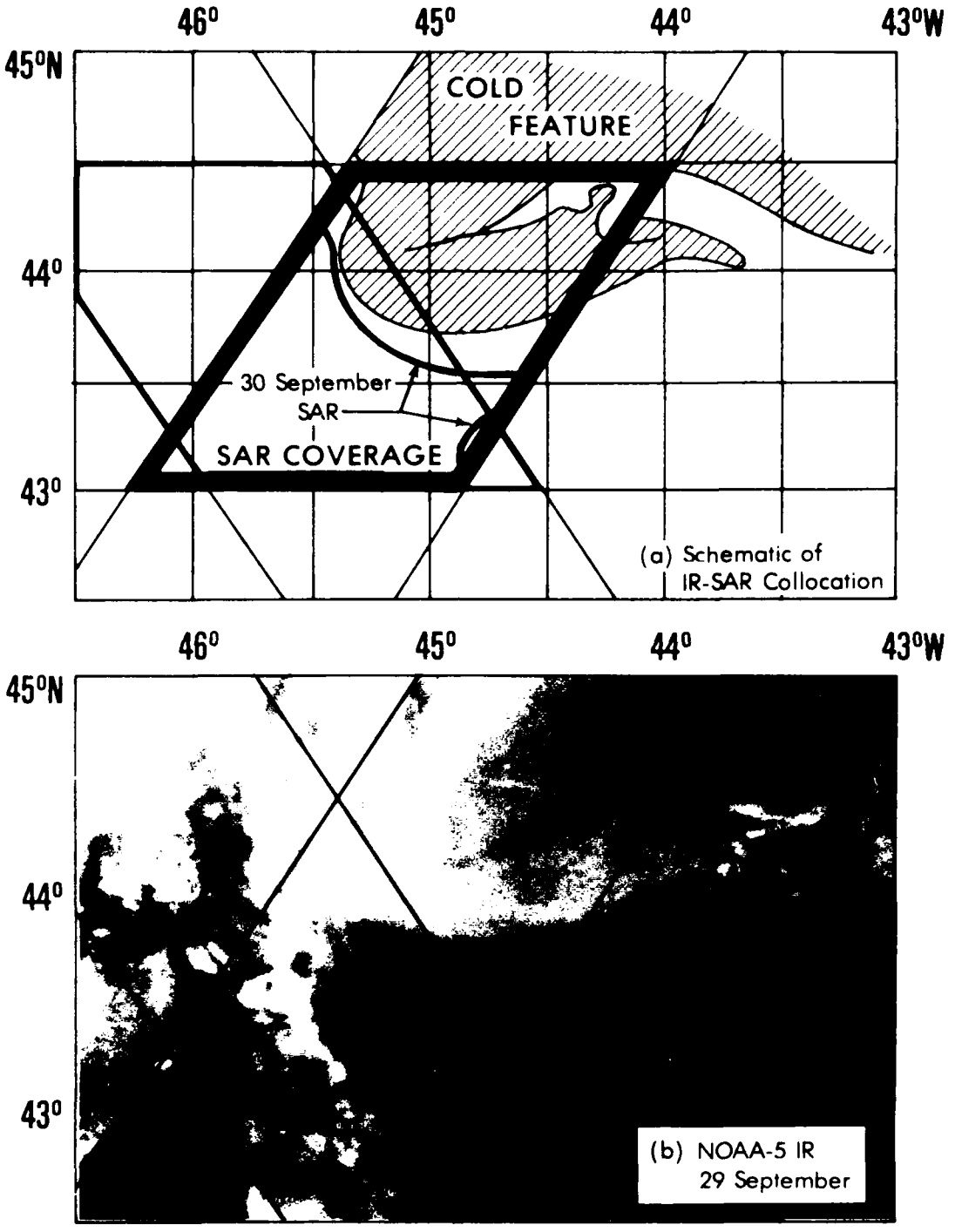

Figure 48. The SAR and infrared imagery for the Newfoundland Seamounts for 29 and 30 September 1978. The schematic shows the SAR frontal defination (heavy line) for 30 September overlain on the area of the cold water (zipped pattern) for 29 September.

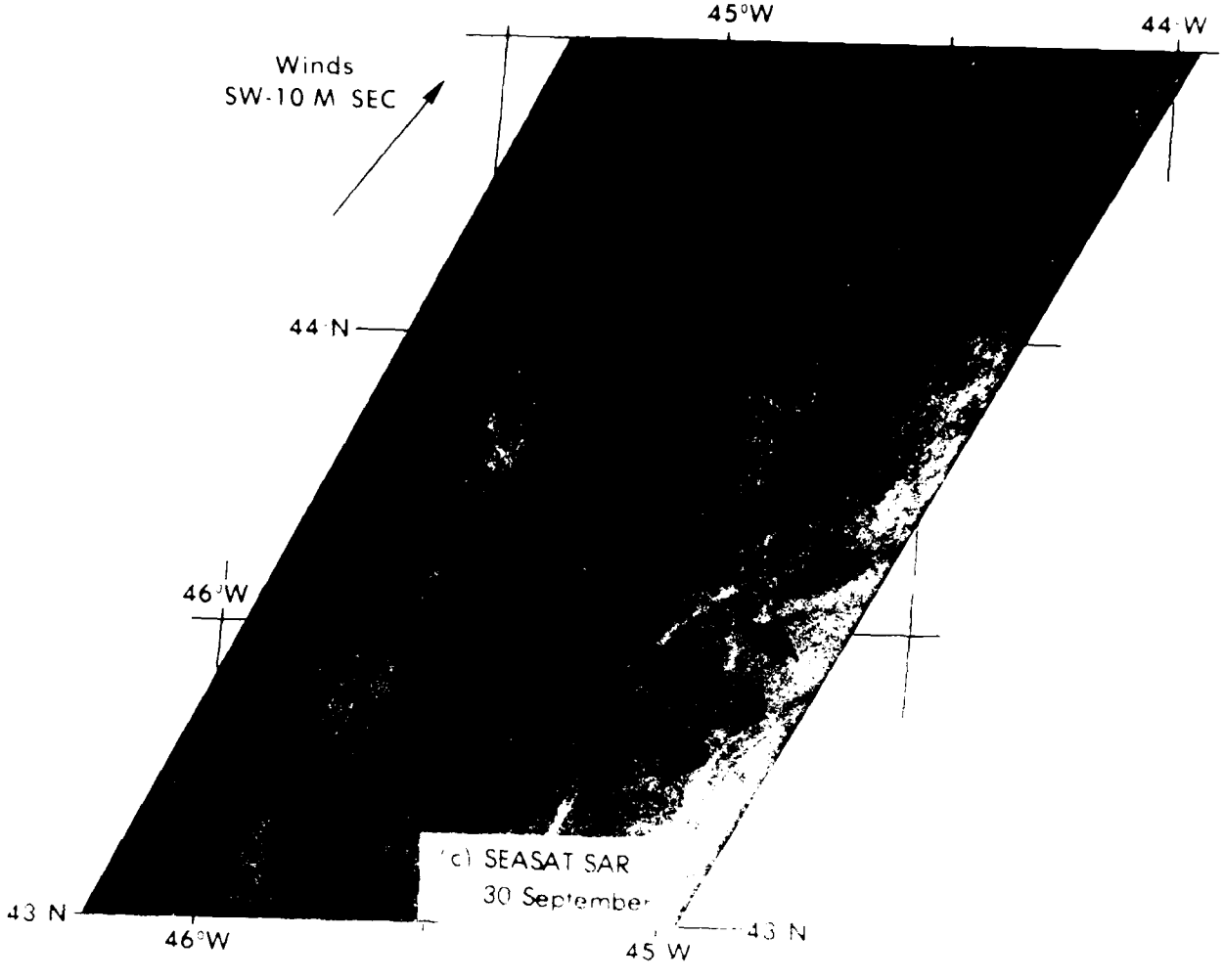

(c) SEASAT SAR
30 September

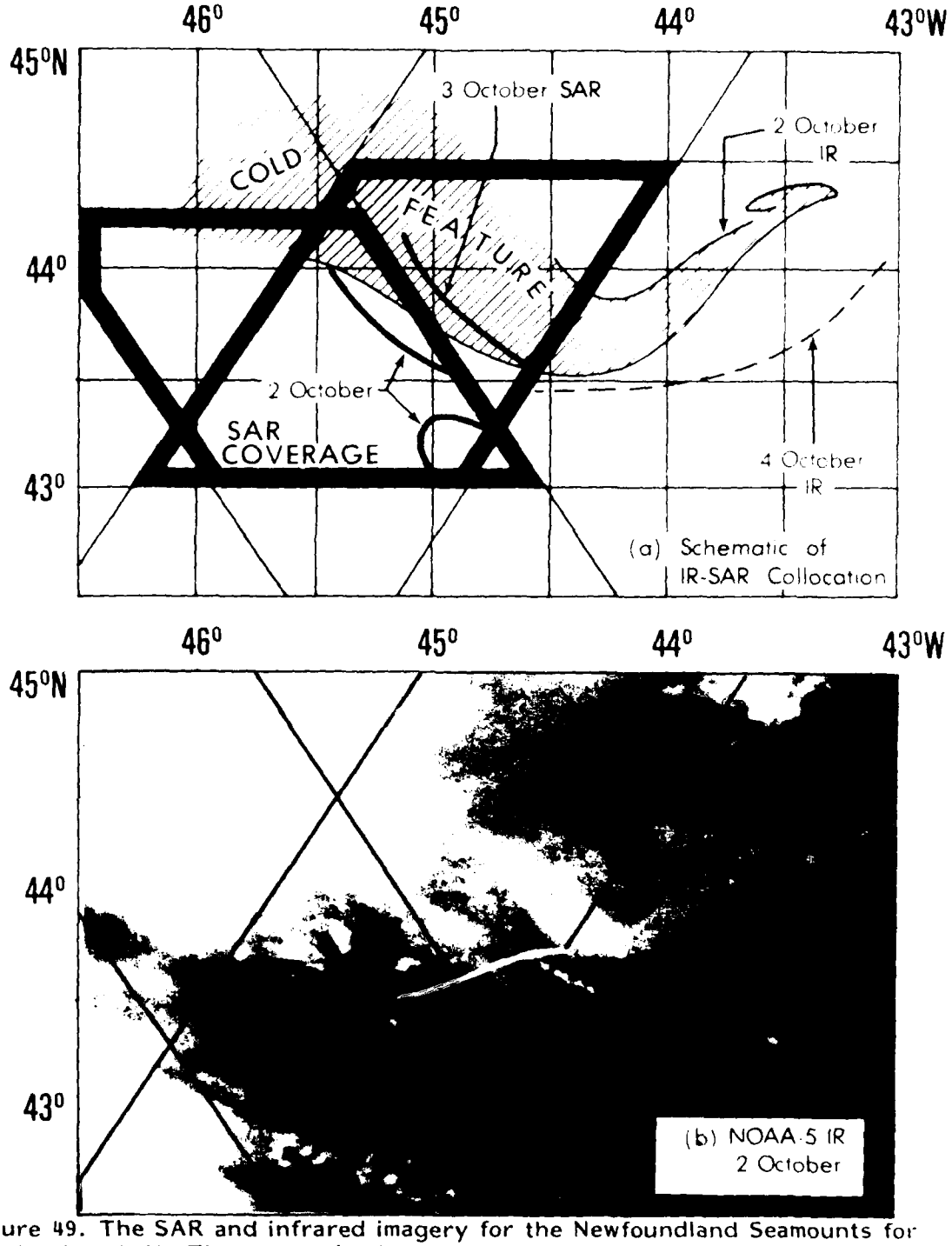

Figure 49. The SAR and infrared imagery for the Newfoundland Seamounts for 2-4 October 1978. The schematic shows the SAR frontal definitions (heavy lines) for 2 and 3 October overlain on the cold water (zipped pattern) for 2 October. Since the swath area of the SAR was cloud covered on 4 October only the 2 October IR image is shown and the 4 October IR area is shown as a dashed line on the schematic. None of the SAR imagery registration have been corrected.

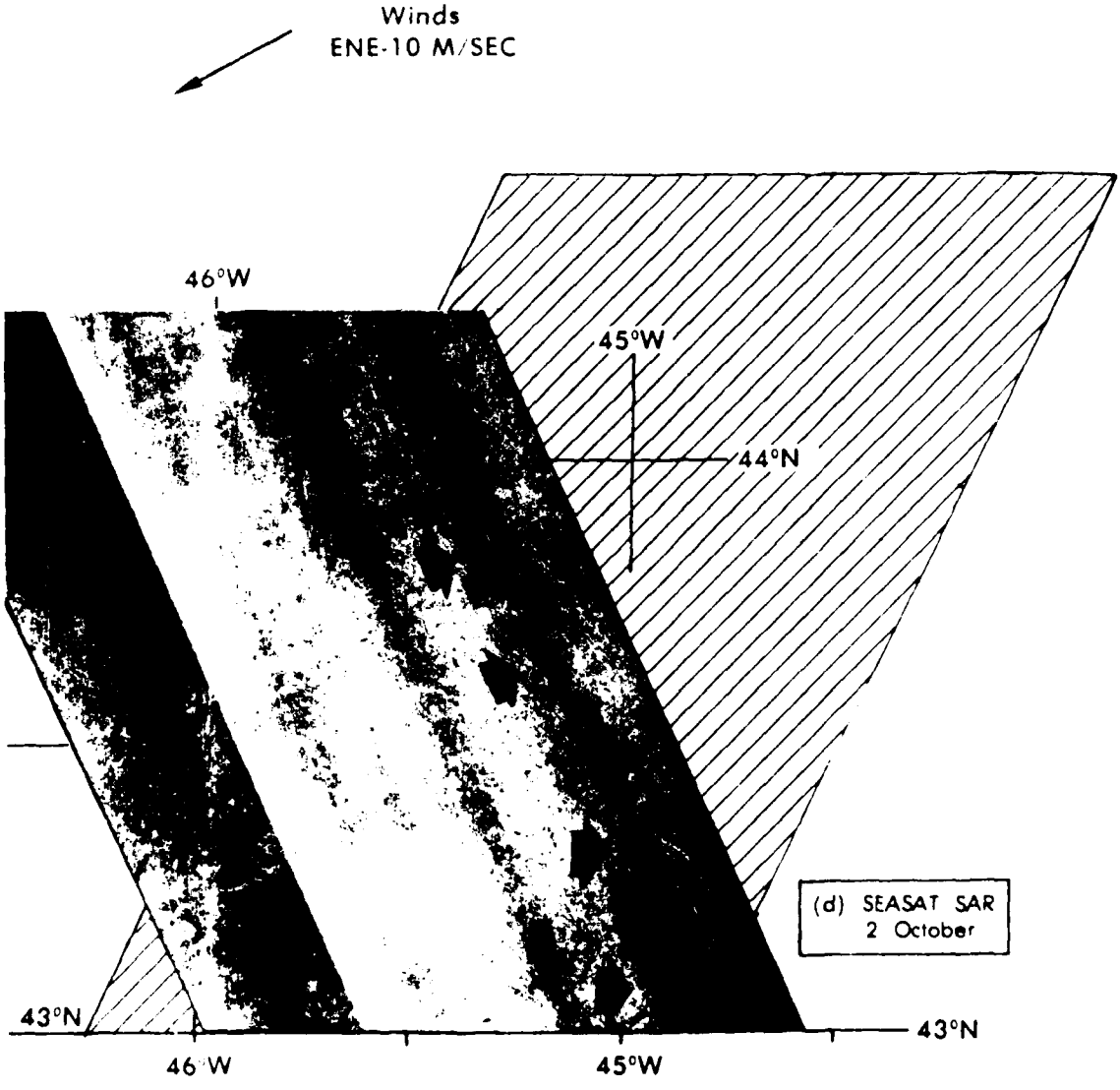
Winds
ENE-10 M/SEC
46°W
45°W
44°N
43°N
46°W
45°W
43°N
(d) SEASAT SAR
2 October

(1)

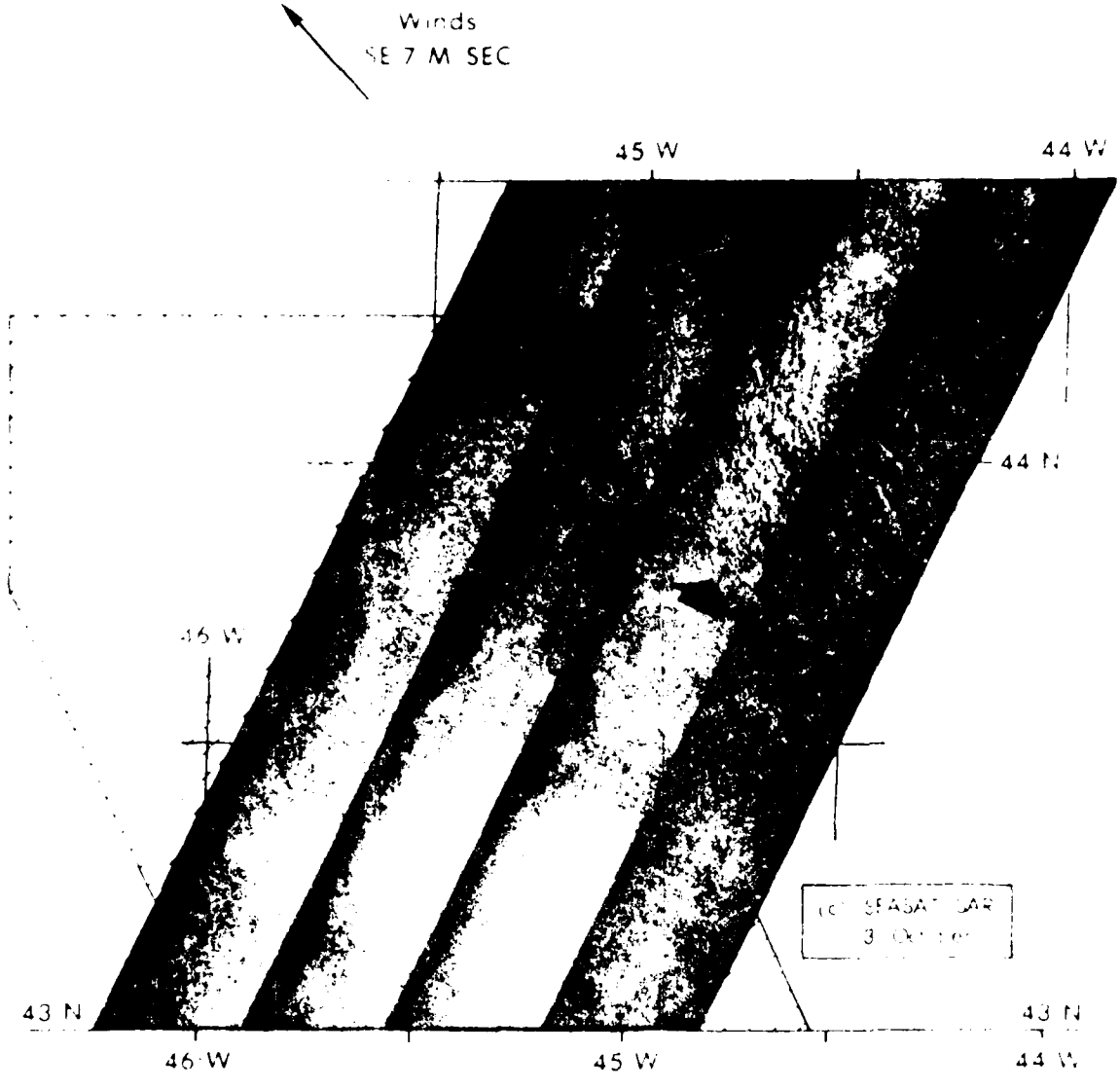

(2)

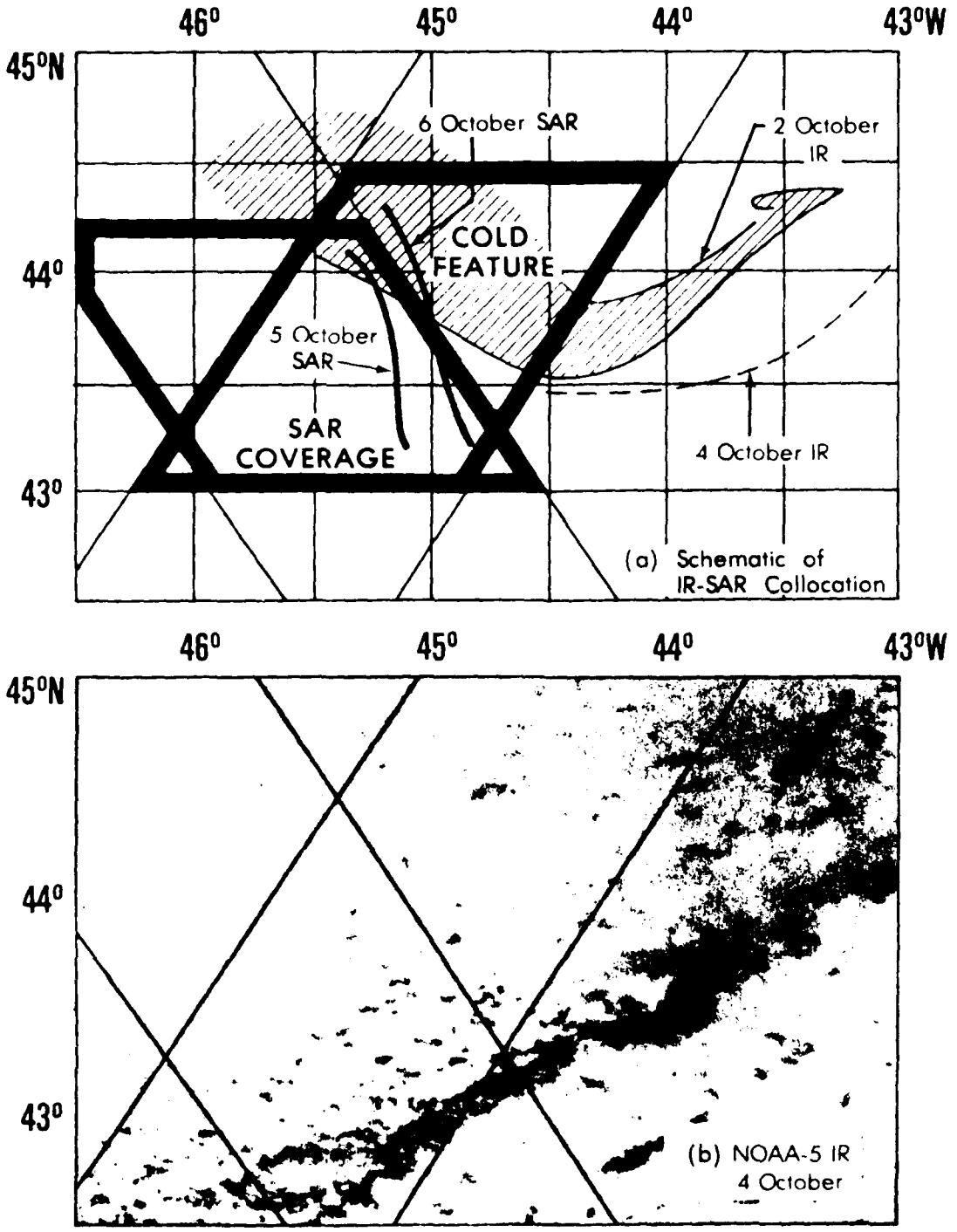

Figure 50. The SAR and infrared imagery for 2, 4, 5, and 6 October. The schematic shows the SAR frontal definitions (heavy lines) for 5 and 6 October overlain on the cold water (zipped pattern and dashed line for 2 and 4 October). Since the swath area was cloud covered on 4 October only the 2 October IR image is shown. None of the SAR imagery registration have been corrected.

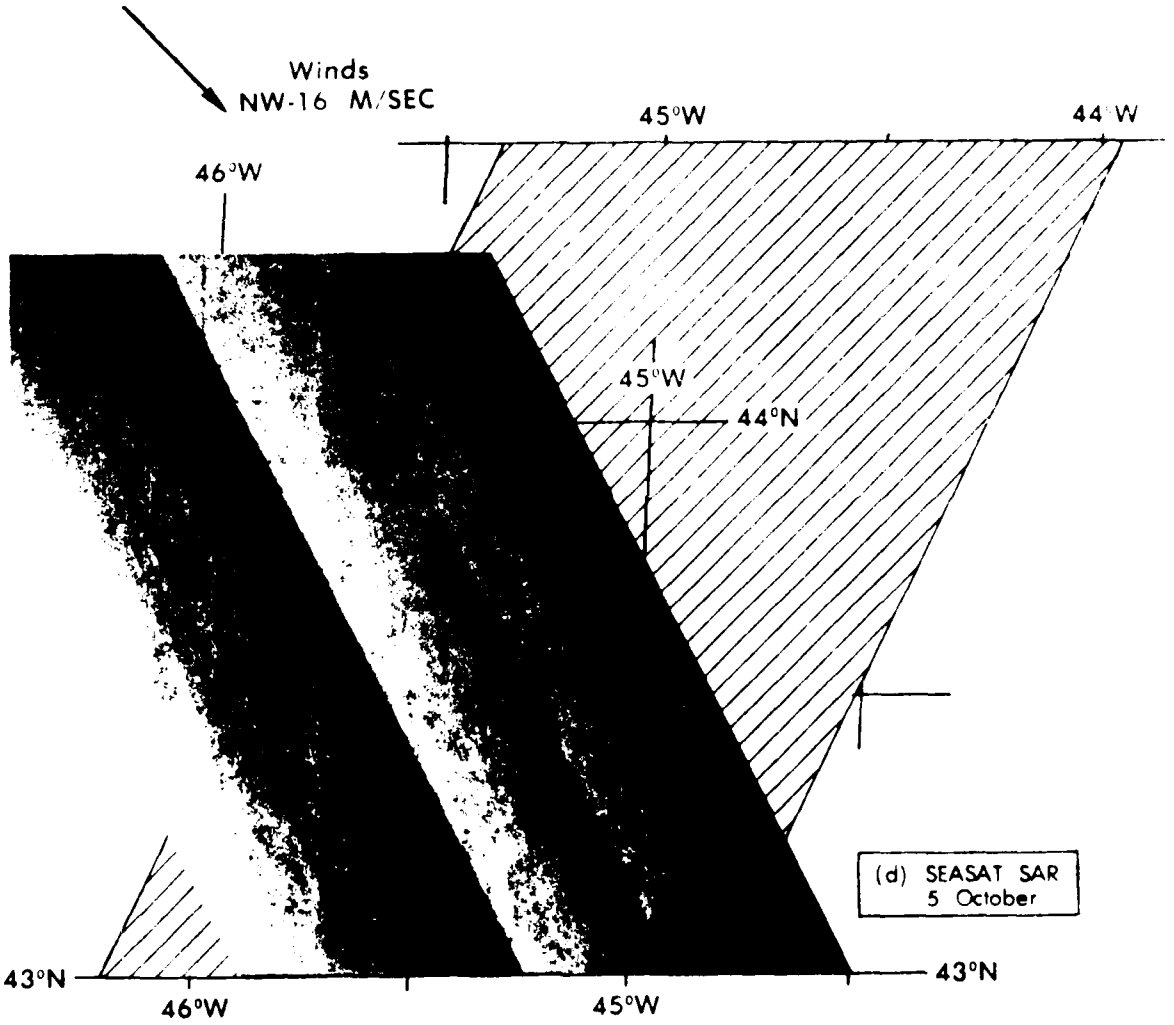
Winds
NW-16 M/SEC
45°W
44°W
46°W
45°W
44°N
43°N
46°W
45°W
43°N
(d) SEASAT SAR
5 October

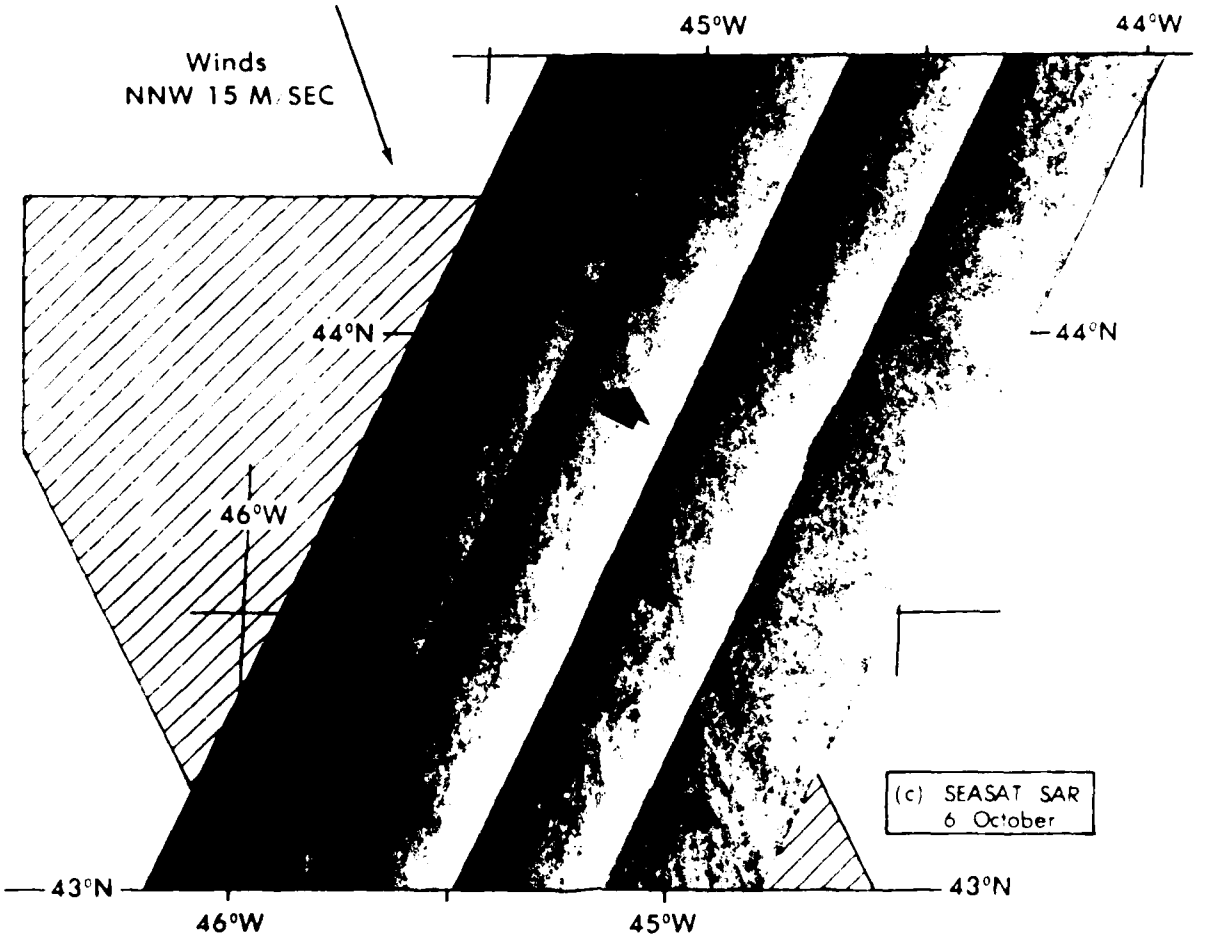
Winds
NNW 15 M/SEC
45°W
44°W
44°N
44°N
46°W
(c) SEASAT SAR
6 October
43°N
43°N
46°W
45°W

(2)

4. Discussion

In comparing the September-October 1979 data, the thermal fronts in the IR imagery are generally found to be delineated by changes in σ_o in the SAR imagery, with location accuracies consistent with the limits of the computer registration of both data sets. This included those instances where the SAR swaths of the ascending and descending orbits crossed.

Correlation is not possible in one case (the Newfoundland Seamount feature on 21 September) and is extremely poor in two cases: the southern thermal front of the eastern ridge feature on 3 October and the western feature on 29-30 September. The following discussion provides possible reasons for these discrepancies.

The patterns in the 21 September SAR image in the area of the Newfoundland Seamounts resemble features reported by other investigators as being caused by strong rain cells (e.g., Fu and Holt, 1982). However, the few ship reports in the area do not indicate rain, and the atmospheric trough (shown by the weather charts to lie to the southeast of the feature [Fig. 40]) should create generally clear conditions. In any case, the environmental event that did occur was obviously strong enough to override the sea-state features related to the thermal front.

The poor showing of the southern front in the 3 October SAR image may be a result of a combination of factors. One of these factors is that winds on 3 October were the weakest of all the times when Grand Banks SAR data were collected (in the Seamount area, they were approximately 5 m/sec). A second, and probably more important, factor is that the 3 October SAR image is the poorest of the SAR images used in this study. Time constraints prevented optically reprocessing the entire 3 October SAR filmstrip to better show features that were obviously subdued in this area, as well as in the other two frontal areas.

The poor correlation of the western ridge feature 29-30 September may be a result of a residual circulation remaining from the 21 September thermal feature. An examination of the 21 September IR image gives an indication that cold water is no longer being pumped into the feature at the surface and that the feature is being cut off from its northern source of cold water (as an example of a strong intrusion of cold surface water--and hence, indicative of a more dynamic connection with the Labrador front--see the cold band of water visible in the southern portion of the eastern ridge feature in Figs. 41-44).

After a given interval of time, mixing in the surface layers caused the feature to lose its surface thermal expression. In the 29 September IR image, the feature is visible only in the northwesterly portion of the sub-area. As mentioned, no thermal feature is present in the comparatively cloud-free IR image of 4 October. However, despite the disappearance of a surface thermal expression, surface rotational circulation evidently remained. This residual circulation is likely the cause of the roughness patterns shown in the SAR image for 30 September and 3, 6, and 9 October.

Although the locations of roughness features in the SAR imagery generally agree with the locations of thermal frontal features in the IR imagery, the roughness features do not show consistent patterns from day to day. These sea state changes are probably the result of atmospheric changes. The work of other investigators (discussed in Part I and in the analyses of Baseline and New Look data) indicates that four atmospheric conditions control the sea conditions across a thermal front:

- wind blowing from the cold to the warm water
- wind blowing from the warm to the cold water
- wind blowing parallel to the front and counter to the current

- wind blowing parallel to the front and with the current

Variations created by a combination of these conditions may occur. Also the relationship (T_a-T_s) across the front affects the degree that the first two conditions apply.

A hindcast study of the environmental conditions on the days that SAR imagery were collected might disclose the causes of the roughness variations. The rest of this section is composed of such a study. It must be emphasized that the study is limited in the amount of available surface data. The wind speed and directions used are derived from surface weather analysis charts and ship reports (none of which were close to the fronts). Thus, accurate air, water, and dew point temperature data ordinarily considered vital for this type study are not available. However, as will be shown, a hindcast study can be made from the available data that, in the author's opinion, gives a fair assessment of the environmental conditions that were present.

Again, because of its persistent location, the Newfoundland Ridge-East feature is chosen to lead the hindcast examination of the three cold water features (Figs. 41-44). As shown in Table G, during the period 21 September-9 October, wind speed over the eastern ridge feature was generally 10 m/sec (with the exception of 3 October when winds decreased to 5 m/sec). However, the direction of the winds varied considerably, and could be said to have "boxed the compass" during the study period. Thus, if the location of the feature is constant and the current is considered to not change, then the only factors that will alter the surface roughness (and, therefore, the radar return) will be wind speed, wind direction, and air temperature.

The SAR swath cut directly across the extrusion and resulted in two fronts being present in each SAR image: one on the northern side of the feature and the other on the southern side. As shown by the two-day intensive examination of a similar ridge feature in Part III, the currents in the area of the northern front should have flowed toward the west (actually west northwest) and the currents at the southern front moved to the east. The central portion should have had an essentially null current.

On 21 September, northwesterly winds were blowing parallel to the fronts and thus, opposed the currents in the northern frontal areas and reinforced the currents in the southern frontal area. In the SAR imagery, the northern and southern fronts are well defined by linear shear patterns. The intensity of the patterns for both fronts are the same with neither the northern or southern front being more prevalent. The roughness patterns in the cold water region are similar to patterns in the cold water regions a short distance away from the immediate area of either front.

Thus, the only marked roughness changes in the SAR image are the shear patterns marking the location of the northern and southern fronts (note that the secondary southern front inside the cold water in the IR image is also shown by a faint line in the SAR image). No change is noticeable across the feature that could be attributable to the change in speed and direction of the currents.

In the next SAR image of the eastern ridge feature--30 September--the winds are the same speed as on 21 September. However, on this date the winds were at right angles to the two fronts--going from the warm to the cold water at the southern front and from the cold to the warm water at the northern front. The result of these wind conditions is that the entire region of the cold feature has a different σ_0 pattern than the warm water regions. The SAR image displays no linear shear patterns at the frontal boundaries as on 21 September, nor are the exact boundaries of the fronts as well delineated. The center

portion of the feature, where currents should be at a minimum, shows essentially the same return as the outer regions of the cold water. Although the entire region of the cold water is well defined by the roughness pattern, the northern portion exhibits the strongest return.

In the 3 October SAR image, the feature is poorly defined (due to the quality of the optical processed image as much as anything else). On this occasion, the wind direction is again parallel to the front. Now, the southeasterly wind should have been opposing the currents at the southern front and reinforcing the currents at the northern front. The northern front shows a more generalized shear area than on 21 September. The southern front is extremely poorly defined. The central portions of the feature show a slightly different σ_o than in the warm water, but the quality of the image precludes any positive statement.

On 6 and 9 October, the winds blew across the northern and southern fronts; although not at as sharp an angle as on 29 September. The northerly winds on 6 October appear to create conditions that cause the southern front in the SAR image to be the better defined. Note that the linear east-west feature splitting the center of the ridge feature in the 9 October SAR image can be faintly seen in the 6 October SAR image. It is unfortunate that no simultaneous IR image is available for comparison to interpret the cause of the linear change.

The hindcast study of the Newfoundland Ridge-East feature provided both expected and unexpected results: the winds blowing from the cold to the warm water created sufficient vertical turbulence to make the frontal boundaries stand out the best. The general settling of the air due to the winds blowing from the warm to the cold water also defined the frontal feature but without as strong a frontal boundary. In general, under both of these conditions, the entire cold water feature had a markedly different σ_o pattern than the warm water, with the warm water pattern being more specular. What cannot be defined is whether there was an offset in the locations of the SAR roughness delineations from the actual locations of the thermal fronts. The location error of the IR images prevented any interpretation. That such offsets may occur is suggested by the intensive frontal surveys discussed in Part III.

Surprisingly, winds blowing parallel to the front, whether blowing with or against the current, produced only shear patterns. No marked difference appeared in σ_o on one side of the cold water feature as compared to the other because of the wind opposing or reinforcing the current.

A continuation of the hindcast study of the environmental conditions of the other two cold water features should show whether these initial results are repeated.

The Newfoundland Ridge-West feature (Figs. 45 and 46) presented several different aspects to the SEASAT-A SAR than the Newfoundland Ridge-East feature. The first is that the frontal area of the western feature within the SAR swath is more circular than the straight fronts lying within the SAR swath of the eastern feature. Thus, a wind from almost any direction is parallel in some places, and at other places is at a right angle to the front or current flow. Although the cold water feature is generally well defined by arcuate wave-like structures by the northerly 10 m/sec winds of 21 September, the best defined area is the southeast quarter. The wave-like structures are probably shear deformations of waves and resemble features seen in the 19 June SLAR imagery (Fig. 32).

The remaining SAR image of the western ridge area graphically shows how the western ridge feature differs from the eastern feature. In the SAR image of 30 September for example, the cold water

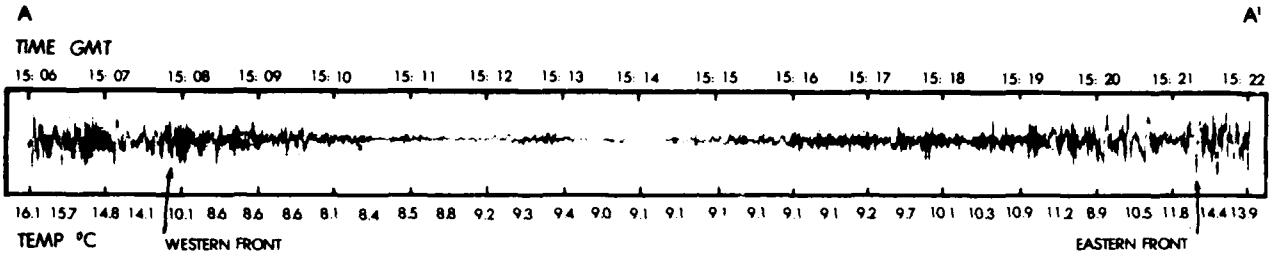

Vertical aircraft movement along line A—A' on 10 May 1979.

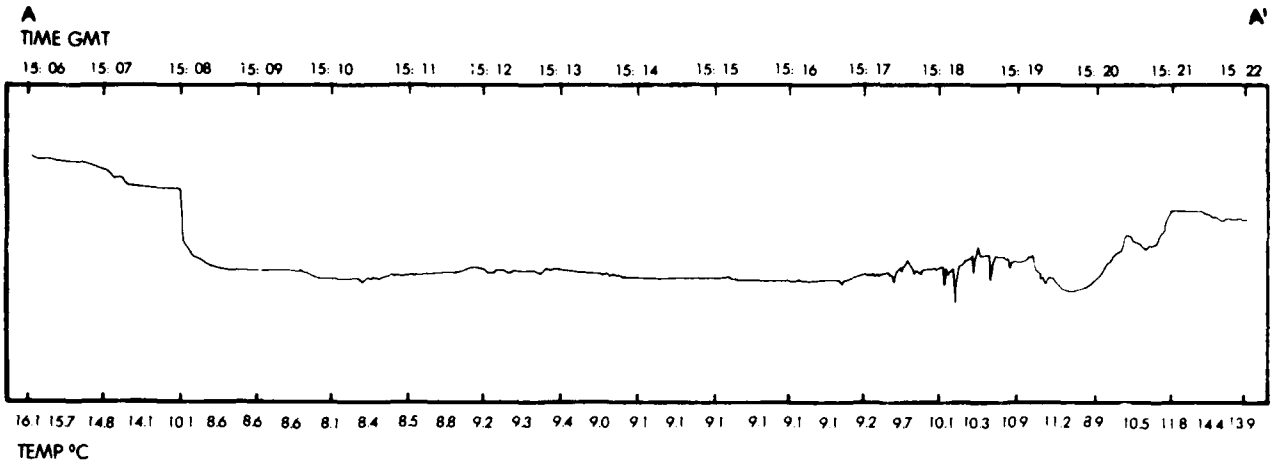

Aircraft PRT trace for line A—A' on 10 May 1979.

Figure 51. An example of the variations in vertical atmospheric turbulence across the western (A) and eastern (A') thermal fronts. A pengraph attached to the vertical accelerometer of the P-3 INS showed the vertical movement of the aircraft as it flew across the frontal structure at an altitude of 300 meters on 10 May. The western front, having the sharpest thermal gradient of the two fronts, showed the quickest atmospheric response. The horizontal wind field, as measured by the aircraft's drift for the same altitude and time, showed no appreciable deviation. This lack of horizontal variability was found in later flights, even when the aircraft flew as low as 70 meters above the water. This example is only one of a number of similiar INS graphs made during the flights. Of particular interest was that during periods when the aircraft was flying through obscuring low clouds or fog with the PRT inactive, the INS graphs indicated changes in vertical turbulence which were shown to be associated with thermal fronts by simultaneous AXBT drops.

surface expression is gone. The roughness pattern shown is probably a circulation feature from the well-mixed surface expression of the cold water. However, without a strong (T_a-T_s), the σ_o variations must be due entirely to wind-current interaction. In Figure 45, the circulation feature can be seen as a poorly defined roughness region that is in the same general area as the 21 September cold water feature in Figure 44. This area of disturbance is repeated in the SAR imagery for 3, 6 and 9 October.

The study of the environmental conditions that generate the σ_o returns in the SAR imagery for the eastern ridge feature indicates that winds blowing parallel to the direction of a current do not generate broad patterns of uniform σ_o in the SEASAT-A SAR imagery. The patterns visible in Figure 45 (and in the imagery for 6 and 9 October) must be due to winds blowing at an angle to the current direction. The curved front of the feature seen in Figure 44 allows such variation to take place.

In the Newfoundland Seamounts region, the cold water frontal boundary also forms a strong curve within the SAR swath. On 30 September, the SAR image shows a strong change in σ_o as the wind blew from the warm water over the cold. The specular return of the warm water in this case sharply contrasts with features in the cold water, which resemble the mottled patterns seen in the 19 June SLAR image (Fig. 32).

On 3 October the winds were parallel to the front. However, while the feature is visible in the SAR image, it is poorly defined. Again, mottled patterns are visible in the cold water. This effect may be the result of the wind blowing across the front outside the SAR swath area, as shown by the diagram in Figure 49. On 6 October, the winds were also parallel to the front and the SAR image displays sharp shear lines that outline the frontal border. On this date, the σ_o from the cold water inside the feature is similar to the warm water outside the feature.

The cross-over imagery formed by ascending SEASAT-A passes also show the Seamounts feature, although with some differences. On 2 October, the ascending SAR image shows a change of σ_o on the edge of the SAR swath. However, it is poorly defined, despite the fact that the wind was blowing from the cold to the warm water--a situation which, in the descending Grand Banks SAR passes, provided the best frontal definition. In the case of the ascending pass for 5 October, the wind was blowing parallel to the front and the SAR image shows the same sharp linear features as the SAR image for 6 October, although it is slightly fainter.

Thus, the western ridge and seamount features show σ_o patterns which define the areas of cold water in much the fashion shown for the eastern ridge feature. In these cases the arcuate structure of the features within the SAR swath accentuated the fact that the wind blowing at right angles to the thermal front and current produced the best defined pattern to delineate the front.

5. Conclusions

From the limited study of several SEASAT-A SAR and NOAA-5 IR imagery, it is found that the roughness patterns in the SAR imagery does delineate the locations of the major thermal fronts shown in the IR imagery.

The comparatively poor accuracy of the NOAA-5 registration prevents defining whether the SAR roughness features lie directly over or are displaced several kilometers to one side of the thermal fronts. The quality of the definition varies from SAR image to SAR image, apparently according to the angle the wind makes with the thermal front and the current. The best conditions for defining the front occurred when the winds were blowing at right angles to the front and current and were moving from the cold to the warm water. The second best conditions occurred when the winds blew from the warm to the cold water. In neither case was the front as

sharply defined as the front in the IR image. In both cases, the broad patterns made by the σ_o changes were the method of definition, with the cold water area having more mottled patterns and the warm water areas having specular, more even patterns.

In those cases where the wind blew parallel to the front, it did not seem to matter whether the wind was blowing with or against the current. The SAR imagery showed linear striations in these cases, which outlined the frontal thermal boundary, with no obvious differences between the cold water σ_o return and the warm water regional return. In those cases containing both effects, such as when the front was curved and the wind encountered the front and current at angles less than 90°, variations of the two conditions took place.

Some of these results seem contradictory to what was found in the studies of the New Look frontal surveys of 16-17 May 1979 discussed in Part V, and the New Look and Baseline SLAR imagery discussed in Part IV. In the frontal surveys, the data indicate that while some roughness induced by air/sea thermal instability was present, the major environmental cause of the measured roughness was the changes in the current field and the interaction of the wind field with the current. The discrepancies in the two results will be further covered in Part VI conclusions.

One interesting result of the comparisons was the possibility that cross-current winds created conditions that allowed the SAR σ_o to delineate a circulation pattern associated with a subsurface thermal structure. In this instance no change in surface thermal conditions was detectable in the IR imagery. This ability could be useful in the study of old cold water rings whose only surface manifestation is a circulation pattern.

Part VI. Conclusions

> The actual appearance of the surface of the open sea . . . is mostly in the sharpest contrast to that of rhythmic regularity. If a wind blows, waves of all different sizes are present, varying in form from long, gently sloping ridges to waves of short and sharp crests. Superimposed on the gentler waves, which may or may not run in the direction of the wind, series of deformations of the surface appear which, from the point of view of physics, can be termed waves only by stretching the definition.
>
> The Ocean, pg. 523, 1942
> by Sverdrup, Johnson, and Fleming

1. Discussion

The main purpose of the Grand Banks Experiment is to examine the ability of specialized radars such as the SLAR and SAR to define ocean fronts. The SLARs used in the experiment were operated aboard U.S. Coast Guard aircraft of the International Ice Patrol. The SAR was part of the suite of microwave sensors aboard SEASAT-A.

The SLAR and SAR are designed to measure waves of certain wavelengths. The SLAR used in this study operated in the K- and X-bands of the electromagnetic spectrum. The SAR operated in the L-band. In the ocean, waves of these dimensions are short-period gravity waves. If the ocean was composed of only such waves, then the demarcation of ocean thermal fronts would be fairly straightforward, since these waves are caused by atmospheric turbulence (which varies with the intensity of the thermal gradients present between the ocean surface and the atmosphere) and do not move far from their area of generation.

However, the ocean surface is not limited to such high frequency waves. The forces which create short-period gravity waves also create long-period gravity waves. These longer-lasting waves are, in turn, modified by currents and other physical processes much in the way discussed in Part I.

It is, however, the σ_o from the short-period gravity waves that the real- and synthetic-aperture radars measure. Experience has shown that the distribution of these short period waves is correlated with larger scale ocean roughness phenomena such as long gravity waves, current shear boundaries, thermal boundaries, and bathymetry. The ability of SLAR and SAR to detect and monitor these large-scale oceanic processes is dependent upon the modulations of the short-period gravity waves by these larger scale phenomena.

This is the problem of the Grand Banks Experiment. In the actual ocean, in an area of complex currents and sharp changes in atmospheric conditions, can the radar return from the regional roughness conditions define the location of actual fronts, and if they can, what are the conditions which allow them to do so?

We tried to set up an experiment to measure those conditions. To begin with, the fronts examined during the Baseline and New Look field surveys were sections of large cold-water structures being extruded from the Labrador Front out over the Newfoundland Ridge and Newfoundland

Seamounts. Analyses of the aircraft, ship, and satellite data taken during the field surveys (Parts II and III) reveal that the extrusions extended deeper than 1000 m and were obviously strongly controlled by the deeper bathymetric features (in the case of the Newfoundland Ridge, this included bathymetric features deeper than 4000 m).

The analyses show that the variations in the regional sea surface temperature and the currents were directly related to these deep cold water extrusions. They show also that the air-sea temperature differences, the interaction of the wind and the current and related local atmospheric factors such as dewpoint and pressure, had marked effect on the magnitude and variation of the local roughness conditions.

The analysis of the data from the intensive aircraft survey of 16-17 May 1979 indicates that well-defined regions of ocean surface roughness existed in the study area, that these roughness regions delineated the frontal boundaries of the cold feature and, in general, that they could be used to define the feature itself.

In addition, studies of the aircraft data indicate that while some roughness induced by air/sea thermal instability was present (Fig. 5), the major cause of the measured variations in ocean roughness seemed to be the interaction of the wave field with the current.

It must be emphasized that the suite of instruments used in the two-day study were incapable of measuring short period waves. The instruments were designed to measure larger-scale ocean roughness such as long period gravity waves, current boundaries, and thermal fronts. As mentioned earlier it is the shorter period waves that are detected by the synthetic- and real-aperture radars.

The next step was to compare these conventional measurements with actual SLAR and SAR data. In the case of SLAR, the comparison of Coast Guard SLAR imagery (Figs. 31 and 32) with simultaneous ocean measurements indicates that certain sea conditions produced certain patterns. Linear features akin to shear striations and aligned parallel to the currents are visible in the imagery in the areas of the warm water near the front. Mottled patterns suggestive of extremely low amplitude, long period waves are present in the imagery in the areas of cold water. Although the mottled patterns show some alignments, these do not coincide with the reports by ship observers nor do they seem to be aligned to the front. Finally, while the regions of the fronts are always indicated in the SLAR imagery, these (with the exception of Fig. 31(a) SLAR image) are not always shown as sharp lines such as seen in infrared imagery of fronts.

The best example of SLAR imagery that had ship data to provide surface truth occurred during Baseline on 19 June 1978. On this occasion analysis of satellite drifter buoy, wave rider buoy, and ship meteorological observations indicated that the thermal air-sea differences over the cold and warm waters were not the major cause of the strong differences of σ_o seen in the 19 June SLAR image. Except for the weak atmospheric front aligned with the ocean front, there was little in the thermal air-sea interaction that would seem to create the strong changes. (T_a-T_s) differences were close to neutral in the warm water and were positive in the cold water. Winds in this instance were moving parallel to the front at speeds greater than 6 m/sec and were reinforcing a current that was moving at 1 m/sec. Previous data showed that shear conditions should have been present at the front, separating the core of faster moving warm water from the cold water. The vertically polarized SLAR imagery during the southern run of the Coast Guard aircraft show patterns indicative of such shear conditions (Fig. 32).

The SAR data are compared in Part V with thermal features in NOAA-5 infrared

imagery, weather charts and to ship-of-opportunity meteorological reports.

These comparisons show that the thermal fronts are always characterized by features in the SAR imagery, including the cross-over regions of the ascending and descending SEASAT-A orbits. The comparisons also showed that these features are similar to features in the SLAR imagery.

A hindcast study using the SAR and infrared imagery and local meteorological reports indicates that the orientation and strength of the regional winds to the thermal front and current seems to be the major factor in the ability of the SAR to depict the front. The study indicated that winds blowing from the cold to the warm water created sufficient vertical turbulence in the warm water to make the frontal boundaries stand out in the SAR imagery as pattern changes of σ_o. The subsidence of the air over the cold water when the winds blow from the warm to the cold water created comparatively calm sea conditions, which also helped define the frontal boundary in the SAR imagery.

This latter condition did not produce as strong a change in pattern as did the wind going from the cold to warm water. In either case the σ_o boundary was not as sharp as the demarcation of the thermal gradients found in the infrared imagery. In this regard the comparatively poor registration of the NOAA-5 imagery prevented ascertaining whether the roughness patterns were offset from the thermal front, as suggested by the INS vertical accelerometer data in Part III (Fig. 51).

In general, the study showed that under either condition, with the wind orthogonal to the front, the entire cold water feature had a marked different σ_o pattern in the SAR imagery than the warm water, with warm water being the more specular and the cold water presenting what can be termed a mottled appearance.

The hindcast study indicated that winds blowing parallel to the thermal front created the poorest conditions to define the thermal front. In addition the conditions produced an entirely different σ_o pattern. These patterns appeared in the SAR imagery as linear striations that were close to, if not directly coincident with, the thermal front. In these instances, the σ_o from the warm water on one side of the front was quite similar to the return from the cold water on the opposite side of the front. The lines of striations occurred with apparently equal strength, whether the winds were opposing or reinforcing the current.

In those instances where the wind was blowing at an angle to the front, modifications of both phenomena appeared in the SAR imagery. This was best demonstrated in those cases where the SAR swath crossed a curved thermal front.

The apparent discrepancy between the results of the SAR and SLAR studies are probably due to the fact that the SLAR studies were limited to a period where the winds were parallel to the front, a situation in which the SAR imagery produced the poorest definition of the thermal front. What was needed to complete the SLAR study was an example of a strong wind blowing at right angles to the front. Such a situation might have been possible with the SLAR image in Fig. 31(c) had not the data had serious navigation errors. Winds blowing across the front produce greater changes of (T_a-T_s) than winds blowing parallel. In fact, on 19 June 1978 the data showed that a weak atmospheric front lay coincident with the cold water.

In examining the SAR imagery for the area of the western ridge feature, the surface thermal gradients are found to be gone in the imagery after 26 September. However, the SAR image still showed roughness patterns similar in location to patterns found when the surface thermal feature was present on 21 and 26

September. The σ_o pattern in this instance was weak as well as poorly defined. If the interpretation is correct that this was residual circulation from the coldwater extrusion, then only the current/wave interactions were responsible for the σ_o in the SAR imagery. This, then, is an example of a σ_o return that did not involve a negative (T_a-T_s).

The patterns in the SLAR and SAR imagery seem to differ from what the same ocean scene would show in reflected sunlight. This is especially true in the case of the mottled patterns inside the cold features. The reason suggested in Part IV for this difference is that the effect is due to Bragg scattering and that the patterns are the result of the constructive/destructive resonant backscatter from the low amplitude, long period waves.

In conclusion, the results of the Grand Banks Experiment are derived from a very limited set of data, with the actual data not as concurrent as originally planned. They do, however, show that satellite- and aircraft-specialized radars such as SAR and SLAR can be used to monitor the location of ocean fronts under nearly all weather conditions. As an operational research tool, such monitoring will require the development of exploitive techniques. Such development will require more extensive data sets than were used in this study. It is suggested that, since satellite SAR is presently unavailable and aircraft SAR is difficult to come by, that the use of the comparatively less expensive aircraft SLAR be used. These radars are currently available from their manufacturers as "off-the-shelf" units.

As far as remote-sensing oceanography is concerned, the input of information that specialized radars can provide (whether from SAR or SLAR) would greatly enhance our synoptic understanding of the dynamic processes taking place in the oceans.

Part VII. References

Apel, J. R. and R. L. Charnel (1974). Ocean Internal Waves Off the North American and African Coasts from ERTS-1. NASA Report SP-351, 1309-1316.

Barber, N. F. (1949). The Behavior of Waves on Tidal Streams. Proc. Royal Soc. London, A, 198, 81-93.

Bowden, K. F. (1948). Some Observations of Waves and Other Fluctuations in a Tidal Current. Proc. Roy. Soc. London, A, 197, 403-405.

Clark, J. R. and P. E. La Violette (1980). The Detection of Moving Oceanic Fronts Using Successive TIROS-N Imagery. Geophys. Res. Lett., 8, 229-232.

Clarke, R. A., R. F. Reininger and A. Warren (1980). Current System South and East of the Grand Banks of Newfoundland. J. Phys. Oceanog., 10, 25-65.

Deacon, E. L. (1961). Aerodynamic Roughness of the Sea. J. Geophys. Res., 67, 3167-3172.

Fett, R. W., P. E. La Violette, M. Nestor, J. Nickerson, and K. Rabe (1978). Chapter 3D, Internal Waves. In Navy Tactical Applications Guide, Volume II: Environmental Phenomena and Effects, Naval Environmental Prediction Research Facility, Monterey, unpaged.

Fett, R. W. and K. Rabe (1977). Satellite Observation of Internal Wave Refraction in the South China Sea. Geophys. Res. Lett., 4, 189-191.

Fortuna, J. and L. Hambrick (1974). The Operation of the NOAA Polar Satellite System. November NOAA Tech. Memo. 60, National Environmental Satellite Service NOAA, Washington, D.C., 127 p.

Fu, L. L. and B. Holt (1982). Seasat Views Oceans and Sea Ice with Synthetic-Aperture Radar. J P L Pub. 81-120, Jet Propulsion Laboratory, California Institute of Technology, Pasadena, Calif., 200 p.

Hayes, J. G. (1980). Ocean Current Wave Interaction Study. J. Geophys. Res., 85:C9, 5025-5031.

Holyer, R. J., P. E. La Violette, and J. R. Clark (1980). Satelite Oceanographic Research Development and Technology Transfer Proceedings of the Fourteenth International Symposium on Remote Sensing of Environment, ERIM, Ann Arbor, Michigan 1, 221-241.

Huang, N. E., D. T. Chen, C. C. Tung, and J. R. Smith (1972). Interactions Between Steady Non-Uniform Currents and Gravity Waves with Applications for Current Measurements, J. Phys. Oceanog., 2:4, 420-431.

Hughes, C. A. (1978). Interim Report on SAR VAL, July 1978. Dept. Def. Res. Est. Pacific Report. Dept. Def. Res. Est., Canada.

Hussey, W. J. (1979). The TIROS-N/NOAA Operational Satellite System, NOAA NESS Tech. Memo. 95, National Environmental Satellite Service/NOAA, Washington, D.C. 35 p.

Islen, C. O. D. (1936). A Study of the Circulation of the Western North Atlantic. Pap. Phys. Oceanog. Meteor., (4), No. 4, 101 p.

Jones, D. R. (1953). Note on Observed Vertical Wind Shear at Low Levels Over the Ocean. Bull. Am. Met. Soc., 53, 59-63.

Kenyon, K. E. (1971). Wave Refraction in Ocean Currents. Deep-Sea Res., 18, 1023-1034.

Koffler, R. (1976). Digital Processing of NOAA's Very High Resolution Radiometer (VHRR) Data. National Environmental Satellite Service/NOAA, Washington, D.C., 7 p.

Kondo, J. (1975). Air-Sea Bulk Transfer Coefficients in Diabatic Conditions. Boundary Layer Met., 9, 91-112.

La Violette, P. E. (1974). A Satellite Aircraft Thermal Study of the Upwelled Waters off Spanish Sahara. J. Phys. Oceanog., 4, 676-684.

La Violette, P. E., L. Stuart, Jr. and C. Vermillion (1975). Use of APT Satellite Infrared Data in Oceanographic Survey Operations. EOS, 56, 276-1282.

La Violette, P. E., S. Peteherych and N. F. R. Gower (1980). Oceanographic Implications of Features in NOAA Satellite Visible Imagery. Boundary-Layer Met., 18, 159-175.

La Violette, P. E. (1981a). Remote Sensing Oceanography: A Synoptic Approach. NORDA Tech Note 100, Naval Ocean Research and Development Activity, NSTL Station, Miss., 16 p.

La Violette, P. E. (1981b). Variations in the Frontal Structure of the Southeastern Grand Banks. NORDA Tech. Note 87, Naval Ocean Research and Development Activity, NSTL Station, Miss.

Liu, P. C. and D. B. Ross (1980). Airborne Measurements of Wave Growth for Stable and Unstable Atmospheres in Lake Michigan. J. Phys. Oceanog., 10:11, 1842-1853.

Longuet-Higgins, M. S. (1961). The Changes in Amplitude of Short Gravity Waves on Steady Non-Uniform Currents, J. Fluid Mech., 10, 529-549.

Longuet-Higgins, M. S. (1964). Radiation Stresses in Water Waves; a Physical Discussion with Applications, Deep-Sea Res., 11, 529-562.

Longuet-Higgins, M. S. and R. W. Stewart (1960). Changes in the Form of Short Gravity Waves on Long Waves and Tidal Currents. J. Fluid Mech., 8, 565-583.

Mann, C. R. (1967). The Termination of the Gulf Stream and the Beginning of the North Atlantic Current. Deep Sea Res., 14, 337-359.

Mann, C. R. (1971). A Review of the Branching of the Gulf Stream System. Proc. R.S.E., 33, 341-349.

McClain, C. R., N. E. Huang, P. E. La Violette (1982). Measurements of the Sea State Variations Across Oceanic Fronts Using Laser Profilometry. J. Phys. Oceanog. 12:11, 1228-1244.

Mountain, D. G. and J. L. Shuhy (1980). Circulation Near the Newfoundland Ridge. J. Mar. Res., 38, 205-213.

Pressman, A. E. and R. J. Holyer (1978). Interactive Digital Satellite Image Processing System for Oceanographic Applications. NORDA Tech Note 23, Naval Ocean Research and Development Activity, NSTL Station, Miss., April, 13 p.

Reininger, R. F. and R. A. Clarke (1975). Circulation Pattern in the Newfoundland Ridge Area, 1972. Proc. Bedford Inst. of Oceanog. 52-67.

Ross, D. B., V. J. Cordone, J. W. Conaway, Jr. (1970). Laser and Microwave Observations of Sea-Surface Conditions for Fetch-Limited 17-25 m/s Winds. IEEE Trans., GE-8, 326-336.

Schule, J. J., Jr., L. S. Simpson, P. S. De Leonibus (1971). A Study of Fetch-Limited Wave Spectra with an Airborne Laser. J. Geophys. Res., 76, 4160-4171.

Schwalb, A. (1972). Modified Revisions of the Improved TIROS Operations (ITOS D-G). National Environmental Satellite Service/NOAA, Washington, D.C., April, NOAA NESS Tech. Memo. NESS 35, 48 p.

Schwalb, A. (1978). The TIROS-N/NOAA A-G Satellite Series, National Environmental Satellite Service. NOAA, Washington, D.C., March, NOAA Tech. Memo. NESS 95, 75 p.

Soule, F. M. (1964). The Normal Dynamic Topography of the Labrador Current and Its Environs in the Vicinity of the Grand Banks of Newfoundland During the Iceberg Season. Woods Hole Oceanog. Inst. Ref. No. 64-36.

Soules, S. D. (1970). Sun Glitter from Space. Deep Sea Res., 17, 191-195.

Strong, A. E. and R. J. De Rycke (1973). Ocean Current Monitoring Employing a New Satellite Sensing Technique. Science 182, 482-484.

Sugimori, Y. (1973). Dispersion of the Directional Spectrum of Short Gravity Waves in the Kuroshio Current. Deep-Sea Res., 20, 747-756.

Sverdrup, H. U., M. W. Johnson, and R. H. Fleming (1942). The Oceans, Their Physics, Chemistry, and General Biology. Prentice-Hall, Inc., 1087 p.

Sweet, W., R. Fett, J. Kerling, and P. E. La Violette (1981). Air-Sea Interaction Effects in the Lower Troposphere Along the North Wall of the Gulf Stream. Monthly Weather Review, 109, 1042-1052.

Weissman, D. E. and T. W. Thompson (1977). Detection and Interpretation of Ocean Roughness Variation Across the Gulf Stream Inferred from Radar Cross-Section Observations. Oceans 1977, Proceedings, 14B1-10.

Worthington, L. V. (1962). Evidence for a Two Gyre Circulation in the North Atlantic. Deep-Sea Res., 9, 57-67.

Worthington, L. V. (1976). On the North Atlantic Circulation. The Johns Hopkins Oceang. Stud., 6, 110 p.

Appendix A: The NOAA, TIROS, and GOES Satellite Data

The non-SEASAT satellites used for the Grand Banks Experiment were GOES, NOAA-4 and 5 and TIROS-N. GOES was used mostly for operational purposes to detect rapid weather and oceanographic changes in the field. NOAA-4 and 5 and TIROS-N were used for the field operation and the post-survey analyses. The primary satellite sensors used in these analyses are the VHRR infrared channel of NOAA-4 and 5 and the AVHRR infrared channel of TIROS-N. Both channels operate within the spectral window of 10.5 to 12.5 microns and present pictures of the earth's emitted infrared energy with a 1.1 km resolution. A description of the NOAA satellite and the VHRR sensor can be found in Schwalb (1972), Fortuna and Hambrick (1974), and Koffler (1976). TIROS-N and the AVHRR sensor are described in Schwalb (1978) and Hussey (1979). Examples of the use of data of these types for oceanographic studies are numerous. Several papers for which the author was responsible may serve as a guide to readers unfamiliar with the application of satellite data to oceanography: La Violette 1974; La Violette et al., 1975; La Violette et al., 1980.

NOAA-4 and 5 data are used for the pre-survey satellite imagery examination and the Baseline data analysis. TIROS-N data are used in the analysis of New Look data. NOAA-5 data are used in the analysis of the SEASAT-A SAR data. NOAA-4 and 5 data are somewhat limited due to the quantitative difficulty in comparing a single infrared image from these satellites' data with other imagery or surface data. This difficulty results because the earth scene shown in each NOAA image is distorted by the projection resulting from the large scan angle at the edge of the satellite sensor field of view and the curvature of the earth. Since the satellite precesses in its orbit around the earth, the same distortion is repeated only after a number of weeks. It is rare that two cloud-free images having oceanic features of interest have the same distortion. Because of problems which include the attitude of the spacecraft and the comparatively poor timing of the spacecraft clocks, it is difficult to reregister the various distortions to a common projection. This was done in Part V of the present study for the hindcast comparison of NOAA-5 infrared and SEASAT-A SAR imagery. In this instance, the registration accuracy of the NOAA-5 imagery was $\pm$20 km.

TIROS-N was launched in October 1978 and its data became operationally available in time for the New Look surveys. The TIROS-N data tapes distributed by NOAA Environmental Data Information Service (EDIS) have incorporated geographic positions derived from ephemeris data. Clark and La Violette (1980), in a study of the accuracy of the geographic positioning incorporated into the data, have measured a mean positioning error in the data of 3.7 km with a standard deviation of 1.7 km. With this degree of accuracy TIROS-N data may be reliably registered into various map projections and an image-to-image quantitative comparison of TIROS-N satellite data is possible. The TIROS-N imagery in the New Look portion of this study have been registered into mercator projections.

The satellite data for this study were received by stations at Wallops Island, Virginia; Toronto, Ontario; and Shoe Cove, Newfoundland. Whenever possible the imagery have been enhanced to show ocean thermal features. The enhancement of the NOAA-5 imagery was done by the Canadian Atmospheric Environmental Service in Toronto, Canada. The registered TIROS-N and NOAA-5 imagery (as well as the computer-composed graphics used in the study) were made using the NORDA-IDSIPS interactive computer. A description of the method used for registering and enhancing the TIROS-N imagery can be found in Holyer et al. (1980), and Pressman and Holyer (1978).

DISTRIBUTION LIST

Department of the Navy
Asst Secretary of the Navy
(Research Engineering & System)
Washington DC 20350

Project Manager
ASW Systems Project (PM-4)
Department of the Navy
Washington DC 20360

Department of the Navy
Chief of Naval Material
Washington DC 20360

Department of the Navy
Chief of Naval Operations
ATTN: OP 951
Washington DC 20350

Department of the Navy
Chief of Naval Operations
ATTN: OP 952
Washington DC 20350

Department of the Navy
Chief of Naval Operations
ATTN: OP 980
Washington DC 20350

Director
Defense Technical Info Cen
Cameron Station
Alexandria VA 22314

Department of the Navy
Director of Navy Laboratories
Rm 1062 Crystal Plaza Bldg 5
Washington DC 20360

Commander
DWTaylor Naval Ship R&D Cen
Bethesda MD 20084

Commanding Officer
Fleet Numerical Ocean Cen
Monterey CA 93940

Commander
Naval Air Development Center
Warminster PA 18974

Commander
Naval Air Systems Command
Headquarters
Washington DC 20361

Commanding Officer
Naval Coastal Systems Center
Panama City FL 32407

Commander
Naval Electronic Sys Com
Headquarters
Washington DC 20360

Commanding Officer
Naval Environmental Prediction
Research Facility
Monterey CA 93940

Commander
Naval Facilities Eng Command
Headquarters
200 Stovall St.
Alexandria VA 22332

Commanding Officer
Naval Oceanographic Office
NSTL Station MS 39529

Commander
Naval Oceanography Command
NSTL Station MS 39529

UNCLASSIFIED

SECURITY CLASSIFICATION OF THIS PAGE (When Data Entered)

REPORT DOCUMENTATION PAGE		READ INSTRUCTIONS BEFORE COMPLETING FORM
1. REPORT NUMBER NORDA Report 49	2. GOVT ACCESSION NO. AD-A136 181	3. RECIPIENT'S CATALOG NUMBER
4. TITLE (and Subtitle) THE GRAND BANKS EXPERIMENT: A Satellite/ Aircraft/Ship Experiment to Explore the Ability of Specialized Radars to Define Ocean Fronts		5. TYPE OF REPORT & PERIOD COVERED Final 6. PERFORMING ORG. REPORT NUMBER
7. AUTHOR(s) Paul E. La Violette		8. CONTRACT OR GRANT NUMBER(s)
9. PERFORMING ORGANIZATION NAME AND ADDRESS Naval Ocean Research & Development Activity Ocean Science and Technology Laboratory NSTL Station, Mississippi 39529		10. PROGRAM ELEMENT, PROJECT, TASK AREA & WORK UNIT NUMBERS
11. CONTROLLING OFFICE NAME AND ADDRESS Same		12. REPORT DATE July 1983 13. NUMBER OF PAGES 126
14. MONITORING AGENCY NAME & ADDRESS(if different from Controlling Office)		15. SECURITY CLASS. (of this report) Unclassified 15a. DECLASSIFICATION/DOWNGRADING SCHEDULE

16. DISTRIBUTION STATEMENT (of this Report)

Distribution Unlimited

17. DISTRIBUTION STATEMENT (of the abstract entered in Block 20, if different from Report)

18. SUPPLEMENTARY NOTES

19. KEY WORDS (Continue on reverse side if necessary and identify by block number)

satellite imagery
infrared
synthetic aperture radar (SAR)
currents
Grand Banks

20. ABSTRACT (Continue on reverse side if necessary and identify by block number)

At various times during 1978-1979. a joint U.S.-Canadian experiment involving ships, buoys, aircraft, and satellites was conducted in the waters southeast of the Grand Banks. The purpose was to determine the ability of satellite- and aircraft-specialized radars (SAR and SLAR) to monitor ocean fronts. The experiment results, detailed in this report, show that these radars are capable of defining thermal fronts under most weather conditions. The degree, as well as the type, of definition depended on the angle the wind made with the thermal

DD FORM 1 JAN 73 1473 EDITION OF 1 NOV 65 IS OBSOLETE
S/N 0102-LF-014-6601

UNCLASSIFIED
SECURITY CLASSIFICATION OF THIS PAGE (When Data Entered)

front and associated currents. Winds blowing parallel to the fronts produced shear lines in the SAR and SLAR imagery. Winds blowing orthogonal to the front produced broad patterns whose changes mark the location of the thermal fronts. This latter definition produced the best delineation of the thermal fronts; however, delineation was more gradual than the sharp thermal gradients marking the fronts seen in satellite infrared imagery. The possible causes of these effects are detailed in this report.